College of Health Sciences

School of Pharmacy

Department of Pharmaceutics and Industrial Pharmacy

Preparation and Characterization of Microcrystalline Cellulose from Tea waste and its Evaluation as a Direct Compression excipient in Paracetamol tablet formulation

By Bihonegn Sisay (BSC, B. Pharm)

December, 2025

Addis Ababa, Ethiopia

Preparation and Characterization of Microcrystalline Cellulose from Tea Waste and Its Evaluation as a Direct Compression Excipient in Paracetamol Tablet Formulation.

By: Bihonegn Sisay

A thesis submitted to the Department of Pharmaceutics and Industrial Pharmacy, School of Pharmacy, College of Health Sciences, Addis Ababa University, in Partial Fulfillment of the Requirements for the Degree of Master of Science in Pharmaceutics under the supervision of Dr. Nisha Mary Joseph, Dr. Tesfaye Gabriel, and Mr. Fantahun Molla.

December, 2025

Addis Ababa, Ethiopia

Addis Ababa University

College of Health Sciences, School of Pharmacy

Department of Pharmaceutics and Industrial Pharmacy

This is to certify that the thesis prepared by Bihonegn Sisay, titled: 'Preparation and Characterization of Microcrystalline Cellulose from Tea Waste and Its Evaluation as a Direct Compression Excipient in Paracetamol Tablet Formulation' submitted in partial fulfillment of the requirements for the Degree of Master of Science in Pharmaceutics complies with the regulations of the University and meets the accepted standards concerning originality and quality.

Approved and signed by the examining committee:

Name	Signature	Date
Dr. Nisha Mary Joseph (Advisor)	Nisha Mary Joseph	11 December 2025
Dr. Tesfaye Gabriel (Advisor)	_____	_____
Mr. Fantahun Molla (Advisor)	_____	_____
Dr. Admassu Assen (External Examiner)		11 December 2025
Mr. Yonas Brhane (Internal Examiner)	_____	_____

ACKNOWLEDGMENT

First and foremost, I would like to sincerely thank my advisors, Dr. Nisha Mary Joseph, Dr. Tesfaye Gabriel, and Mr. Fantahun Molla, for their invaluable guidance and support throughout my research thesis, from its initial stage to completion.

I would also like to forward my heartfelt appreciation to Addis Ababa University for the scholarship rendered to me and for the financial support. I am also grateful to the School of Pharmacy, Department of Pharmaceutics and Industrial Pharmacy, for its technical support, including laboratory access and materials. My sincere thanks also go to the department's staff, especially Ato Fikade Tefera, for their assistance.

I would also like to thank Ethiopian Pharmaceutical Manufacturing (EPHARM) for providing me with access to their laboratory facilities and donating Paracetamol directly compressible raw material, as well as other pharmaceutical excipients. I sincerely thank Adama Science and Technology University for providing the laboratory equipment for the characterization study. I am also grateful to Addis Ababa Science and Technology University for helping me with the laboratory activity and data interpretation. I also thank Ethio Agri Ceft PLC and East African Agri-business PLC for donating the raw materials of tea fibre and tea leaf waste.

Finally, I would like to thank the Ethiopian Public Health Institute and the Armauer Hansen Research Institute for sponsoring my MSc study. I am also happy and grateful to have had all my colleagues, from the Traditional and Modern Medicine Research Directorate staff, especially Mrs. Frehiwot Teka and Mr. Baye Akele, throughout my journey.

TABLE OF CONTENTS

LIST OF TABLES

LIST OF FIGURES

ABBREVIATIONS AND ACRONYMS

AHP	Alkaline Hydrogen Peroxide
BNC	Bacterial Nanocellulose
BPA	Baird-Parker Agar
BP	British Pharmacopoeia
BSC	Biopharmaceutics Classification System
CF	Compression Force
CrI	Crystallinity Index
C.I	Carr's Index
CNC	Cellulose Nanocrystals
DI	Direct Compression
DP	Degree of Polymerization
DSC	Differential Scanning Calorimetry
FAO	Food and Agriculture Organization of the United Nations
FTIR	Fourier Transform Infrared Spectroscopy
F1	Paracetamol tablet formulated using TLW-MCC
F2	Paracetamol tablet formulated using TFW-MCC
F3	Paracetamol tablet formulated using Avicel pH-101
H. R	Hausner's Ratio
HPLC	High-Performance Liquid Chromatography
MCC	Microcrystalline Cellulose
NFC	Micro Fibrillated Cellulose
Mid	Middle
MFC	Micro Fibrillated Cellulose
Min	Minimum
NCC	Nanocrystalline Cellulose
PA	Peak Area
PCM	Paracetamol
Pb	Bulk density
Pt	Tapped density

RD	Reference Drug
RSD	Relative Standard Deviation
SDA	Sabouraud Dextrose Agar
SD	Standard Division
SEM	Scanning Electron Microscope
STD	Standard
TLW	Tea Leaf Waste
TFW	Leaf Fiber Waste
TW	Tea Waste
TGA	Thermogravimetric analyzer
TSA	Tryptone Soya Agar
TSB	Tryptone Soya Broth
USP	United States Pharmacopeia
UV	Ultraviolet
WRS	Working Reference Standard
XLD	Xylose-Lysine Deoxycholate
XRD	Xray diffraction

ABSTRACT

Lignocellulosic biomass is an abundant and renewable resource derived from plants, mainly composed of lignin, cellulose, and hemicellulose. Cellulose has long chains of β-D-glucopyranose units joined by β-1,4-glycosidic linkages. Therefore, this research explores the valorization of tea waste (TW), a plentiful agricultural byproduct in Ethiopia, as a sustainable raw material for producing microcrystalline cellulose (MCC). Few studies have evaluated tea waste as a source of cellulose. Therefore, this study aimed to prepare and characterize microcrystalline cellulose from TW. The study involved extracting cellulose from Tea leaf waste (TLW) and Tea fiber waste (TFW) through a sequence of chemical treatments, including alkaline processing and bleaching. The isolated cellulose was then converted to MCC via acid hydrolysis. The hydrolysis conditions, including temperature and time of hydrolysis, were systematically optimized using a CCD, with the highest yield of 86.79% achieved at 100°C for 30 minutes with a 2.5 M HCl concentration.

The resulting MCC powders were thoroughly characterized and compared to a commercial standard (Avicel PH-101). Analytical techniques, including XRD, FTIR, SEM, and thermal analysis, confirmed the successful production of MCC from both TW sources. The samples exhibited the characteristic chemical structure of cellulose, with crystallinity indices ranging from 62.48% to 70%, and morphological changes indicative of successful hydrolysis. Furthermore, key physicochemical and powder flow properties, such as pH, moisture content, bulk density, and angle of repose, were evaluated and found to comply with pharmacopeial standards, demonstrating their suitability as pharmaceutical excipients. The practical application of the TW-derived MCC was evaluated by formulating paracetamol tablets via direct compression. The tablets produced (F_1 with TLW-MCC and F_2 with TFW-MCC) were compared against tablets containing Avicel PH-101 (F_3) and a commercial reference product. All formulated tablets met the required BP standards for weight variation, hardness, friability, and disintegration time. Crucially, dissolution testing revealed rapid drug release, with over 85% of the paracetamol dissolved within 10 minutes, and assay results confirmed uniform drug content within the acceptable range of 90-110%. In conclusion, MCC with excellent tableting properties was successfully isolated from tea waste, establishing it as an effective, sustainable, and locally relevant excipient for the pharmaceutical industry.

Keywords: Tea waste, Microcrystalline Cellulose, Direct compressible excipient, Characterization, Formulation, Paracetamol tablets

1. INTRODUCTION

1.1 Background

Biomaterials derived from lignocellulosic biomass are considered environmentally friendly materials for use in the preparation of various products. Scientists and researchers have given considerable thought to applying it to the preparation of biodegradable composite goods. One way to create a sustainable environment is to use the widely accessible agricultural waste that comes from plant fiber (Nguyen, 2023).

Among the major components of lignocellulosic biomass, plants are rich in cellulose, a fibrous, naturally occurring carbohydrate polymer. Globally, about 50 billion tons are produced annually and cellulose is composed of long chains of β-D-glucopyranose units joined by β-1,4-glycosidic bonds. There are numerous applications for microcrystalline cellulose (MCC), one of the derivatives that can be produced from cellulose. Applications for MCC powder are typically micrometer-sized (1–100 μm) (Bahreini, 2022). MCC is a partially depolymerized cellulose that is made by applying mineral acids to cellulose. It is a crystalline, fine, white, odorless, nontoxic, and biocompatible powder with a high mechanical strength, a large surface area, and a low density. These characteristics make MCC a common choice for excipients, used as anticaking agents, emulsifiers, binders, dispersants, emulsion stabilizers, thermal stabilizers, and carriers for tableting and quick drying in the food and pharmaceutical industries (Jamshaid *et al*., 2017).

The use of wood pulp as a raw material in traditional MCC preparation techniques destroys forests and trees. Plant cell walls are composed of lignin, cellulose, hemicellulose, and microfibrils. Additionally, improvements have been made in the independent use of the three components to achieve full functional conversion, including direct combustion, and to allow for more thorough utilization (Figure 1). Fibers derived from plant wastes, particularly agricultural residues, may therefore be a viable substitute for wood pulp (Tseng *et al*., 2022).

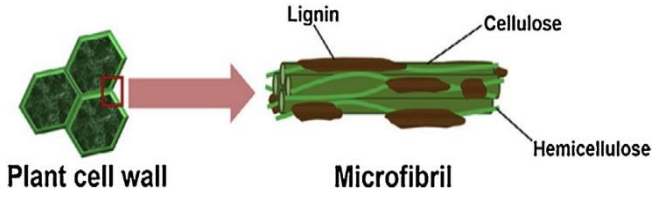

Figure 1. Composition of the plant cell wall in lignocellulosic (Bahreini, 2022).

Tea is grown year-round in small and large gardens in the southern and southwestern wooded hills, where an elevation of 2,100 meters is ideal. Domestic use accounts for more than half of the 7000 tons produced annually, and most of the tea that is exported is black tea. Tea plants were introduced to Ethiopia in 1927 due to their increasing popularity, but the industry has faced difficulties over the years. Although more land was allocated for tea production in 2020, production did not keep pace (Dechassa & Merga, 2022).

1.2. Classification of Cellulose

Cellulose can be classified in various ways, according to its substrate specificities, reaction mechanisms, structural similarities, or sizes. Cellulose can be categorized into two types based on size: microcellulose and nanocellulose. The latter is further sub-classified into three types, based on size, namely nano- or micro-fibrillated cellulose (MFC), nanocrystalline cellulose (NCC), and bacterial nanocellulose (BNC) (Borhana *et al.*, 2021).

The size range of nanocellulose is 5 nm to 100 nm. The difference between nano-fibrillated cellulose (NFC) and micro-fibrillated cellulose (MFC) is that MFC is usually produced by chemical treatment, while NFC is usually produced by chemical pretreatment followed by high-pressure homogenization. MFC or NFC can be found in wood, sugar beetroot, hemp, flax, and potato tubers. 20–50 nm is the average diameter. Equally, nanocrystalline cellulose usually measures 100 nm in length and 5–70 nm in diameter. Numerous things, including bacteria, algae, plants (wood, cotton, hemp, flax, wheat straw, mulberry bark, ramie, and tunicin), microorganisms, and animals (tunicates), can cause NCC (Trache *et al*., 2016).

Bacterial nanocellulose is another form of nanocellulose that can be made from non-plant sources. The engagement of microorganisms in the biopolymer sector is essential because of their quick development, which enables high yields and year-round product availability. Microorganisms can be used to produce BNC primarily in two ways: static culture and stirred culture. A thick, leather-like white BNC pellicle that accumulates at the air-liquid contact is used in static culture. The agitated culture combines. The cellulose is synthesized by the agitated culture and disseminated throughout the culture media, resulting in irregular pellets or suspended fibers (Foroughi *et al*., 2021). It is preferable to produce bacterial cellulose through static culture because earlier research has shown that bacterial cellulose from a static culture has higher mechanical strength and yield than that from an

agitated culture. Additionally, microbial mutations, which are more likely to happen in an agitated culture, may hinder the production of BNC. Static cultures have the drawback of requiring more space and time to develop. Plants, bacteria, algae, and other substances can all produce cellulose. In the primary cell wall of oomycetes, many kinds of algae, and green plants, BNC plays a critical structural role. Reports state that the degree of polymerization in cellulose varies between 250 and 10,000 glucosyl units. Copolymers, which are polymers made up of two or more different monomers, can generally show both moderate and high levels of polymerization (Foroughi *et al*., 2021).

1.3. Cellulose Extraction Techniques

There are some types of cellulose production techniques, such as chemical treatment, mechanical treatment, a combination of chemo-mechanical processes, and bacterial production of cellulose, and the synthesized microcrystal and nanocrystal cellulose produced from cellulose (Figure 2).

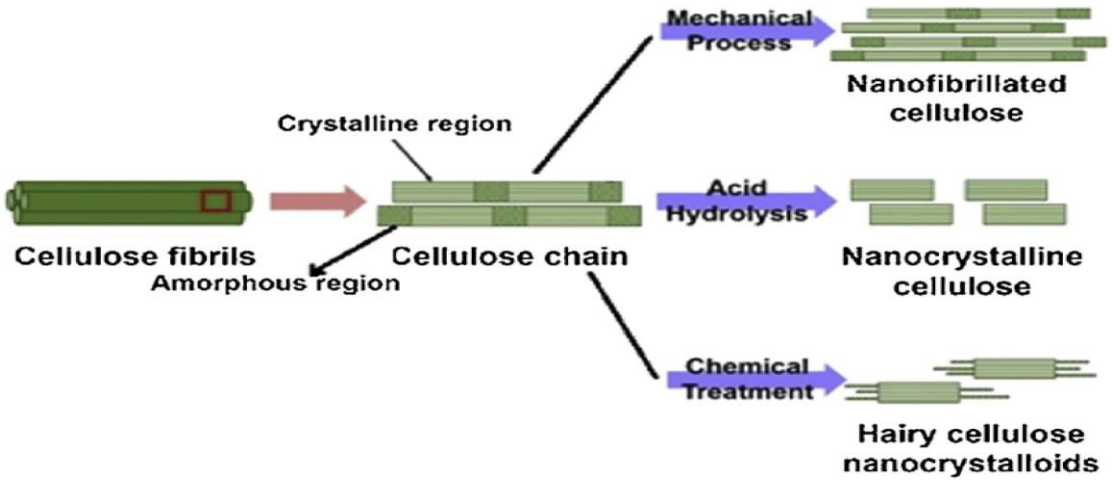

Figure 2. Extraction of Cellulose from Lignocellulosic biomass (Omran *et al*., 2021).

1.3.1. Mechanical Extraction

One method of mechanical extraction is high-pressure homogenization. High-pressure homogenization, a technique used for large-scale nanocellulose production, involves forcing the material down an incredibly small channel or orifice using a piston and high pressure (between 50 and 2000 MPa). The processes of high-pressure homogenization, grinding, crushing, and steam explosion are all part of mechanical cellulose extraction. This is a nanocellulose isolation technique that is safe

for the environment. On the other hand, employing this approach carries the risk of mechanical damage to the crystalline structure. Grinding is another mechanical method, and by spinning grindstones at a speed of about 1500 rpm, shear stress is applied to the fiber in the process of grinding, which separates nanocellulose from fiber (Bacakova *et al*., 2019). Water evaporation occurs as a result of the heat generated by friction during the fibrillation process, enhancing the extraction procedure. Furthermore, cellulose fiber is also extracted by crushing, and in cold environments, microcellulose is produced using this technique. The cellulose that is generated has a size that falls between 0.1 and 1μm. To produce nanocellulose, this procedure can be employed as a pretreatment before high-pressure homogenization. The extraction of cellulose is accomplished by steam explosion, which is a low-energy approach. It might be regarded as a pretreatment even though lignin is not entirely removed. The fiber obtained after using this procedure requires mechanical modification (Alemdar & Sain, 2008).

1.3.2. Chemical Extraction

Chemical extraction methods include degumming, chemical retting, alkali treatment, and acid soaking. These treatments also affect other components of the fiber microstructure, such as hemicellulose, pectin, and other non-cellulosic components. One use of the chemical extraction process is alkali or acid retting. Although mechanical extraction is less costly, fibers are less damaged when using this extraction method (Jamshaid *et al*., 2017). After being cleaned and heated, the fiber is soaked in an alkaline or acidic solution. This method can improve some fiber properties. By eliminating the pectin and gummy substance, degumming is one of the chemical extraction methods intended to maintain the shape of ramie fiber. Another chemical process is chemical retting. Fibers contain less lignin and water as a result of this process. While chemical retting can remove more lignin, it is less effective at removing moisture than alkali and acid retting. Combining chemical and mechanical extraction methods can guarantee a higher lignin removal efficiency; mechanical processes are frequently performed after chemical treatment (Kumar *et al*., 2006).

1.3.3. Bacterial Production of Cellulose

Apart from originating from plants, certain bacteria belonging to the genera Acetobacter, Pseudomonas, Agrobacterium, Alcaligenes, Rhizobium, or Sarcina can also manufacture cellulose

fibers by extracellular biosynthesis. According to this viewpoint, Acetobacter xylinum (Gluconacetobacter xylinus), a Gram-negative strain of acetic acid-producing bacteria, is the most effective source of bacterial cellulose (Sharma *et al*., 2019). Cellulose biosynthesis produces bacterial cellulose, which is then extracted as ribbon-shaped fibrils that are less than 100 nm wide and as fine as 2-4 nm long. These bacterial cellulose microfibrils will accumulate in the extracellular medium. In contrast, nanocellulose can be obtained by mechanical or chemo-mechanical means. Similar to cellulose microbially derived from plants, BNC microfibrils in CNC can also be converted into bacterial nanocrystals through an acid hydrolysis process (Liang *et al*., 2023).

1.4. Microcrystalline cellulose

The pure, partially depolymerized cellulose with the formula (C6H10O5) n is known as MCC. Alpha cellulose is treated with mineral acids to prepare it. This polysaccharide polymer is made up of linear chains of β-1,4-d-glucopyranosyl units that link several hundred to over ten thousand β (1 → 4) linked D-glucose units (Figure 3). The flexible material utilized in the fabrication of MCC is pulp generated from fibrous plants, like coniferous wood. Another potential source of cellulose for MCC is cotton. Wood is a significant source of pharmaceutical-grade MCC, requiring a high-quality pulp. Such a hardwood source has layers of cellulose chains that are securely bound together by cross-linking polymer lignin's strong hydrogen bonds (Kale *et al*., 2018). Hardwoods (deciduous broad leaves) and softwoods (evergreen conifers) can be utilized for that purpose. These woods vary not only in terms of their chemical makeup, which includes the amounts of cellulose, hemicellulose, and lignin. However, also in terms of their structural arrangement, or the parts that are comparatively more crystalline or amorphous. Acid hydrolysis of the amorphous parts is more likely to yield shorter, more crystalline fragments, like the MCC (Yohana *et al*., 2019).

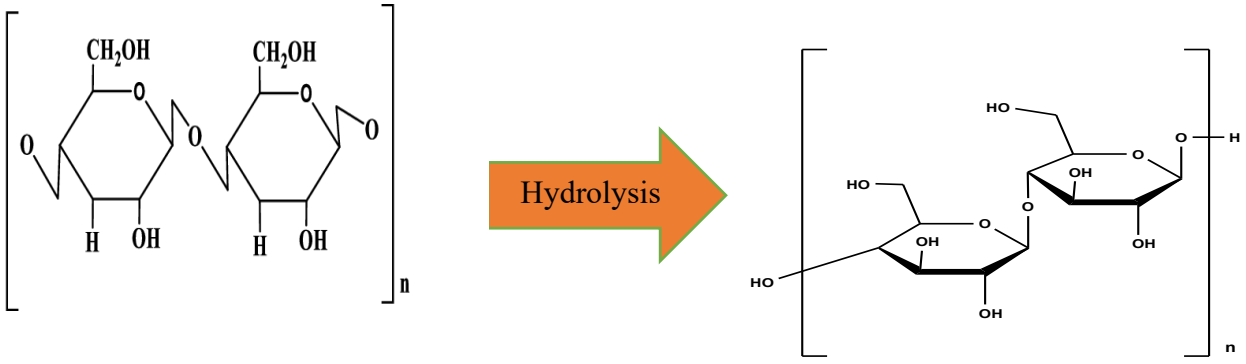

Figure 3. Chemical structure of Cellulose and Microcrystalline cellulose (Kale *et al.,* 2018).

1.4.1. Microcrystalline cellulose preparation techniques

Highly pure MCC has been extracted from plant cell walls using an assortment of techniques, including radiation-enzymatic, steam explosion, extrusion, and hydrolysis with acids and alkalis. Depending on the type and age of the plant, different natural sources may have varying amounts of cellulose. The natural bio-composite known as lignocellulosic is made up of nanoscale domains of cellulose, hemicellulose, lignin, and extractives. From a technological standpoint, determining the amount of lignin is essential to efficiently optimizing the pretreatment process needed to isolate pure cellulose pulp. It is believed that the most challenging chemical to extract from lignocellulosic materials is lignin. These procedures are frequently used as a pretreatment to speed up the hydrolysis process that produces MCC (Haafiz *et al*., 2014).

The raw lignocellulose is subjected to two stages of steam treatment. The first step involves removing the steam-treated lignocellulose to recover cellulose with a low degree of polymerization. In the second step, a strong mineral acid is impregnated into the cellulose to hydrolyze it into MCC. The crystalline domains that are more resistant to acid assault stay mostly intact when exposed to acidic solutions, while the para-crystalline or amorphous regions preferentially cleave. This was investigated using HCl or H2SO4, and the impact of the acid on the characteristics of the generated MCC was looked at (Yildirim & Candan, 2020). They demonstrated that the type of acid used did not affect the crystallinity or size of the crystallites. The laser diffraction particle size analyzer showed that the composition of the acid can affect the MCC particle size, contingent on the natural sources utilized. After H2SO4 hydrolyzed the bagasse-MCC, the thermal analysis revealed good thermal stability. Another study, which was based on the hydrolysis approach using 1-2.5 M HCl at 105 °C, employed a variety of pulping techniques to produce MCC from cotton, flux, and various wood species (both soft and hardwood). When sulfuric or hydrochloric acid is present, various hydrolysis processes can generate high-grade MCC at temperatures as high as 160°C (Andersson, 2006).

In the field of biotechnology, alkaline hydrogen peroxide (AHP) pretreatment has been employed for cellulose saccharification and bioethanol production, among other applications. MCC was prepared using an AHP-pretreated sample, and its potential for application in bio-composites was further characterized. Consequently, by examining the morphological changes, spectra, crystalline behavior, and thermal characteristics of the isolated MCC, the impact of the alkaline hydrogen peroxide

pretreatment was ascertained. Additionally, it has been documented that raw cellulose is treated with 14-20% sodium hydroxide in a process known as steeping, which utilizes alkaline solutions. This method is used in the manufacturing of cellulose derivatives and viscose cellulose. After treatment, the cellulose is pressed to extract the majority of the sodium hydroxide (Kharismi *et al*., 2018).

The pressed cellulose is then broken down, aged, and subjected to carbon disulfide to produce viscose cellulose. However, alkaline treatment of cellulose has not been used for manufacturing MCC. Current methods for MCC production involve acidic hydrolysis of the amorphous cellulose part, followed by separation of the crystalline portion. MCC can also be created using pressurized steam at temperatures ranging from 180 to 350°C. While acid should not be used at high temperatures, safety concerns remain related to the application of high pressure and temperature. The process for manufacturing MCC involves enzymatic hydrolysis to produce cellulose with high crystallinity. Although a high-temperature and pressure environment is not necessary, the process requires a reaction time of 24-48 hours, which may not be practical for commercial purposes. The amorphous (fibrous) regions of the purified cellulose are removed using established techniques. Natural cellulose material will swell when treated with aqueous sodium hydroxide, with the extent of swelling influenced by factors such as temperature, treatment duration, caustic concentration, fiber tension, and assembly parameters swelling occurs (Sergejs Trusovs and Northridge, 2002).

1.4.2. Characterization of microcrystalline cellulose

Many researchers have investigated the structure and properties of MCC using a range of complementary techniques. These investigations include, for instance, FTIR, 13C NMR, X-ray diffraction, thermal analysis, and electron microscopy techniques (Demirayak, 2016).

One of the most popular spectroscopic methods for studying polymers is infrared spectroscopy. The method offers various sampling approaches that are both sensitive and quick, while the instrumentation remains reasonably priced. A compound's most distinctive physical characteristic is most likely its infrared absorption spectrum, which is sometimes referred to as a molecule's fingerprint. The method was initially used as a tool for the identification of reasonably pure compounds. For a variety of uses, the most often utilized range was the mid-infrared area, which is located between 4000 and 400 cm -1 (Kačuráková & Wilson, 2001).

FTIR involved standard tasks, including interpreting infrared carbohydrate data. They are, however, essentially restricted to a few numbers of monomers as well as the polymers starch and cellulose. Nonetheless, a broad range of carbohydrates, including commercial sugars, starch, cellulose, pectin, carrageenans, hemicelluloses, hyaluronates, etc., and their low molecular weight models, are being used in biochemical, biological, and food industry applications (Owolabi *et al*., 2016).

Based on their atomic structure, crystalline solids can be identified using XRD. Because the wavelengths of X-rays are in the order of a few angstroms, which is about equivalent to the interatomic distances in crystalline solids, diffraction occurs. A crystalline solid's diffraction pattern can be created using a diffractometer (Ouwmeester, 2015). X-ray beams are reflected off the parallel atomic layers within a molecule over a variety of diffraction angles during this XRD examination. There is a possibility of constructive or destructive interference because the X-ray beam only has one particular wavelength (Adeleye *et al*., 2022). When the reflected rays are in phase (constructive interference), a diffractogram displays a peak at particular angles. The molecule or chemical combination can be identified using the diffraction pattern. X-ray diffraction can be used to identify crystalline materials based on their atomic-scale structure. XRD is a versatile, nondestructive technique that offers thorough information about the chemical composition and crystalline structure of both natural and synthetic materials. X-ray crystallography is used to create unparalleled high-resolution structures of biomolecules and complexes from the solid phase (Kian *et al*., 2017).

High-resolution images of a sample's surface can be obtained using scanning electron microscopy. Scanning electron microscopy images are useful for determining the surface structure of the subject because of their distinctive three-dimensional appearance, which is a result of the technique used to create them. In a SEM, electrons can be thermionically radiated or released by field emission from a tungsten or lanthanum hexaboride cathode, and they can then be accelerated in a vacuum towards an anode (Adeleye *et al*., 2022). Electromagnetic deflection coils, an objective lens, and electromagnetic condenser lenses are utilized to scan the sample's surface with the electron beam. The main imaging technique involves gathering low-energy secondary electrons that the sample's surface releases (Picker & Hoag, 2002). The electrons are detected by a scintillation material that produces light flashes from the secondary electrons. The light flashes are then detected and amplified using a photomultiplier tube. A transmission electron microscope's resolution is usually orders of magnitude higher than a scanning

electron microscope. However, because the latter relies on surface processes rather than transmission, it can image large samples and has a much larger depth of view, resulting in images that faithfully capture the three-dimensional structure of the sample (Kian *et al.*, 2017).

To produce 5-hydroxymethyl furfural and levulinic acid, which are desirable precursors for catalytic conversion into chemicals and hydrocarbon fuels, MCC is also utilized in the production of glucose. The method of determining a material's thermal behavior under different circumstances is called thermal analysis. The temperature at which a thermal standstill occurs is another way that thermal analysis identifies a material's changes. Clarification of the excipients' stability, compatibility, and phase transition was further aided by TGA and DSC studies. In the literature that describes thermogravimetric analysis, differential thermal analysis, and differential scanning calorimetry were used to examine the thermal behavior of MCC. These were utilized to aid in the comprehension of potential chemical reactions leading to the depolymerization of MCC (Haji Badri, 2016).

The glass transition temperature (Tg), which separates amorphous and semicrystalline polymers like MCC, is the critical temperature at which a polymer's material characteristics significantly change. Therefore, knowing the Tg is essential for characterizing MCC and determining the Tg of MCC using differential scanning calorimetry at standard heating rates. found that dry cellulose had a Tg of 230°C, which decreased with increasing water content. Although cellulose has been extensively studied, the nature of the glass transition of MCC has not yet been completely characterized because the amorphous areas only comprise 30% of the overall material (Picker & Hoag, 2002).

The higher signal dispersion of ^{13}C NMR allowed for the resolution of the matrix polysaccharides. Through changes in the intensity of specific 13C NMR signals, cross-polarization NMR studies allow for the indirect determination of proton NMR parameters by combining the best features of both nuclei. the extensive application of cross-polarization NMR, which was recently used to evaluate the amount of cellulose present in the primary cell walls of plants. Since nuclear spin relaxation processes can be sensitive to molecular dynamics, the corresponding temporal constants provide helpful criteria for differentiating between mobile and immobile elements in cell walls, such as nanocrystalline (amorphous) and crystalline domains (Khili *et al*., 2019). The intermediate states are referred to as mesomorph domains or para-crystalline isolation of cell walls. Nuclear magnetization is altered during each relaxation step, moving from a disturbed state to an equilibrium state. The processes are

complicated by spin diffusion, which is the transfer of spin information between nearby nucleus pairs. Millisecond time intervals can be used to transfer proton spin data over nanoscale dimensions. Therefore, the experimental values of proton spin relaxation time constants reflect mean values for protons inside a specified volume, irrespective of the ^{13}C signal used to monitor proton relaxation. Different carbon atoms inside a molecule may have different experimental values observed because ^{I3}C spins scatter over a longer time (Newman *et al*., 1996).

1.4.3. MCC as a pharmaceutical excipient

A pharmaceutical excipient is a material that is added to a drug formulation in addition to the active pharmaceutical ingredient (API) to help with the drug's production, stability, delivery, or patient acceptability. It basically refers to anything in a drug that isn't the actual drug. As tableting technology advances, excipients must have high weight consistency and superior compressibility. Disintegrants, lubricants, glidants, antiadhesives, and fillers (also known as diluents) are the primary excipients. Colorants, flavors, sweeteners, coating agents, plasticizers, wetting agents, buffers, and adsorbents are examples of secondary excipients. Even when used infrequently, direct compression binders maintain their effectiveness and provide better tablet properties. Certain diluents, like microcrystalline cellulose, enhance the compression mix's tablet ability or compatibility, which qualifies them for use in medication formulation. Certain diluents, such as microcrystalline cellulose, improve the compatibility or tablet-forming ability of the compression mix, making them suitable as dry binders as well (Shlieout *et al*., 2002)

MCC is widely regarded as the diluent with the best binding properties and is also one of the most trusted DC binders. MCC is used as a binder/diluent in the preparation of oral tablets and capsules, and for the wet granulation and direct compression techniques. Due to the small particles, MCC provides some lubricant and disintegrant properties, which are advantageous in direct tableting. Small quantities of MCC bind efficiently with other materials, especially poorly water-soluble MCC is complemented by a high dilution potential, which is the best in MCC. The broad range of particle sizes provides optimum packing density and coverage of other materials (Demirayak, 2016).

The most used direct compression excipient is still MCC, which is also a great excipient. It can be used as a lubricant, absorbent, filler or diluent, anti-adherent, strong dry binder, and tablet disintegrant.

MCC is generally thought to be the diluent with the best binding properties and is one of the suggested direct compression binders. It functions as a binder/diluent in formulations for oral tablets and capsules that use both wet granulation and direct compression processes. It also has some lubricating and dissolving properties that are useful for direct tableting (Yohana Chaerunisaa *et al*., 2019).

MCCs can effectively bind other materials in small amounts, particularly active pharmacological compounds that don't work well as tablets. While the wide variety of particle sizes allows for the best possible packing density and covering of other materials, MCC has a high potential for dilution (Krivokapić *et al*., 2020). Among the others, MCC has been the most favored diluent due to its low bulk density. An excipient with a wide particle size distribution, ideal packing density, and high dilution potential on a weight basis will cover a medication and other excipient components. MCC is offered for sale in a variety of particle sizes, densities, and moisture grades, each with unique qualities and uses. The grades Avicel pH 101 and pH 102 are the most noticeable. The term pH refers to MCC's pharmaceutical-grade product, with the original grade being called Avicel pH 101. Although pH 102 is available as a partially agglomerated product, it offers slightly improved fluidity and a larger particle size distribution. There is no discernible change in the compressibility between the two grades (Landín *et al*., 1993).

1.4.4. Tea waste as a source of MCC

The tea leaf, also known by its botanical name, Camellia sinensis, is a tiny, native Asian evergreen shrub that grows to a height of three to six feet. Based on data from the Food and Agriculture Organization of the United Nations (FAO), the production of tea worldwide increased to 5.07 million tons in 2013. After the tea leaves are chopped off and dried, a waste product known as tea leaf waste fibre (TLWF) is removed. Tea leaf waste fibre is created in large quantities during industrial production when tea is extracted for beverages and instant tea. The negative environmental effects of disposing of tea waste can be reduced by finding more uses for it in various industries as an inexpensive source of biomass. For this reason, maximizing the TLW's residual value is essential. Even though tea leaves have many industrial applications, little research has been done on the characteristics or isolation of cellulose from TLW (Rahman *et al.*, 2017).

MCC is made of local agricultural residues (bagasse, rice straw, cotton stalks, and bleached pulps). Because wood and cotton are the main industrial sources for cellulosic fibers, they serve as primary feedstock in MCC production. Then, it is not easy to provide all sectors with the right amount of wood and cotton at a competitive price due to the competition among many other applications (furniture, pulp and paper industry, building products) connected with water vapor or in direct competition (combustion of wood for energy, textile for the use of cotton). In addition, not all areas have access to cotton or wood; therefore, non-woody cellulose is the only alternative. Consequently, there has been a great deal of interest sparked by the study of various sources, including aquatic plants, herbaceous plants, grass, crops, and their byproducts. Compared to wood, these non-woody plants often have less lignin. Bleaching techniques, therefore, require less energy and chemicals (Trache *et al*., 2016).

As per recent statistics, the globe generates approximately 6.3 million tons of tea waste each year, and this amount is predicted to grow in the coming years with the global consumption of tea rising to 7.4 million tons (Azum et al., 2021). Reportedly, Azum *et al.* have conducted for MCC extraction from various biomass sources by using different chemical methods. Prepared MCC from tea waste through water boiling, grinding, alkaline, and bleaching ($NaClO_2/HCl/H_2O_2$) before the hydrolysis process with hydrochloric acid (Tseng *et al*., 2022).

Tea waste (TW) is made up of cellulose, hemicellulose, and lignin from lignocellulosic material. Cellulose (16–30%), hemicelluloses (68.2%), and lignin (18.8%) were found in waste tea. Tea trash can be used to produce crystalline cellulose derivatives due to its high cellulose concentration. Both hemicellulose and lignin are also amorphous polymers, whereas cellulose is a semicrystalline polymer occurring in nature. The hydroxyl of the inner monosaccharide of lignin and carbohydrates in pulp are combined on ether, the hydroxyl of lignin and carboxyl in uranic acid during hemicellulose is bonded on ester. These are the two binding manners between carbohydrate units and lignin. The alkaline-resistant property of the first linkage is significantly lower than that of the second or subsequent linkages (Rahman *et al*., 2017).

Tea factory waste has been working as a raw material for the synthesis of cellulose nanocrystals and microcrystals, which have been successfully applied as a strengthening in polymer composites. Studies have shown that MCC isolated from oolong tea processing waste retains its inherent thermal stability and cellulose structure. Moreover, black tea waste has been reported to contain a relatively

high cellulose content of approximately 28.3%, making it a promising feedstock for cellulose nanocrystal production. Overall, tea waste represents a cellulose-rich, readily available, and abundant biomass that can be effectively applied for the production of value-added MCC (Debnath *et al*., 2023).

Ethiopia produced 7,400 tons of tea in 2013 compared to 15 tons in 1976. Nevertheless, tea is currently grown on just 3,099 hectares of the more than 150,000 hectares of arable land. After water, tea is the most popular beverage worldwide. Around 7.3 billion kilograms of tea were consumed worldwide in 2023 (Dechassa & Merga, 2022). According to a recent study, tea is one of the most popular drinks in the world, with 6.3 million tons used globally as of right now and an anticipated increase to 7.4 million tons by 2025. With the significant increase in tea consumption, there has been a corresponding rise in the production of industrial tea waste. This results in the underutilization of valuable agricultural resources and contributes to environmental degradation. Around 5 million tons of tea waste are produced annually worldwide. This includes waste tea leaves, buds, and pruned stems (Kumar *et al.*, 2006).

1.4.5. Application of Tea waste for pharmaceuticals

Drug delivery, tissue engineering, wound dressing, pharmaceutical excipients, biosensors, and medical devices are among the pharmaceutical fields (Trache *et al*., 2016). Due to their high lignin concentration and low inorganic content, wastes from the tea business must be utilized efficiently through scientifically advanced procedures. It is crucial to address these waste utilization and management challenges in a manner that aligns with sustainable practices and innovative solutions to ensure industrial advancement and environmental protection. Describe in detail one such technology that uses tea trash to its full potential, with ease of use. Potential health benefits of catechin-based capsules: consumers can now reap the benefits of catechins without having to drink numerous cups of green tea. This meets the growing need in our daily lives for supplements high in antioxidants. The liquefiable carbon source offers innovative methods for pharmaceutical applications that improve the future of medicine (Chowdhury *et al*., 2016).

The ability of the created carbon quantum dots to sense dangerous pollutants in water bodies is currently being investigated. Based on these discoveries, the research team has filed several patents. By bringing intelligence to product packaging, micro and nano-crystalline cellulose designed for

intelligent packaging meets the changing needs of contemporary industries and customers. A sustainable method of managing these wastes that helped strengthen the circular economy. The vast volume of tea waste is used for the creation of inexpensive adsorbents, which lowers the costs associated with treating wastewater and water (Sikdar *et al*., 2020).

1.5. Direct compression method of tablet formulation

Direct compression is a popular and extensively utilized tableting technique in the pharmaceutical industry due to its cost-effectiveness, speed, and efficiency. The most effective way to make tablets is by direct compression, which involves the fewest steps in the production process. This approach is good for handling water-sensitive active components and has lower capital and energy costs in addition to its straightforward process (Kamlesh, 2012). This includes the used filler-binder, also known as the direct compression excipient. It significantly impacts the processability of the formulation and the overall characteristics of the finished tablet, including hardness, disintegration, and dissolution of the powders. Several issues with direct compression, including poor flowability, uneven tablet weight, inadequate tablet strength, lack of content uniformity or segregation, and dissolving failure, can arise from the use of improperly specified or poorly managed raw materials. Therefore, choosing the right excipient and ensuring that it improves the formulation's performance, quality, and consistency is essential to the success of direct compression (Kokott *et al*., 2021).

Additional direct-compression fillers are now available for purchase, including Avice (microcrystalline cellulose), which was the first effective dry binder, and filler starch, a partially pregelatinized starch that maintains its disintegrant properties while offering improved flowability and compressibility compared to regular starch. The direct-compression revolution began with spray-dried lactose, which was the first of these vehicles. A dicalcium phosphate that flows freely and can be compressed, several sugars that can be directly compressed, including different kinds of sorbitol and mannitol (Kamlesh, 2012). The low compressibility characteristics of spray-dried lactose have been improved by increasing the agglomeration of the smaller crystals, thereby solving browning problems caused by contaminants present in the mother liquors. This paralleled important innovations in tablet press technology, such as accurate positive die feeding and precompression stages, which now possible to achieve direct compression tableting. The bulk of tablets that were produced could now be compressed directly, thanks to the availability of excipients and equipment by the early 1980s.

It's critical to comprehend why this hasn't happened (Bandelin, 1999). Aspirin is a marketable example of a direct compression tablet granulation equipped with the dry granulation technique. The literature review indicates that tablets of many low-dose drugs, such as paracetamol, ibuprofen, felodipine, diazepam, and nitroglycerin, have been prepared by direct compression (Shwetha *et al*., 2019).

1.6. Paracetamol and Its Physicochemical Properties

Paracetamol (acetaminophen) is a commonly used analgesic and antipyretic medication well-defined by a collection of physicochemical properties that strongly determine its formulation, stability, and biological performance. With a pKa of around 9.5, it is a to some extent acidic molecule that is mainly unionized at physiological pH. Regardless of its limited water solubility, this unionized form helps explain its comparatively robust membrane permeability. As a result of endothermic dissolution, paracetamol's limited aqueous solubility rises with temperature. Its solubility can also be enhanced through co-solvents, pH alteration (within stability limits), or solid-state manufacturing procedures such as creating cocrystals or amorphous dispersions (Ogemdi, 2019).

From a solid-state standpoint, paracetamol exists in numerous polymorphic forms, with Form I being the commercially relevant stable form. Although it is more difficult to make consistently, Form II is metastable and provides superior compressibility, which may improve tablet ability. The crystalline nature of Form I results in slightly poor compaction qualities, typically needing excipient. With a melting point of 168–170 °C, paracetamol is susceptible to thermal deterioration at high temperatures, resulting in the formation of colored contaminants through oxidation and breakdown. However, it is usually stable in neutral aqueous settings; it is also vulnerable to hydrolysis in extremely acidic or basic conditions. With its combination of high permeability (BCS Class I), moderate solubility, and chemical stability under suitable formulation conditions, paracetamol remains one of the most adaptable and extensively formulated active pharmaceutical ingredients (Edrees *et al*., 2017).

Paracetamol is chosen as a model drug in direct compression because it is well-studied, safe, and analytically convenient, yet poses realistic formulation challenges due to its poor compressibility and flow properties. This makes it an excellent representative compound for testing and optimizing direct compression processes. It is also readily available in the market currently and serves as a raw material for the pharmaceutical industry. Because of its poor compressibility, it’s often used to test the

performance of new excipients, co-processed materials, or powder flow improvers in direct compression formulations (Gawshinde *et al*., 2024).

1.7. Statement of the problem

First, successfully isolating and characterizing microcrystalline cellulose from tea waste involves overcoming technical challenges related to extraction methods, purification techniques, and analyzing the final product. Tackling these issues is crucial to ensure consistent and reliable results, which are essential for its potential use in pharmaceuticals as a directly compressible excipient and for stabilizing emulsion drug formulations.

The availability of high-quality, affordable excipients is a major concern in the pharmaceutical industry, especially in Ethiopia. Consequently, the shortage of suitable excipients hampers the development of locally tailored pharmaceutical formulations and can lead to reliance on imported materials, which are often expensive and may not meet the specific needs of the Ethiopian pharmaceutical market. Additionally, utilizing agricultural waste such as tea waste to produce pharmaceutical excipients presents an opportunity to address environmental and waste management challenges. However, the feasibility and technical practicality of this method must be carefully examined to ensure the final product complies with the necessary quality standards for pharmaceutical use (Dechassa & Merga, 2022).

The problem statement highlights the need to address the challenges of sourcing affordable excipients locally and the potential benefits of utilizing agricultural waste for pharmaceutical applications from an Ethiopian perspective. By clarifying these issues, this study hopes to help find a long-term, locally appropriate solution to these problems and open the door for improvements in Ethiopia's agricultural and pharmaceutical industries.

1.8. Significance of the study

Firstly, Ethiopia is one of the leading producers of tea in Africa, and thus, the generation of tea waste is substantial. By repurposing this waste into a valuable pharmaceutical excipient, this research contributes to sustainable waste management and aligns with global and local efforts towards environmental sustainability and waste reduction. This could positively impact the tea industry in

Ethiopia, paving the way for innovative waste utilization practices and potentially opening new revenue streams for tea producers.

Moreover, the pharmaceutical industry in Ethiopia, like in many developing nations, often faces challenges related to the cost and availability of high-quality excipients for drug formulation. By exploring the potential of microcrystalline cellulose from a readily available source, this study would have the potential to contribute to the local pharmaceutical industry by providing a cost-effective and locally sourced excipient. Furthermore, the research could potentially spur interest and investment in the utilization of other agricultural and industrial waste products for pharmaceutical and other industrial applications, fostering innovation and economic growth within the country (Dechassa & Merga, 2022).

This work advances science by converting a low-value agricultural waste (tea waste) into a high-value pharmaceutical excipient (microcrystalline cellulose), demonstrating its suitability for direct compression tablet formulation. It supports sustainable excipient development, broadens the knowledge base of cellulose sources, and promotes environmentally friendly approaches in pharmaceutical manufacturing.

In summary, this study would have the potential to not only address environmental concerns and contribute to sustainable waste management but also to positively impact the pharmaceutical industry and health care accessibility in Ethiopia. It could pave the way for a more sustainable and cost-effective approach to pharmaceutical production and contribute to the broader goal of promoting economic growth and innovation within the country. Therefore, the current work efforts to address the following research questions

- What are the cellulose and microcrystalline cellulose yields of tea (fiber and leaves)
- What are the physicochemical characterization parameters of the MCC that is extracted from tea waste
- What physicochemical evaluation parameters are essential to determine the quality of tablets prepared by direct compression
- Does tea waste MCC compare favourably to commercial MCC

1.9. Objectives of the study

1.9.1. General objective

To prepare, characterize, and formulate MCC from tea waste and evaluate it as a direct compressible excipient

1.9.2. Specific objectives

- To isolate Cellulose & Microcrystalline cellulose from tea waste
- To Characterize Cellulose & MCC from tea waste
- To formulate tablets using tea waste MCC as a directly compressible excipient
- To evaluate the physicochemical parameters of the prepared paracetamol tablets and compare them with commercial products.

2. EXPERIMENTAL

2.1. Materials

Tea (*Camellia sinensis*) byproducts and stalks were collected from local tea manufacturer Ethio Agricefts and East African agri-business PLC. Two plant parts were collected from two selected companies. The site is located in Bonga in the southwest region (East African agri-business PLC) and Dukem around the Oromia region (Ethio Agricefts).

2.2. Chemicals and solvents

Ammonium Hydroxide solution (28%) (Sigma-Aldrich, Germany), Hydrochloric acid (37%) (Surechem products Ltd, England), Sodium chlorite 5% (Surechem products Ltd, England), Hydrogen per- oxide (50%, V/V) (CICAMCF, Ethiopia), Formic acid (99%), (Surechem products Ltd, England),), Acetic acid (99.5%) (Neolab Pvt. Ltd) and ethanol (95%, v/v), Distal water and Sodium hydroxide (Loba Chemie Pvt. Ltd.,, India), Zinc chloride (Merck chemicals), Potassium iodide (BDH Chemical Pvt. Ltd), Iodine (Sigma-Aldrich, Germany), Potassium bromide (Sigma-Aldrich, Germany), Acetone (Surechem products Ltd, England), Toluene (VWR lab products Pvt. Ltd) was obtained from Armauer Hansen Research Institute (AHRI), EPHI and the rest was purchased from local market. Excipients used in the formulation of paracetamol (Anqiu Lu'an, China) included microcrystalline cellulose (Sigma Aldrich, Germany), Magnesium stearate (Sigma Aldrich, Netherlands), sodium starch glycolate (SBF Pharma, India), and purified talc (Sigma-Aldrich, Netherlands).

2.3. Hemicellulose, Lignin, and Extractives in biomass determination

The amounts of the three lignocellulosic material components (Extractives in biomass, hemicellulose, and lignin) in tea leaf and tea fiber waste were determined using the Mansor *et al.* 2019 method. Acetone, sodium hydroxide (NaOH 0.5 mol/L), sulfuric acid (98%), and barium chloride solution were the four chemical types used in the experiment (Mansor *et al.*, 2019).

2.3.1. Determination of the amount of extractives in biomasses

60 mL of acetone was added to 1 g of each waste (TLW and TFW) (A). A hot plate was used to keep the temperature at 90°C for two hours. The sample was dried for two hours at 105–110°C in an oven until its weight remained constant (B). The formula used to determine the amount of extractives was Extractives (g) = (A) - (B) (Mansor *et al.,* 2019).

2.3.2. Determination of the amount of hemicellulose in biomasses

1g of each type of tea waste (TLW and TFW) that had been processed to remove extractives (designated as B) was mixed with 150 milliliters of NaOH solution (0.5 mol/L). The mixture was maintained at 80°C for 3.5 hours using a hot plate. After that, deionized water was used to thoroughly wash the sample until no sodium ions (Na+) were left in it. Using pH paper, the presence of Na+ was verified, with a target reading close to 7. After that, the sample was dried in an oven set at a temperature between 105 and 110°C until its weight (C) remained constant. The amount of hemicellulose (g) = (B) – (C) was used to calculate the amount of hemicellulose (Mansor *et al.,* 2019).

2.3.3. Determination of the amount of lignin in biomasses

1 g of each type of tea waste (TLW and TFW), both free of extractives (B), was mixed with 30 mL of 98% sulfuric acid. Using a hot plate to regulate the temperature, the mixture was boiled for one hour at 100 °C after being allowed to sit at room temperature for twenty-four hours. Following boiling, the mixture was filtered, and the solid residue was cleaned with deionized water until the sulphate ions were no longer visible. A 10% barium chloride solution was added to an acidified sample to detect sulphate ions. The absence of a white precipitate indicates the absence of sulphate ions. The sample was then dried in an oven at 105-110°C until a constant weight was achieved (D). The final weight of the residue was recorded as the lignin content, with the amount of lignin (in grams) equal to D (Mansor *et al*., 2019).

2.4. Preparation of cellulose from tea waste

All the tea factories generate large quantities of tea waste, including the discarded leaves, buds, and stems of tea. After washing the fiber and plant waste to remove dust, the tea waste was cut into smaller

pieces and then dried. Then, the tea waste was boiled in distilled water at a ratio of 1:10 seven times to remove soluble components. The resulting tea waste was filtered and dried at 65°C for 3 days, then crushed into powder by a blending machine, as depicted in Figure 4.

Stage one involved alkaline pretreatment with a 10% NaOH concentration, a solid-to-liquid ratio of 1:10, and a water bath (Daihan Scientific, Korea) at 90°C for 1.5 hours. After repeated washing and filtration, the resulting pulp was treated with 2.5% NaOH for 1 hour. The material was then filtered and washed with distilled water, followed by treatment in a water bath (Daihan Scientific, Korea) at 90°C for 1.5 hours using a solution composed of 20% formic acid, 20% acetic acid, and 7.5% hydrogen peroxide in a 2:1:2 ratio. The treatment was carried out at a waste-to-liquor ratio of 1:10, with continuous washing using hot water. Lastly, bleaching was performed using 10% hydrogen peroxide in an alkaline medium of 10% NaOH solution at a 1:10 fiber ratio. The process was primarily carried out at room temperature, followed by heating in a water bath at 70°C for 30 minutes. After repeatedly washing the residue with hot distilled water, it was dried for one day at 60˚C in an oven (Jeio Tech, Korea) until its weight remained constant (Gabriel *et al.,* 2020).

2.5. Preparation of microcrystalline cellulose from the isolated cellulose

An acid hydrolysis procedure was used to extract MCC from cellulose. To hydrolyze the amorphous domains of cellulose fibers and separate the microcrystalline particles, acidic hydrolysis was carried out for 30 minutes at 100 °C in a 2.5 N HCl solution. The mixture was then filtered and neutralized with distilled water. After that, distilled water and 5% NH3OH were used to wash the mixture at room temperature. After that, it was repeatedly cleaned with distilled water until the filtrate was odourless and clear. Finally, the isolated MCC was dried in a dry oven to achieve constant weight and stored in a refrigerator at 4°C (Figure 4). The MCC experiment analysed the effects of four variables: temperature, time of hydrolysis, acid concentration, and yield. The first three are dependent, and the fourth is an independent variable (response) (Zhao *et al*., 2018, Azum *et al*., 2021).

The optimization study was conducted using Design of Experiments (DOE) based on the results of preliminary tests. For clarity, the three process parameters investigated in the optimization study were labelled as A, B, and C, representing temperature, reaction time, and solvent concentration, respectively.

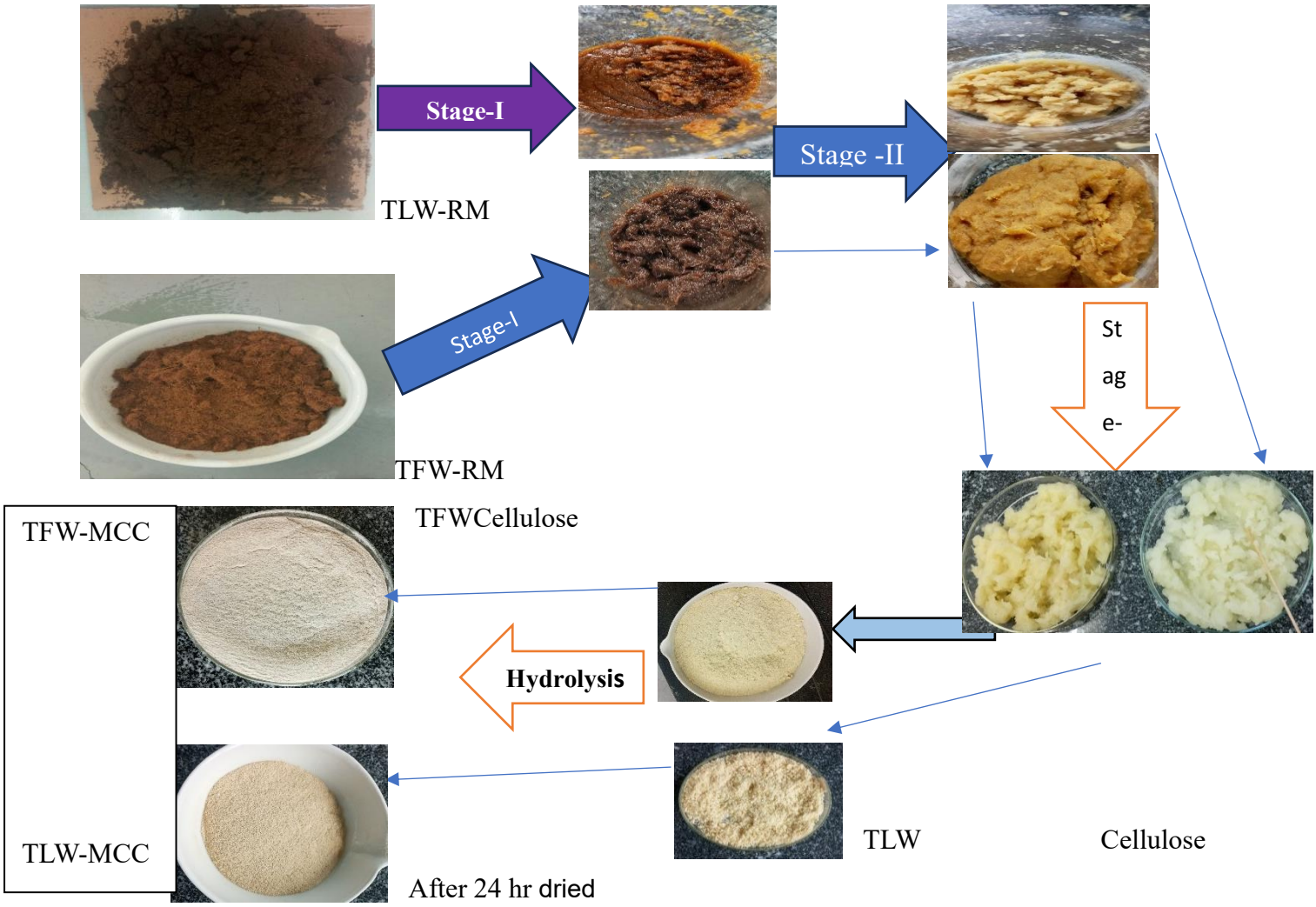

Figure 4. Schematic diagram of the Cellulose and Microcrystalline Cellulose extraction from Tea waste.

2.6. Characterization of Cellulose and Microcrystalline Cellulose

2.6.1. Fourier Transform Infrared

To investigate the modifications in functional groups brought about by different treatments, the FTIR spectra were captured using an attenuated total reflection Fourier transform infrared. Potassium bromide was combined with the dried and ground samples, and the mixture was then compressed into pellets (1-2mg sample and 100-200mg potassium bromide). MCC with KBr for FTIR because KBr is transparent and allows for clear spectra; slight peak shifts do not come from the KBr reaction. The

sample was measured on a Spectrum 65 FT-IR, PerkinElmer (Llantrisant, UK), in the range 4000-400 cm-1, resolution 4 cm-1, number of scans 4 in potassium bromide pellets (Hospodarova *et al*., 2018).

2.6.2. X-ray diffraction (XRD)

X-ray diffraction (XRD-7000S, SHIMADZU, Japan) equipped with Cu Kα radiation in the 2θ range 5 - 55° with a step size of 0.02°, was used under the operational conditions of 40 kV-40 mA. All of the samples were performed with a ramp rate of 2°/min (Kunusa *et al.*, 2018). The Detector instrument, Scintillation detector, and Measurement mode, Continuous scan, had the Crystallinity Index (CrI) calculated using the following formula samples.

$$\text{Crysallinity Index (\%)} = \frac{\text{Total Area of the Crystalline Peaks}}{\text{Total Area of the crystalline and amorphous Peaks}} \times 100 \ldots \text{Eq.1}$$

The d-spacings were calculated using Bragg's equation

$$d=\frac{n\lambda}{2sin\,\theta} \ldots\ldots\ldots \text{Eq.2}$$

where n is an integer; λ is the wavelength of the X-rays, θ is the scattering angle, and d is the distance between the atomic layers (lattice spacing).

The crystallite sizes were calculated from the Scherrer equation as follows:

$$L=\frac{K\lambda}{\beta cos\,\theta} \ldots\ldots\ldots \text{Eq.3}$$

Where k is the Scherrer constant (0.94), β is the FWHM (full-width half maximum) of the lattice plane reflection in radians, L is the size of the crystallite (nm), λ is the X-ray wavelength (0.15418 nm), and θ is the corresponding Bragg angle (reflection angle) (Trache *et al*., 2014).

2.6.3. Thermal analysis

The thermal properties of the cellulose and MCC samples were investigated by Differential Thermal Gravimetry (DTG-60H, SHIMADZU, Japan) on a simultaneous thermal analyzer, with a sample

weighing between 6 and 10 mg. Under nitrogen, each sample was heated from room temperature to 800°C at a rate of 5°C per minute. For every sample, data from TGA and derivative thermo-gravimetric analysis were acquired (Azubuike & Okhamafe, 2012).

2.6.4. Morphological characteristic

The morphological characteristics of cellulose and the MCC at different treatment stages were examined with a scanning electron microscope (JEOL, Japan). The cellulose-water slurry was examined visually for fibrillation. Using scanning electron microscope systems and an accelerating voltage of 20 kV, the morphological analysis of cellulose fibers and microfibrils was carried out (Chen *et al*., 2011).

2.7. Evaluation of physicochemical properties of microcrystalline cellulose powder

Organoleptic properties, such as MCC samples' color, odor, and physical attributes, were assessed and documented in compliance with pharmacopeia guidelines (USP, 2012). After adding 5 g of each sample to a Falcon tube and shaking it with 40 mL of water for 20 minutes, the supernatant solution was centrifuged at pH 5.0–7.5 (Getachew *et al*., 2023).

Water-soluble substances were evaluated using 5g of the sample, which was added, and then shaken for 10 minutes with 80 mL of water using vacuum assistance to pass through filter paper (Whatman No. 42 or equivalent) into a vacuum flask, and the filtrate was transferred to a tared beaker and evaporated until dry without charring. Finally, dry at 105°C for 1 hour, cool in a desiccator, and weigh the acceptance criteria where the weight difference between the residue and the weighed (USP, 2012).

10 g of the sample was placed on a chromatographic column with an internal diameter of about 20 mm, and 50 mL of ether free of peroxide was run across the column to examine ether-soluble substances. Use a fume hood air current to evaporate the eluate to dryness in an evaporating dish that has already been dried and tared. After all of the ether has evaporated, dry the residue at 105° C for 30 minutes, allow it to cool in a desiccator, and then weigh it. Moisture content determination was determined by oven, placing a 1g sample at 105°C for 3 h, and the acceptance criteria were not more than 7.0% (USP, 2012).

Calculation% moisture content $=\frac{W2-W3}{W2-W1}*100$……Eq.4

W1 = weight of empty Petridis in grams

W2 = weight of Petridis + sample before drying in grams

W3 = weight of Petridis + Sample after drying in grams

In another physicochemical quality parameter total ash method, the samples (1g) were weighed into a dry silica crucible of known weight, then incinerated at 450°C in a muffle furnace for 6 hours until free from carbon. The crucible was cooled and weighed, and the percentage of the total ash was calculated using the following equation.

Total Ash value = $\frac{z-x}{y}*100$…… Eq.5

Where X- the weight of the empty crucible, and Y is the weight of the MCC sample taken, and the weight of the crucible + ash (after complete incineration) (Angupale *et al*., 2023).

2.8. Degree of Polymerization

The viscometry method was employed at a temperature of 25°C to calculate the extracted MCC's average degree of polymerization (DP). The MCC sample was dissolved in a 1:100 ratio with dimethyl sulfoxide (SRLchem, India) solvent. The flow time was recorded, and relative viscosity, ηr, was determined based on the recorded flow time using a viscometer (MCR102, Modular Compact Rheometer, Austria). Then, intrinsic viscosity, η, was determined according to the following equation in $cm^3\ g^{-1}$ (Zeleke *et al*., 2022). The result shows an average of three measurements.

$\log[\frac{\eta r-1}{C}] = \log[\eta] + 0.13[\eta]C$…….6

Hence, $\eta = \frac{\eta r}{C}$

Where C is the solution concentration of the sample in g/ml. The average degree of polymerization was then determined from this formula: $DP^{0.905} = 0.75[\eta]$.

2.9. Microcrystalline Cellulose Powder Property Study

Several standard techniques, such as Carr's index, Hausner's ratio, bulk and tapped densities, and the angle of repose, were used to assess the flow characteristics of the individual samples based on USP-30/NF-25 (2022). A funnel with a 10 mm stem diameter was used to measure the angle of repose. The funnel, which was held 10 cm above the bench, was filled with a 25g powder sample and covered with fresh paper. The cone-shaped heap's height (h) and radius (r) were measured in centimeters. The angle was computed as follows:

$\alpha = \tan^{-1}(h/r)$ …… Eq.7 α is the angle of repose.

Bulk Density (ρb) was determined after weighing and pouring the samples (5 g each) into a 25 mL measuring cylinder that was angled 45 degrees to avoid tapping, and the volume was noted. Next, the bulk density was determined (USP, 2022).

$$\rho b = \frac{M}{V} \text{ ……Eq.8}$$

Where ρb - bulk density, m - mass, and v - volume.

Tapped Density (ρt) was determined after weighing and pouring the sample (5 g each) into a 25 mL measuring cylinder. The samples were tapped on a level surface from a height of 2 cm until a constant volume was achieved. After recording the final volume, the tapped density was computed (USP, 2024).

$$\rho t = \frac{M}{V} \text{…… Eq.9}$$

Where ρt- tapped density, m – mass, and v – final volume

Carr's Index (C.I). The Carr's Index (%) of the sample was determined using the equation below:

$$C.I. = \frac{\rho t - \rho b}{\rho t} \times 100 \text{……. Eq.10.}$$

Hausner's Ratio (H.R). This was determined using the equation below.

$$H.R = \frac{\rho t}{\rho b} \ldots\ldots\ldots \text{Eq.11.}$$

Where ρt -Tapped density, and ρb - Bulk density

Porosity and True Density were calculated using a 25 mL pycnometer container filled to the capacity with xylene, and the weight was recorded. A portion of the xylene was drained away before adding the sample (1.0 g) to the bottle. The extra fluid was wiped off after more xylene was added to the bottle until it reached the mark. The weight of the bottle was recorded for the second time. The porosity and true density were calculated using the following formulas (Rajr, 2013).

$$\text{True density} = \frac{W}{a+w-b} \times SG \ldots\ldots\ldots \text{Eq.12}$$

Where w is the weight of the powder, a is the weight of the bottle + solvent, b is the weight of the bottle + solvent + powder, and SG is the specific gravity of xylene (0.86).

The porosity was calculated as:

$$\text{Porosity} = \left(1 - \frac{\text{bulk Density}}{\text{true density}}\right) \times 100 \ldots\ldots\ldots \text{Eq.13}$$

Determination of swelling capacity was done using a 1 g sample and placing it in a 15 mL measuring cylinder, then tapping it. The tapped volume occupied by the sample was recorded as V_1. Distilled water was then added up to the mark, and the cylinder was left undisturbed for 24 h (Angupale *et al*., 2023). The new volume occupied by the sample was recorded as V_2, and the swelling capacity (%) were calculated using the equations below:

$$\text{Swelling capacity} = \frac{v2-v1}{\text{v1}} \times 100 \ldots\ldots\ldots \text{Eq.14}$$

Where V1 - initial volume of the sample, V2 - final volume of the sample

2.10. Moisture sorption capacity

A petri dish was evenly covered with one gram of each of the powdered TLW-MCC, TFW-MCC, and Avicel PH-101, which had been precisely weighed. After that, the samples were kept at 25°C in a sizable desiccator filled with saturated salt solutions of potassium chloride (RH = 85%), sodium chloride (RH = 75%), calcium chloride (RH = 30%), and sodium hydroxide (RH = 20%) as well as distilled water (RH = 100%). After a month of equilibration, the weight gain was noted. The MCC samples' water sorption capacities were reported as a percentage of moisture absorption. The average of three replicate determinations was used to present the results. The following formula was used to determine water absorption based on the weight difference: Moisture sorption capacity = $(W_2 - W_1) / W1 \times 100$, where W_1 is the initial weight before exposure and W_2 is the weight after exposure (Mihranyan *et al*., 2004).

2.11. Particle size and Size distribution

The particle size distribution and particle size of MCC from TLW, TFW, and Avicel pH-101were determined with a laser diffraction particle-size analyzer (Master Sizer, UK). The measurement range covers particles from 0.05 to 900 µm, with a 3000RFmm active beam length (2.40 mm). The following parameters were used for the analysis: polydisperse, standard-wet, presentation (3OHD), and sample unit (MS1: Small Volume Sample Dispersion Unit). Background readings were taken using ultra-pure distilled water as the dispersing medium, and Obscuration was maintained between 10% and 30%. Measurements were taken in triplicate, and the mean values with their standard deviations were calculated. Data analysis was performed with the 90Plus Particle Sizing 166 software version 3.93 (New York, USA), which determines the particle size distribution based on the diffraction pattern. Key parameters that were calculated, such as D10, D50, D90, narrow distribution (low Span), and wide distribution (high Span), were plotted as particle size versus volume distribution (Krivokapić *et al*., 2020).

$$\text{Span}=\frac{D(v,0.9)-D(v,0.1)}{D(v,0.5)} \quad \ldots\ldots\ldots\ldots\ldots 15$$

2.12. Compatibility studies between the Paracetamol drug and microcrystalline cellulose using the FT-IR method

For the FTIR analysis, physical mixtures of the three studied MCCs were prepared. All the FT-IR spectra were recorded using an iS50 ABX (USA) FT-IR spectrometer. With a spectral resolution of 1 cm-1 and 8 readings/point, the spectra were captured between 4000 and 550 cm-1. Individual Components were prepared with pure samples of the API and each excipient to establish baseline spectra. Mixing the API with each excipient at relevant concentrations means a 1:1 ratio, then run using FT-IR. Peak comparison has examined the spectra for any shifts, changes in intensity, or the appearance of new peaks in the mixtures compared to the individual components. Finally, potential chemical interactions based on spectral changes were identified. For instance, a reduction in peak intensity, the arrival of new absorption peaks, or the vanishing of existing peaks may indicate interactions between the API and excipient (Dinte *et al*., 2013).

2.13. Microbial enumeration tests and Tests for specified microorganisms of Microcrystalline Cellulose Powder

Media used for the Total aerobic Bacterial Count test were tryptone soya Agar (TSA) and Tryptone soya Broth (TSB) 1 g of each sample was prepared and diluted in 100ml TSB (Homoginate A), then 1ml from the dilution/ enriched media was inoculated into TSA, and incubated at 35 - 37 °C for 3-5 days. A total fungal count (TFC) was determined using TSB and SDA (Sabouraud Dextrose Agar) media for testing. 1 g of each sample was prepared and diluted in 100 mL of TSB, then 1 mL of the dilution/enriched media was inoculated into SDA and incubated at 25°C for 5 days. Using TSB, MacConkey broth, and MacConkey agar, *Escherichia* coli was tested by taking 1 g of each sample. The solution was prepared and then diluted to a total volume of 100 mL TSB and incubated for 24 hours. On the second day, 1 mL of Homogenate A was taken and diluted with 100 mL of MacConkey broth, and incubated for 24 hours. On the third day, 1 mL from the dilution (Mac B) was inoculated into Mac A and incubated at 35- 37 °C for 72 hrs (Gholizadeh *et al*., 2019). The method for *Salmonella t*esting involved media testing using TSB and Xylose-Lysine Deoxycholate (XLD) agar. One gram of each sample was prepared and diluted in 100 mL TSB, then incubated for 24 hours. On the second

day, 1 mL of Homogenate A was taken and inoculated into XLD agar, then incubated at 35-37°C for 18-72 hours (Gholizadeh *et al*., 2019).

For *Staphylococcus aureus* testing, the media used included TSB and Baird-Parker agar (BPA). 1gram of the sample was prepared and diluted in 100 mL of TSB, then incubated for 24 hours. On the second day, 1 mL of Homogenate A was taken and inoculated into BPA, then incubated at 35-37°C for 18 to 72 hours (Gholizadeh *et al*., 2019). For *Pseudomonas aeruginosa* testing, the media used were TSB and Cetrimide agar. One gram of the sample was prepared and diluted in 100 mL TSB, then incubated for 24 hours. On the second day, 1 mL of Homogenate A was taken and inoculated into Cetrimide agar, then incubated at 35-37°C for 18-72 hours (Gholizadeh *et al*., 2019).

2.14. Development of Model Drug Formulation

Formulations of tablets containing paracetamol as a model drug have been developed, as confirmed in Table 1. In a cube mixer set to 200 rpm, all ingredients (apart from magnesium stearate) were combined with paracetamol for ten minutes. The combined powder was then run through a sieve with a 1 mm mesh size. To lessen the friction of compression forces and speed up the disintegration time, magnesium stearate was then added and mixed for an additional three minutes. A single-punch 12/32 flat compaction machine (B3B, B3B, Manesty machines, England) was used to compress the powder mixtures directly into tablets. The die/punch was set to 12.00 mm diameter at a predetermined compression pressure (Figure 5). The tablets produced were stored in a desiccator for a couple of weeks preceding further evaluation of uniformity of weight, hardness, dimension, friability, disintegration, assay, and dissolution (Widodo *et al.*, 2022; Tomar *et al.*, 2017).

Table 1. Formulation of paracetamol tablets using isolated microcrystalline cellulose and Avicel 101.

Name of material	F1	F2	F3	Quantity in %	Quantity for one batch (400 tabs)	Quantity for three batches (1200 tabs)
Paracetamol DC90%	✓	✓	✓	70.42	100gm	300gm
MCC	TLW	TFW	Avicel 101	22.0	31.24gm	93.72gm
Sodium starch glycolate	✓	✓	✓	4.0	5.68gm	17.04gm
Magnesium stearate	✓	✓	✓	1.96	2.78gm	8.34gm
Purified talc	✓	✓	✓	0.90	1.28gm	3.79gm

"✓" indicates the material used during formulation, considering 10% for contingency (waste), F_1 was formulated by using TLW-MCC, F_2 was formulated by using TFW-MCC, and F_3 was formulated by using Avicel PH-101, Paracetamol DC90%. The hardness test was conducted on five randomly selected tablets from each formulation, with their hardness measured using the hardness tester (Sotax MT50, India). Furthermore, the thickness and diameter of the tablet were measured using the same hardness tester. The friability test was conducted as another parameter. For this test, 20 tablets were de-dusted and weighed collectively (W1). They were then transferred to a friability test apparatus (Sotax F2, India) and rotated at 25 rpm for 100 revolutions. After this process, the tablets were removed from the friability tester, de-dusted again, and reweighed (W_2) (Angupale *et al*., 2023). Using the two weight values, the friability of each batch of tablets was calculated accordingly. The following equation.

$$\text{Friability (\%)} = \frac{w1-w2}{w1} * 100 \ldots\ldots \text{Eq.16}$$

A tablet disintegration device was used to perform the disintegration test *in vitro*. In total, 900 milliliters of distilled water were used as the disintegration medium in a beaker that was maintained at 37 ± 0.5 °C. Each tube of the disintegration apparatus (ERWEKA, ZT304, Germany) had a basket

with six tablets from each batch. Each tablet's time to portion into tiny pieces and move through the mesh was noted, and the average time was computed (Hitesh Chaturvedi1 *et al*, 2022).

Figure 5. Schematic diagram of formulated Paracetamol tablet F_1(A), F_2(B), and F_3(C).

2.15. Methods of *In-vitro* dissolution profile and Assays for Paracetamol Tablets

2.15.1. *In-vitro* dissolution studies

Using a Type II (paddle-type) dissolution apparatus, the dissolution test was conducted in accordance with the BP pharmacopeia. Phosphate buffer (pH 5.8) containing 40.83g of monobasic potassium phosphate (KH2PO4) and 0.864g of sodium hydroxide in 6,000 ml of water served as the dissolution medium. An adjusted dissolution tester (Lab India, DS800, India) and 900 ml of phosphate buffer were added to each of six dissolution vessels. The vessels were then kept at 37 ± 0.5 °C for 60 minutes at a speed of 50 rpm. After 10, 20, 30, 40, 50, and 60 minutes, the samples were removed, and in every dissolution experiment, a new buffer solution was added right away in their place. 1.8 mL of the sample was added to a 50 mL volumetric flask, and it was subsequently diluted with phosphate buffer until it reached the desired level. Weighing out 25 mg of the paracetamol working standard, then adding it to a 50 ml volumetric flask and diluting it with phosphate buffer, was the standard procedure. A 50 ml volumetric flask was then filled with 1 ml of the solution, which was diluted with phosphate buffer until it reached the desired level. Since the standard and sample concentrations were then equal, the collected dissolution samples were filtered once every minute. Then, the absorbance of paracetamol using a UV-VIS spectrophotometer (U.V-1800 Double Beam Spectrophotometer, SHIMADZU Corporation, JAPAN) was determined at 243nm wavelength against a blank phosphate buffer, pH 5.8, which has been filtered. Finally, the percentage of paracetamol released at each time

was calculated by dividing the absorbance of the sample by the absorbance of the standard and multiplying by one hundred (BP, 2009).

The independent model simple technique, which makes use of the difference (f1) and similarity (f2) components, was used to compare the dissolution profiles in this study. Factor f1 displays the percentage difference (dissimilarity) between the two dissolution profiles. f2 is the reciprocal square root transformation of the logarithm of the sum squared error. It shows the average percentage of similarity between two dissolution profiles. It is acceptable to have f1 levels between 0 and 15 and f2 values between 50 and 100. f1 value greater than 15 indicates significant dissimilarity, whereas a f2 value greater than 50 indicates substantial similarity (Santos Júnior *et al*., 2014)

$$f_1 = \{[\sum_{t=1}^{n} n|Rt - Tt|] / \sum_{t=1}^{n} nRt]\} * 100 \ldots\ldots\ldots\ldots \text{Eq.17}$$

$$f_2 = 50 * \log \{[1+(\frac{1}{n}) \sum_{t=1}^{n} * (R_t - T_t)^2]^{-0.5} * 100\} \ldots\ldots\ldots\ldots \text{Eq.18}$$

A stock solution of paracetamol was prepared by dissolving 25 mg of pure Paracetamol DC powder in 25 ml of phosphate buffer at a pH of 5.8. This solution was stirred for 5 minutes and then brought to a final volume of 50 mL, achieving a concentration of 0.5 mg/ml. To produce stock solutions, this concentration was serially diluted to final concentrations of 0.25, 0.50, 0.75, 1, 1.25, and 1.5 mg/ml. The absorbance of these solutions was measured in a UV spectrophotometer at 243 nm, resulting in a calibration curve that plotted absorbance against concentration (Figure 19).

2.15.2. Assay of formulated paracetamol content

The determination of the drug content or assay in paracetamol tablets using High-Performance Liquid Chromatography (LC 2030C 3D, Shimadzu Corporation, Japan) involves an efficient approach to quantify the active ingredient in the tablet formulation. First, a suitable mobile phase, typically a mixture of water and methanol (3:1), was prepared to ensure optimal separation of paracetamol from other excipients in the tablet. Sample preparation of the paracetamol tablet involved weighing 20 tablets in each batch and crushing them using a mortar and pestle. Transfer the powder equivalent to average weight (355mg) by converting the equivalent into 100mg then the powder was added into a 200 volumetric flask, added 100ml of the mobile phase (methanol and water) was Shaken by a

mechanical means for 10 minutes, and sonicated for 5minute finally, dilute up to volume by mobile phase filter using Whatman no1 filter paper. The final concentration of the sample became 0.5ml/mg, and the working reference standard (WRS) preparation was also the same sample preparation, which means 100mg WRS weighed and transferred into a 200ml volumetric flask, then diluted by mobile phase and filtered using Whatman No. 1 filter paper then transferred into both sample and standard vials, ready for HPLC.

The chromatographic system of HPLC Model-LC, the Shimadzu HPLC system, is equipped with a UV detector at 243nm wavelength, which is the absorption maximum for paracetamol. The sample was injected into the chromatographic column, where it underwent separation based on its interaction with the stationary phase (typically a C18 column). The flow rate was 1.5ml/min, and the injection volume was 10µL. The mobile phase elutes the drug, and as it passes through the detector, the paracetamol's concentration is measured by the peak area (PA), height, Height, tailing factor (peak quality), theoretical plate, and finally the concentration of paracetamol concerning retention time. The results were expressed as a % of the labeled drug content. $(\frac{\text{PA sample}}{\text{PA Standard}}*100)$, ensuring that the paracetamol tablets meet the required pharmacopeia standards for dosage accuracy in percent (90-110) (BP, 2009).

2.16. Statistical Analysis of Data

The measurements for the powder property study, physicochemical tests, and degree of polymerization were performed in triplicate, including calculations of standard error and standard deviation, and confidence intervals. The optimization results were analyzed using a Central Composite Design (CCD) within the framework of Response Surface Methodology (RSM). The characterization study included FTIR, XRD, compatibility studies, and thermal analysis data interpretation using OriginPro 2019b 64-bit. Size distribution, particle size, distribution volume, and specific surface area were analyzed using Master Sizer (3OHD). The dissolution profile/*in vitro* release test data were analyzed with GraphPad Prism software and Microsoft Excel to compare each formulation. SPSS one-way ANOVA followed by Tukey Post Hoc Test was used to compare the assay or drug content of F1, F2, F3, RD, and WRS at a 95% confidence level ($\alpha = 0.05$); therefore, the level of significance was set at $P<0.05$.

3. RESULTS AND DISCUSSION

3.1. Composition of the untreated raw materials

The amounts of extractives, hemicellulose, and lignin in TLW and TFW were determined using a chemical analysis method. The extractive content in TLW was 23%, while in TFW it was 18%. The amounts of hemicellulose and lignin in TLW were 25% and 19%, respectively. Additionally, the amounts of hemicellulose and lignin in TFW were 30% and 21%, respectively. Extractives content was high in TLW, but hemicellulose and lignin content were high in the TFW. In this study, the results were comparable to other raw materials like teff straw, enset fiber, sugarcane bagasse, and coffee hull. The ultimate physicochemical properties of cellulose and microcrystalline cellulose derived from tea waste are greatly influenced by its extractive concentration. To produce high-purity cellulose and MCC appropriate for a variety of uses, non-cellulosic compounds such as tannins, polyphenols, and other extractives must be effectively removed using procedures including bleaching and alkaline treatment (Nasution *et al*., 2017, Gabriel *et al*., 2020).

3.2. Yield of Cellulose and Optimization of the Yield of Microcrystalline Cellulose

The yield of Cellulose 23.57±1.55% from tea leaf waste and 28.5±1.02% Tea fibre waste was obtained. Finally, the yields were 66.7±1.6% from tea leaf waste and 86.7869±1.80% from tea fibre waste, the MCC powder.

The yields of MCC prepared under various selected conditions are presented in Table 2. The highest MCC yield, recorded at 86.52%, was achieved under conditions of 100°C, a reaction time of 30 minutes, and a 2.5M HCl concentration (run 4). In contrast, the lowest MCC yield, 54.56%, was observed in run 19, where the MCC was prepared at 100°C for 5 minutes using a 2.5M HCl concentration. This optimization result was comparable to some literature (Fitrya *et al*., 2021). The design consists of 20 experimental runs (8 factorial points, 6 axial points, and 6 replicated runs (centre points)).

Table 2. The yield of microcrystalline cellulose is prepared under different designated conditions.

Run	Space Type	A: Temperature (°C) Factor 1	B: Time of hydrolysis (Minutes) Factor 2	C: Acid Concentration (M) Factor 3	Yield (%) Response
1	Center	100	30	2.5	83.5
2	Factorial	80	15	3	71.24
3	Factorial	80	15	2	60.6
4	Center	100	30	2.5	**88.52**
5	Center	100	30	2.5	**84.53**
6	Factorial	80	45	2	73.05
7	Axial	133.636	30	2.5	71.07
8	Factorial	120	15	3	76.2
9	Axial	66.3641	30	2.5	80.2
10	Factorial	120	15	2	78.2
11	Factorial	80	45	3	81.01
12	Factorial	120	45	3	59.03
13	Axial	100	30	3.3409	79.1
14	Axial	100	30	1.6591	78.6
15	Axial	100	4.77311	2.5	56.34
16	Center	100	30	2.5	**85.12**
17	Center	100	30	2.5	**84.82**
18	Center	100	30	2.5	**85.07**
19	Axial	100	55.2269	2.5	54.56
20	Factorial	120	45	2	56.82

3.2.1. Model of selection

Both linear and quadratic models were fitted to the experimental data to determine the most appropriate relationship between the dependent and independent variables. Model selection was based on statistical parameters such as the coefficient of determination (R^2), adjusted R^2, significance of the regression coefficients (p-values), and visual inspection of the data trend. If the quadratic term was statistically

significant ($p < 0.05$) and resulted in a higher adjusted R^2, the quadratic model was considered the better fit, indicating a nonlinear relationship (Table 3) (Osubor, 2017).

Table 3. Summary of statistical model fit statistics used for model selection.

Fit Summary report

Source	Sequential p-value	Lack of Fit p-value	Adjusted R^2	Predicted R^2	
Linear	0.8220	< 0.0001	-0.1234	-0.5148	
2FI	0.3220	< 0.0001	-0.0671	-0.6420	
Quadratic	**< 0.0001**	**0.2011**	**0.9620**	**0.8824**	**Suggested**
Cubic	0.2011		0.9764		Aliased

Model Summary Statistics

Source	Std. Dev.	R^2	Adjusted R^2	Predicted R^2	PRESS	
Linear	11.75	0.0540	-0.1234	-0.5148	3537.49	
2FI	11.45	0.2699	-0.0671	-0.6420	3834.52	
Quadratic	**2.16**	**0.9800**	**0.9620**	**0.8824**	**274.71**	**Suggested**
Cubic	1.70	0.9938	0.9764		*	Aliased

The significance of the model is indicated by its F-value of 54.46. The likelihood that an F-value this large could be caused by noise is 0.01%. Model terms are considered significant when the P-value is less than 0.0500. In this instance, important model terms in Table 3 are A, B, C, AB, AC, A^2, B^2, and C^2 as seen in Table 4. The model terms are not significant if the values are higher than 0.05. Model reduction may enhance the model if it contains a large number of unnecessary terms (apart from those needed to support hierarchy). In comparison to the pure error, the lack of fit is negligible, according to the lack of fit F-value of 2.22. A large lack of fit F-value has a 20.11% probability of being caused by noise. Non-significant lack of fit is good, as it means the model fits in Table 3 (Osubor, 2017).

Table 4. ANOVA for the response surface quadratic model.

Source	Sum of Squares	DF	Mean Square	F-value	p-value	
Model	2288.60	9	254.29	54.46	< 0.0001	significant
A-Temperature	70.39	1	70.39	15.07	0.0030	
B- Time of hydrolysis	27.34	1	27.34	5.86	0.0361	
C-Acid concentration	28.28	1	28.28	6.06	0.0336	
AB	461.62	1	461.62	98.86	< 0.0001	
AC	42.27	1	42.27	9.05	0.0131	
BC	0.2926	1	0.2926	0.0627	0.8074	
A^2	157.35	1	157.35	33.70	0.0002	
B^2	1570.98	1	1570.98	336.43	< 0.0001	
C^2	67.71	1	67.71	14.50	0.0034	
Residual	46.70	10	4.67			
Lack of Fit	32.19	5	6.44	2.22	0.2011	Not significant
Pure Error	14.51	5	2.90			
Cor Total	2335.30	19				

Final Equation in Terms of Coded Factors: Yield = +85.24 -2.27A-1.41B+1.44C-7.60AB-2.30AC+0.1912BC-3.30A^2-10.44B^2-2.17C^2……. Eq19

Since the difference is less than 0.2, the adjusted R^2 of 0.9620 and the predicted R^2 of 0.8824 are in reasonable agreement. The signal-to-noise ratio is measured by adequate precision. The stronger the correlation between the experimental and predicted values, the closer the R-squared value is to 1. A ratio of more than four is ideal, and an adequate signal is indicated by a ratio of 20.884. The design space can be navigated using this model (Table 5A). For specific levels of each factor, predictions regarding the response can be made using the equation expressed in terms of coded factors. By default, the factors' high and low levels are denoted by the numbers +1 and -1, respectively. The coded equation is useful for identifying the relative impact of the factors by comparing the factor coefficients (Victoria *et al.*, 2023).

Final Equation in Terms of Actual Factors Yield = -217.84933 + 2.87296A +5.15822B +68.45318C - 0.025321AB -0.229875AC + 0.025500BC - 0.008261A^2- 0.046404B^2-8.67057C^2 ..... Eq20. For specific levels of each factor, predictions regarding the response can be made using the equation expressed in terms of actual factors. In this case, each factor's levels should be stated in its original units. Since the intercept is not at the centre of the design space and the coefficients are scaled to account for the units of each factor, this equation should not be used to calculate the relative impact of each factor. The response variable is the yield. (Sayed, 2025).

Table 5A. Statistical data for ANOVA and Constraints.

Statistical data for ANOVA (A)			
Parameters	Value	Parameters	Desirability
Std. Dev.	2.16	R^2	0.9800- Selected
Mean	74.38	Adjusted R^2	0.9620
C.V. %	2.91	Predicted R^2	0.8824
		Adeq Precision	20.8838

Constraints

Name	Goal	Lower Limit	Upper Limit	Lower Weight	Upper Weight	Importance
A: Temperature	is in range	80	120	1	1	5
B: Time of hydrolysis	is in range	15	45	1	1	5
C: Acid concentration	is in range	2	3	1	1	5
Yield	maximize	54.56	88.52	1	1	5
Std Err (Yield)	is in range	0.88133	1.76849	1	1	5

The CCD for optimizing MCC yield used three independent variables: temperature, Time of hydrolysis, and Acid concentration, each tested at five levels (low, high, centre, and two axial points). The goal was to determine the combination of factor levels that maximizes the yield, which varied between 54.56% and

88.52% within the tested experimental domain**.** Response (yield) constraint assigned implies yield MCC (%) was the response of this study, and maximization of yield was the objective function. Yields obtained within the domain of Central Composite design ranged from a minimum value of 54.56% at conditions 100 °C, 55.23 min, and 2.0 M HCl to attain a maximum value of 88.52% at conditions 100 °C, 30 min, and 2.5 M HCl. Therefore, the major restriction during optimization is to obtain maximum yield with respect to temperature, time, and acid concentration within their limits (Table 5) (Gao *et al*., 2020).

Table 5B. Experimental design details indicating the highest, lowest, and axial points of the independent variables

Independent variable	Coded symbol	Lowest level (-1)	Highest level (+1)	Axial level (-α)	Axial level (α)	Centre point (0)
Temperature (°C)	A	80	120	66.36	133.64	100
Time of hydrolysis (min)	B	15	45	4.77	55.23	30
Acid concentration (M)	C	2.0	3.0	1.659	3.3409	2.5

The closer the values between the actual and predicted values, the better the model's fitness. A scatter plot that illustrates a model's performance by contrasting its predictions with actual data points is called a predicted vs. actual plot. This 6A figure, which shows how closely the points align with a 45-degree diagonal line (when forecast equals actual value), is used in optimization to evaluate how well a model's output matches the actual outcomes (Chijioke *et al*., 2020). Figure 6B represents the graph of residuals vs. predicted, where the prediction made by the model is on the x-axis, and the accuracy of that prediction is on the y-axis. Figure 6(C) shows a normal plot of residuals, which indicates that all the residuals are collected along the inclined line, and there is no significant deflection from the normal probability line. The distance from line zero shows how bad the prediction is for that value. Positive values of residuals on the y-axis mean that the prediction was too low, whereas negative values mean that the prediction was too high. A scattered graph of residual vs. predicted is considered to be an ideal graph in Figure 6 B. The plot of residuals in Figure 6D indicates normal % Probability, showing where each residual should fall if the data were perfectly normally distributed. Internally studentized residuals" show how many standar deviations each actual residual is from zero after adjusting for leverage, letting you spot outliers or non-

normal patterns. (Singh & Goyal, 2016).In Figure 7 in the normal probability plot of residuals, points that align closely with the red reference line indicate that the residuals are normally distributed. Deviations from the line suggest potential issues with normality, such as the presence of outliers or skewness in the data (Gao etal.,2020).

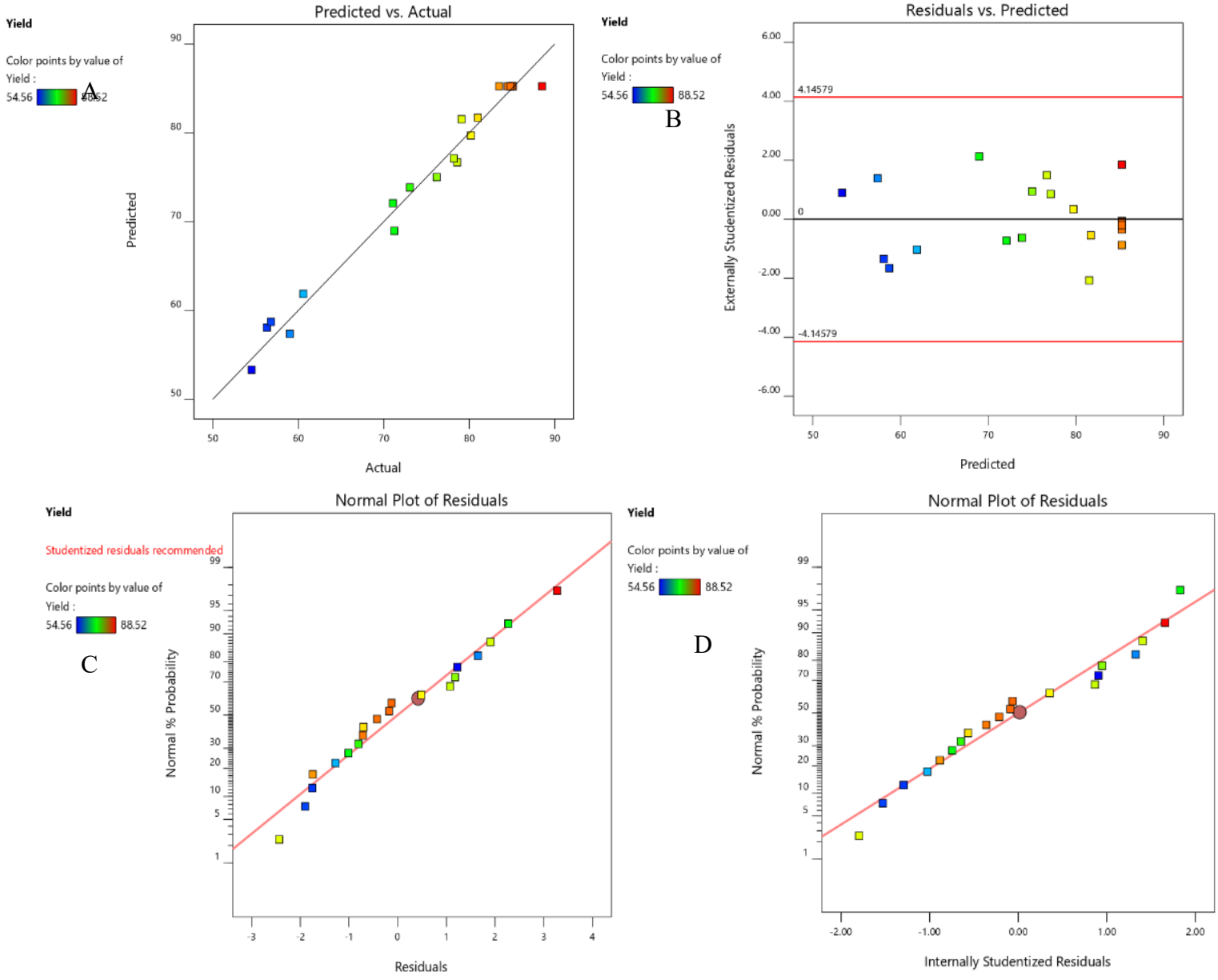

Figure 6. Predicted vs Actual (A), Predicted vs Actual (B), Normal plot of residuals (C), Externally studentized vs Normal plot of residuals (D) for the yield of microcrystalline cellulose.

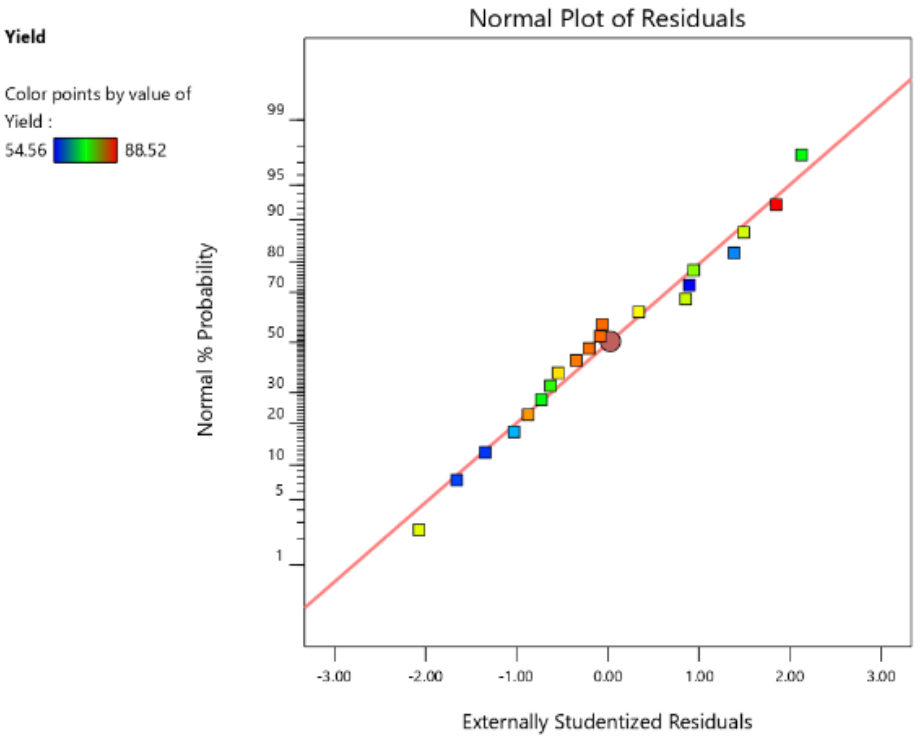

Figure 7. Externally studentized vs normal plot of residuals of microcrystalline Cellulose.

3.2.2. Response surface analysis

The 3D graph illustrates the interaction between two independent variables, temperature and acid concentration, and the time of hydrolysis, as well as the impact of these factors on a dependent variable, yield (expressed as a percentage). The graph appears to be part of an optimization study aimed at maximizing yield (Figure 8). The contour lines on the base of the graph represent lines of equal yield. These lines help visualize how the yield changes with temperature, acid concentration, the time of hydrolysis, and the combinations of temperature, acid concentration, and time (Zeleke *et al*., 2024).

The area with the highest yield, indicated by the warmer colours, is located in the top-left corner of the graph. This indicates that maximum yield is achieved at a high temperature of around 120°C and with a long hydrolysis time of approximately 45 minutes, resulting in a peak yield of 86.7869%. As the temperature increases, the yield also increases, and similarly, extending the hydrolysis time leads to an increased yield. Therefore, based on this graph, to achieve a higher yield at an acid concentration of 2.85353M, it is recommended to use a higher temperature and prolong the hydrolysis time (Figure 8A) (Sayed, 2025).

The color of the surface likely indicates the yield value; warmer colors (red and orange) typically represent higher yields, while cooler colors (yellow, green, and blue) suggest lower yields. The area with the maximum yield, marked by the warmest color in the top left corner, is reached at a relatively high acid concentration (close to 3M) and lower temperatures (around 80-90 °C). The highest yield observed in this area is 86.7869%. Analysis of the variables shows that as temperature increases; the yield generally decreases. Conversely, as acid concentration increases, the yield typically rises until it reaches its peak around 3 M. Therefore, to achieve a higher yield, it is advisable to use a lower temperature combined with a higher acid concentration during the reaction, as shown in Figure 8B (Akhabue, 2017).

The color of the surface indicates the yield value; warmer colors (red/orange) represent higher yields, while cooler colors (yellow/green/blue) signify lower yields. The area with the maximum yield, which is the highest yield achieved, is located in the top right corner of the graph. This indicates that the maximum yield occurs at a relatively high acid concentration (around 3M) and a longer hydrolysis duration (about 45 minutes). The highest yield that can be achieved is 86.7869%. As the hydrolysis time increases, the yield generally increases as well. Similarly, an increase in acid concentration also tends to lead to a higher yield. Based on this graph, with a temperature of 83.91°C, it is recommended to use a higher acid concentration and a longer hydrolysis time to achieve a better yield in the hydrolysis reaction (see Figure 8C) (Tiwari *et al*., 2013, Zeleke *et al*., 2024).

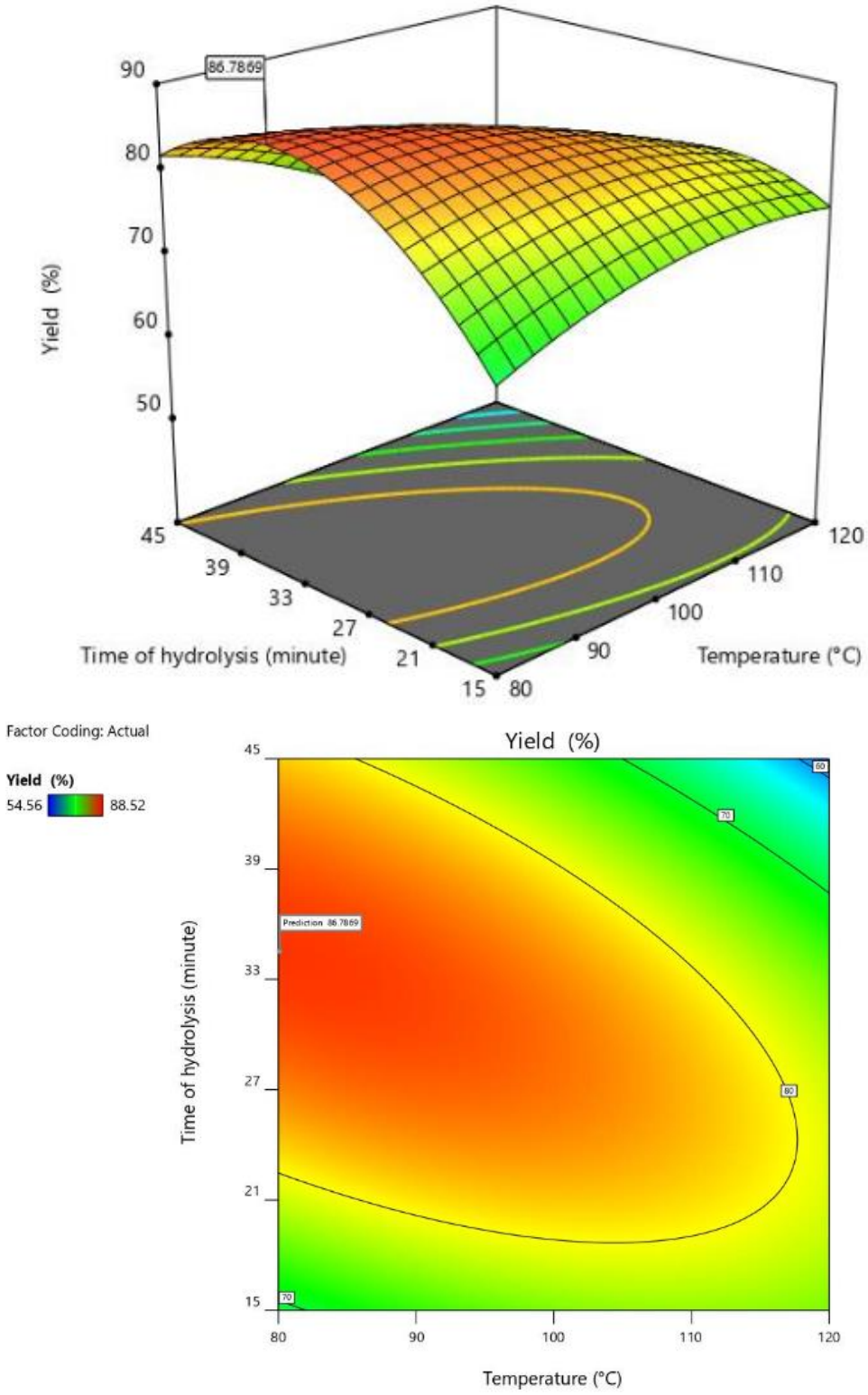

Figure 8A. The 3D and Contour plots of Temperatures and Time of hydrolysis on Microcrystalline cellulose yield.

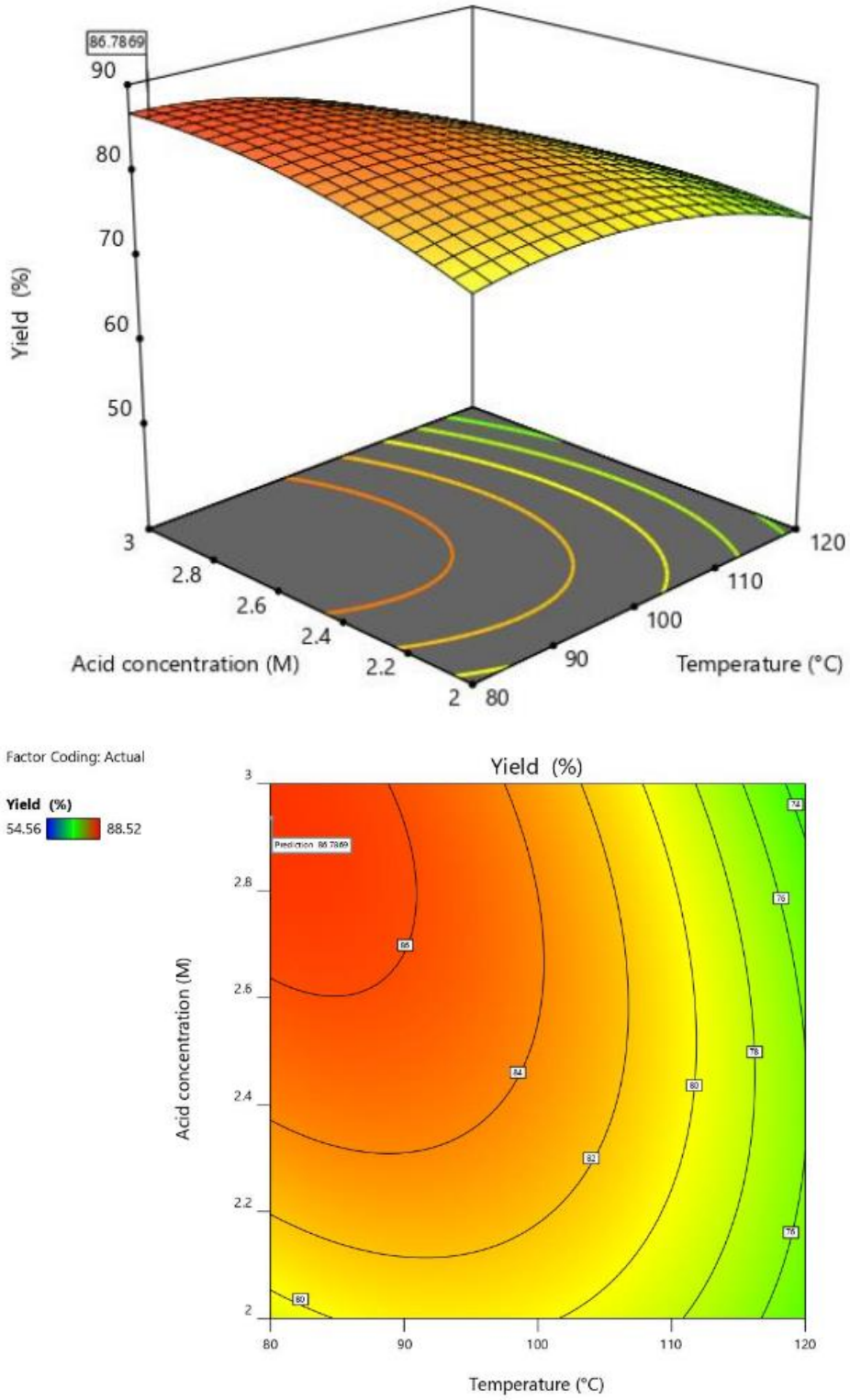

Figure 8B. The 3D and Contour plots of Temperature and acid concentration on microcrystalline cellulose yield.

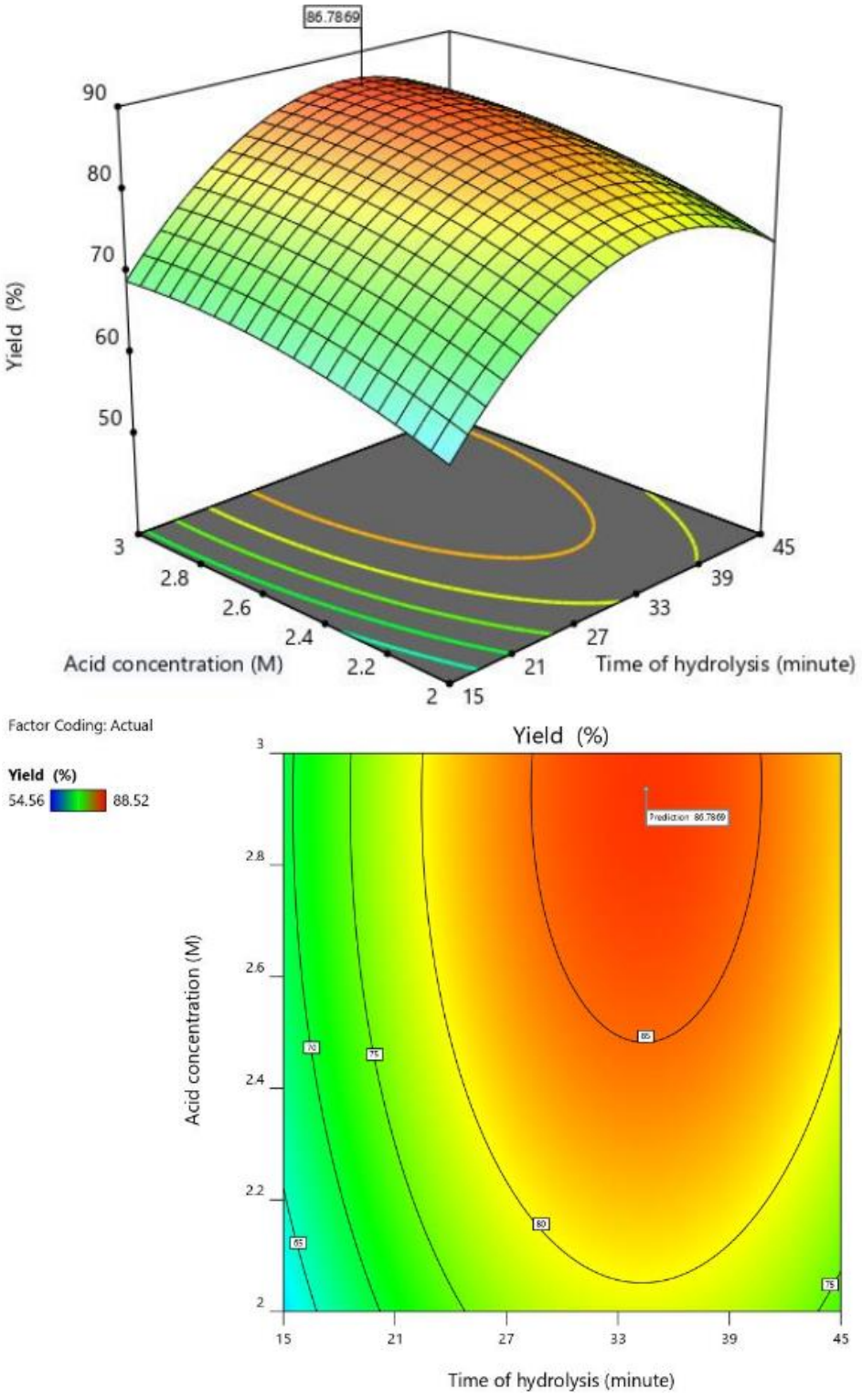

Figure 8C. The 3D and Contour plots of time of hydrolysis and acid concentration on microcrystalline cellulose yield.

3.2.3. Confirmation test of the model

The 3D surface shows the yield achieved at different combinations of these variables. To validate the model, the proposed experiment design identified an optimal run based on the experimental data, providing the maximum MCC yield (as shown in Table 6). This suggested optimal run was performed, and the actual yield of 87.448% obtained was compared to the predicted yield of 86.430%. The average percentage error between the actual and predicted yields was calculated and recorded. The resulting average percentage error of 1.163% was well below the 5% threshold, confirming that the predicted model was accurate and acceptable for practical use (Tiwari *et al*., 2013).

Table 6. Optimization validation of the yield of isolated MCC.

Number	Temperature (°C)	Time of hydrolysis (min)	Acid concentration (M)	Predicted yield (%)	Actual Yield (%)	Std Err (Yield)	Desirability
1	80.136	34.525	2.936	86.787	87.871	1.234	0.949
2	80.051	34.551	2.939	86.787	87.879	1.243	0.949
3	80.263	34.423	2.929	86.786	87.856	1.218	0.949
4	83.069	35.395	3.000	86.538	87.623	1.238	0.942
5	99.953	29.981	2.501	85.254	86.011	0.881	0.904
				86.430	87.448		

An overlay plot in an optimization or design-of-experiments study shows where multiple response constraints are simultaneously satisfied. It is one of the clearest tools for understanding trade-offs among responses. The best combination of variables for the maximum possible response exhibited a desirability of nearly one. The yellow shaded region in Figure 9(A, B, C) indicates the area that satisfies the imposed criteria. In the shaded region, the optimum conditions were a Temperature of 80.1054 °C, a time of hydrolysis of MCC of 34.5257 minutes, as the combined effect, Time of hydrolysis (34.5257 minutes), and Acid concentration of 2.936M, as the combined effect of Temperature of 80.1054 °C and Acid concentration of 2.936M. Under these conditions, the software predicts the yield of MCC 86.7869% (Gangolu *et al*., 2019).

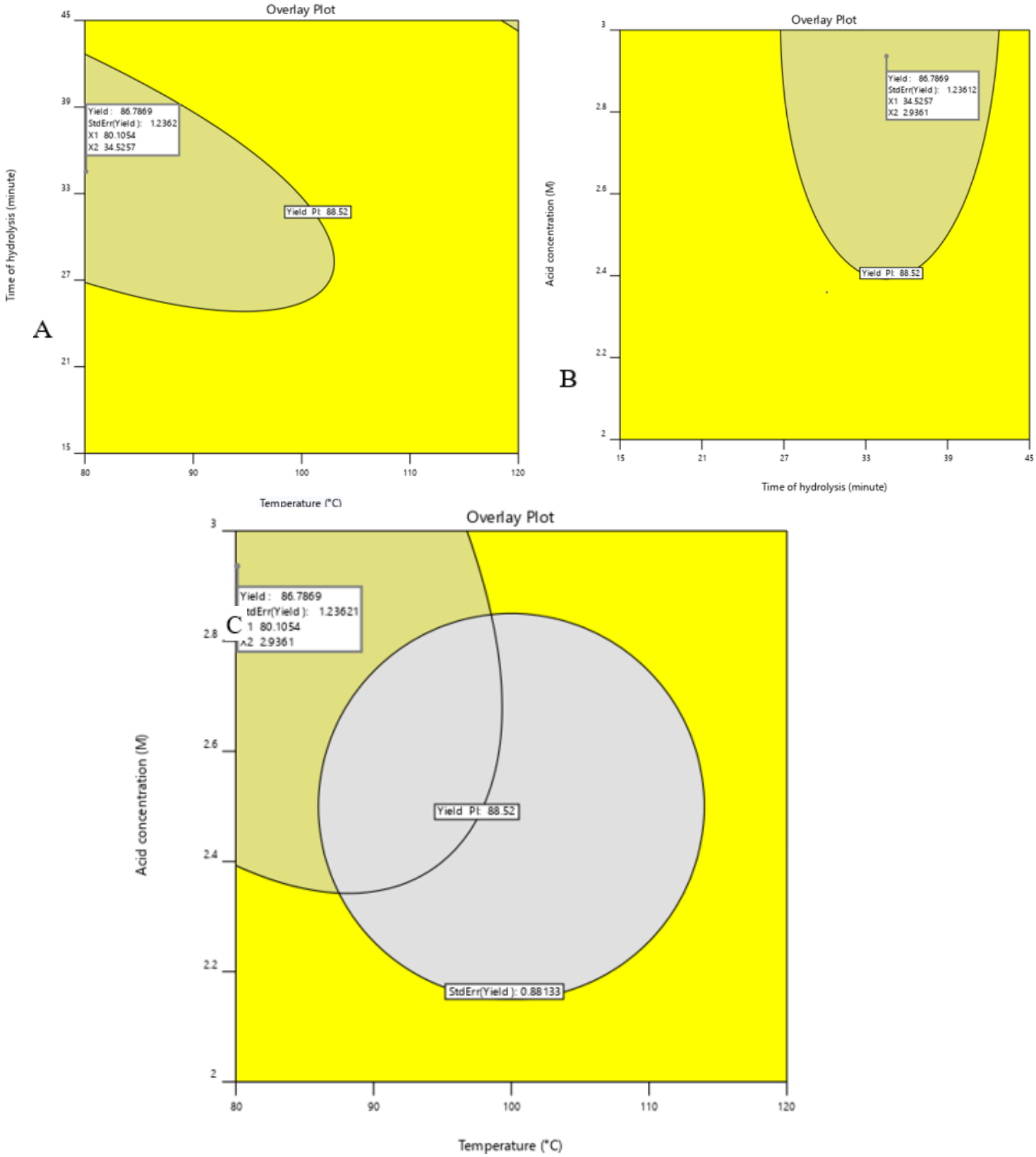

Figure 9. The overlay plot of the optimization study of microcrystalline cellulose.

3.3. Characterization study results

3.3.1. FTIR spectra analysis

The broad peak observed between 3200–3500 cm^{-1} is attributed to the O-H stretching vibrations, which are characteristic of the hydroxyl groups visible in cellulose. O-H stretching was indicated from a sample (TFW, TLW) and standard cellulose at 3432cm^{-1}, 3420cm^{-1}, and 3428cm^{-1}, respectively. The intensity and position of this peak can indicate hydrogen bonding, with variations in intensity across the samples possibly suggesting differences in the degree of bonding or moisture content. Peaks around 2900 cm^{-1} are associated with C-H stretching vibrations in cellulose from the sample (TFW, TLW), and standard cellulose at 2920cm^{-1}, 2920cm^{-1}, 2924cm^{-1} spectra were observed. The intensity of this peak is often related to the aliphatic C-H bonds present in the glucose units of cellulose. Peaks near 1600–1650 cm^{-1} represent the O-H bending mode of absorbed water or moisture in cellulose (As depicted in Figure 10) (Pachuau *et al*., 2014).

Variations in the water content may be the cause of variations in this peak's sharpness or intensity among the samples. The CH_2 scissoring motion, a property of cellulose, is represented by a peak at about 1430 cm^{-1}. The peak around 1370–1380 cm^{-1} is typically attributed to cellulose's C–H bending. The presence of cellulose structures is indicated by their appearance in the spectra of all three samples. These are frequently ascribed to C-O and C-C stretching vibrations in the cellulose backbone at about 1200–1300 cm^{-1}. Usually linked to C-O stretching in the cellulose structure, the peak at 1030–1060 cm^{-1} is specifically connected to the glycosidic bonds that connect glucose units (Getachew *et al*., 2023).

Interpretation of the FTIR Spectrum for Microcrystalline Cellulose broad peak around 3200–3500 cm^{-1} (O-H Stretching). As with standard cellulose, this peak corresponds to O-H stretching vibrations. The broadness of the peak is related to the hydrogen bonding between the hydroxyl groups within the cellulose structure (Getachew *et al*., 2023). In samples (TLW, TFW) and standard MCC around 3432cm^{-1}, 3417$cm^{-1,}$ and 3417$cm^{-1,}$ respectively were broader and less intense spectra were observed. In MCC, this peak might appear slightly sharper or more defined than in untreated cellulose, reflecting the more crystalline nature of MCC. The peak at 2900 cm^{-1} (C-H Stretching) is associated with the C-H stretching of the methylene groups in the cellulose backbone. From Figure 10, the MCC sample (TFW, TLW, STD) 2920cm^{-1}, 2920cm^{-1}, and 2909 cm^{-1} visible O-H Stretching were observed, which results are comparable with other literature (Panaitescu *et al.*, 2020). Similar to cellulose, this peak is consistent across MCC samples, but the intensity

may differ depending on the purity and crystalline nature of the MCC. Peak around 1650 cm^{-1} (O-H Bending) represents water absorption or moisture content within the cellulose structure. Since MCC is generally a dehydrated form of cellulose, this peak is typically less pronounced than in MCC, indicating lower moisture content. Differences in this peak between TFW-MCC (1638cm^{-1},), TLW-MCC (1635cm^{-1}), and STD-MCC (1635cm^{-1}) could suggest varying levels of water absorption. The peak at 1430 cm^{-1} (CH_2 Scissoring) is characteristic of cellulose and is also present in MCC (TFW, TLW, STD), related to the CH_2 scissoring motion within the glucose units.

A signature peak for cellulose and MCC (TFW, TLW, and STD) was 1373 cm-1, 1379 cm-1, and 1373 cm-1, respectively. The peak at 1370 cm^{-1} (C-H Bending) represents C-H bending in the cellulose backbone. The consistency of this peak across all samples confirms the MCC structure. The peak in the range of 1050–1060 cm^{-1}, corresponding to C-O stretching, is attributed to the C-O bonds in the cellulose chains and is frequently observed in the FTIR spectra of MCC (TLW, TFW, standard) at 1055cm^{-1}, 1051cm^{-1}, and 1055cm^{-1} C-O stretching was observed. In MCC, the more crystalline nature may cause this peak to shift slightly or appear sharper than in standard MCC (Figure 10). Overall, the FTIR analysis confirmed the presence of key functional groups in our sample, and the comparison with many literature spectra suggests that the sample composition is consistent with other similar compounds. The result is similar peak positions and peak intensities with the literature (Pachuau *et al*., 2014, Aridi *et al*., 2010).

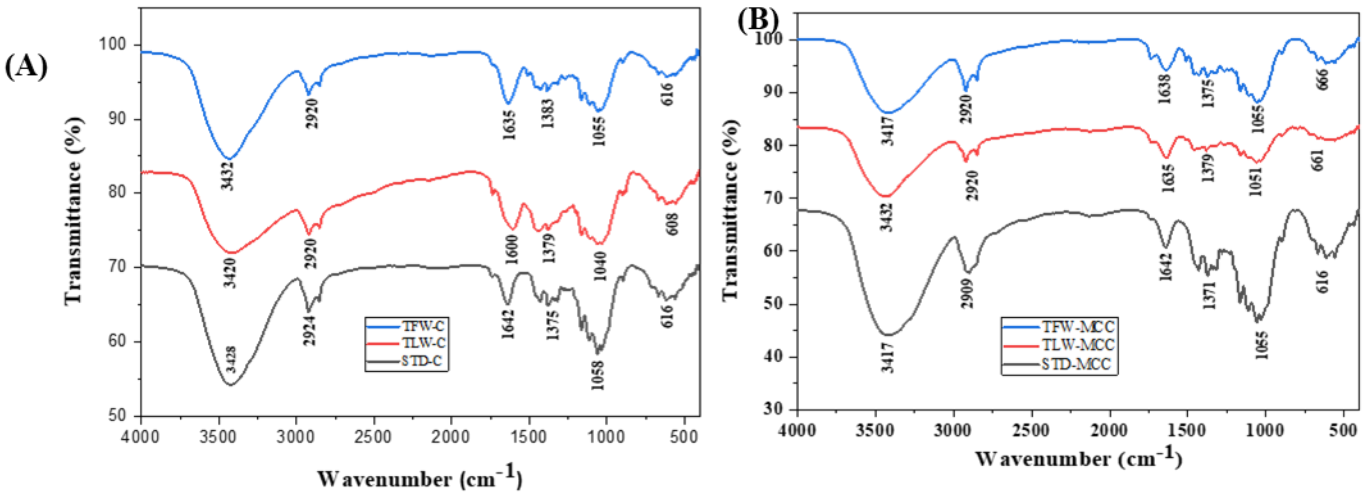

Figure 10. FTIR of cellulose (A) and Microcrystalline Cellulose (B).

3.3.2. Thermal analysis

In the TGA, the weight loss of the samples is plotted against temperature, indicating the thermal stability and decomposition pattern. Both cellulose and MCC exhibited initial weight loss starting around 100°C. There's a small initial weight loss for both samples and STD, likely due to the evaporation of moisture. This weight loss was in the first stage (0-200°C) in TLW, TFW, and standard cellulose, 9.01%, 6.75%, and 5.60% respectively, corresponding to the degradation of the polymeric component of the sample (Adel *et al*., 2010; Tarchoun *et al*., 2019). Major weight loss (decomposition) of the sample from 200°C to 400°C (TLW, TFW, and Standard cellulose 60.10%, 67.22%, and 80.20% respectively). This range shows the most significant weight loss, corresponding to the thermal degradation of cellulose. For the standard cellulose, the weight loss begins around 250°C and becomes more rapid around 350°C, with a total weight loss of around 50-60% by 400°C. In addition, Standard cellulose > TFW-Cellulose > TLW-Cellulose, the decomposition starts earlier, around 200°C, with a similar weight loss to 400°C. However, the onset of decomposition is at a slightly lower temperature compared to STD-C, suggesting reduced thermal stability due to fiber treatments. In the cellulose samples, the weight loss follows a similar trend, but the exact temperatures vary slightly depending on the sample processing. Final weight loss started around 0-800°C (Standard cellulose (99.32%) > TFW-Cellulose (99.31%) > TLW-Cellulose (85.68%)), and all samples experienced further weight loss, representing the breakdown of the remaining carbonaceous material. The final residual weight (char residue) at 800°C was Standard cellulose (0.68%), TFW-Cellulose (0.69%), and TLW-Cellulose (14.32%), with TLW-Cellulose having the highest residual weight. All sample results were consistent with the literature, and a similar study was conducted by Trache *et al*. (2014).

The DTA curves help identify the points of endothermic (heat absorption) and exothermic (heat release) reactions, which are typically related to phase changes, decomposition, or combustion reactions. Endothermic peaks were observed at around 100-150°C, with all samples showing a small endothermic peak. Cellulose STD at 350°C and TLW cellulose at 290°C show an endothermic peak on thermograms of cellulosic materials, but TFW cellulose shows no endothermic peak. This peak results from the evaporation of loosely bound water on the sample's surface. The exact values of the DTA signal range between -2 and -8 µV, depending on the sample. Additionally, significant exothermic peaks (decomposition) appear between 200-400°C (Cellulose STD at 400 °C, TFW Cellulose at 350°C, 650°C, and TLW at 300°C was observed). These peaks correspond to the thermal degradation of the fiber, with different samples showing slightly varying peak temperatures. For standard cellulose, the peak temperature occurs around 350°C, with

a DTA signal near -10 μV, indicating the decomposition of cellulose. Both samples exhibit similar exothermic peaks, but their temperatures are slightly lower, ranging from 300 to 350°C, indicating that these fibers decompose earlier than the untreated samples. At high-temperature reactions above 400°C, further exothermic reactions occur, related to the combustion of the remaining carbon-based materials in the composite. These reactions vary between samples but typically occur around 450-600°C.

Thermogravimetric analysis of MCC samples shows how weight changes with temperature, indicating the thermal stability of the microcrystalline cellulose-based composites. The initial weight loss, mainly due to moisture evaporation, is observed at around 0-200°C for MCC samples, whereas non-MCC samples likely display a different pattern. This weight loss is generally attributed to the evaporation of surface-bound moisture. The weight loss in this region was roughly 2-10% for TFW MCC (8.08%), TLW MCC (7.52%), and Standard MCC (7.14%). Central weight loss (decomposition of MCC and Cellulose) between 200°C and 400°C, the MCC samples show significant weight loss, indicating the thermal decomposition of cellulose and other organic components (Abu-Thabit *et al*., 2020). From Figure 11, at the above temperature, the weight loss was TFW MCC, TLW MCC, and Standard MCC, which were 76.83%, 70.16%, and 85.13%, respectively.

The standard MCC begins to lose weight around 250°C and continues to degrade rapidly, with a major weight loss of 350-400°C. At 400°C, the sample has lost about 50-85% of its mass, similar to the behavior observed in the cellulose (STD-C). However, the sample started decomposing slightly earlier, around 200°C, and experienced significant weight loss in the 200-350°C range. This suggests that the approach to MCC may reduce its thermal stability, leading to earlier decomposition (Fortunati *et al*.,2013).

The final weight loss began at higher temperatures, around 0-800°C, of MCC samples TFW (97.83%), TLW (97.78%) and the Standard was 98.54%. The MCC samples continue to lose mass, but at a slower rate, indicating the combustion of the remaining carbon-rich residues. The residual weight (char yield) left after complete decomposition is around 10-20%, similar to the non-MCC samples. The residual weights of TFW MCC, TLW MCC, and Standard MCC were 2.17%, 2.22%, and 1.46%, respectively. The char residue indicates the inorganic or highly thermally stable components that remain after heating, typically the by-products of lignin or other non-decomposable materials (Abu-Thabit *et al*., 2020).

Differential thermal analysis provides insights into the heat flow associated with physical and chemical transitions in the MCC samples, such as moisture loss, decomposition, and combustion. The observations

for MCC samples endothermic peaks indicated that moisture loss started around 100-150°C. There is a small endothermic peak for all MCC samples, indicating the loss of moisture and standard MCC at 350°C. The DTA signal at this point ranges from -2 to -5 uV, consistent with the initial weight loss seen in the TGA. Moreover, Exothermic peaks indicate the decomposition of MCC. The main exothermic peaks, corresponding to the decomposition of microcrystalline cellulose, occur between 200-450°C. For STD-MCC, the exothermic peak occurs at approximately 400°C, TFW MCC 400°C and 450 °C, and TLW MCC 450°C, with the DTA signal reaching around -8 to -10 μV. This exothermic reaction represents the thermal breakdown of the cellulose chains in the MCC, accompanied by the release of heat. In both, the exothermic peaks occur slightly earlier, around 250-300°C, suggesting that the thermal treatment affects the stability of the cellulose structure in MCC (Picker & Hoag, 2002).

At High-Temperature reactions (Char Combustion) temperatures beyond 400°C, further exothermic reactions occur, likely due to the combustion of the remaining char or carbonized materials. These reactions arise around 450-600°C, with minor exothermic peaks in the DTA signal. The extent of these reactions varies slightly between the MCC samples, but overall, the residual material (10-20% weight) after 800°C remains similar across samples (Haji Badri, 2016).

The thermal stability of the untreated MCC sample is relatively high, with decomposition starting around 250°C and a major exothermic peak at 350°C. It exhibits similar thermal degradation behavior to untreated cellulose. Both samples, having undergone some form of thermal treatment, show slightly lower thermal stability compared to STD-MCC. The decomposition begins earlier, around 200-250°C, and the exothermic peaks are shifted to lower temperatures. This suggests that thermal treatments might weaken the cellulose structure, making it more susceptible to decomposition at lower temperatures. However, the overall weight loss and residue formation are comparable to STD-MCC (Figure 10).

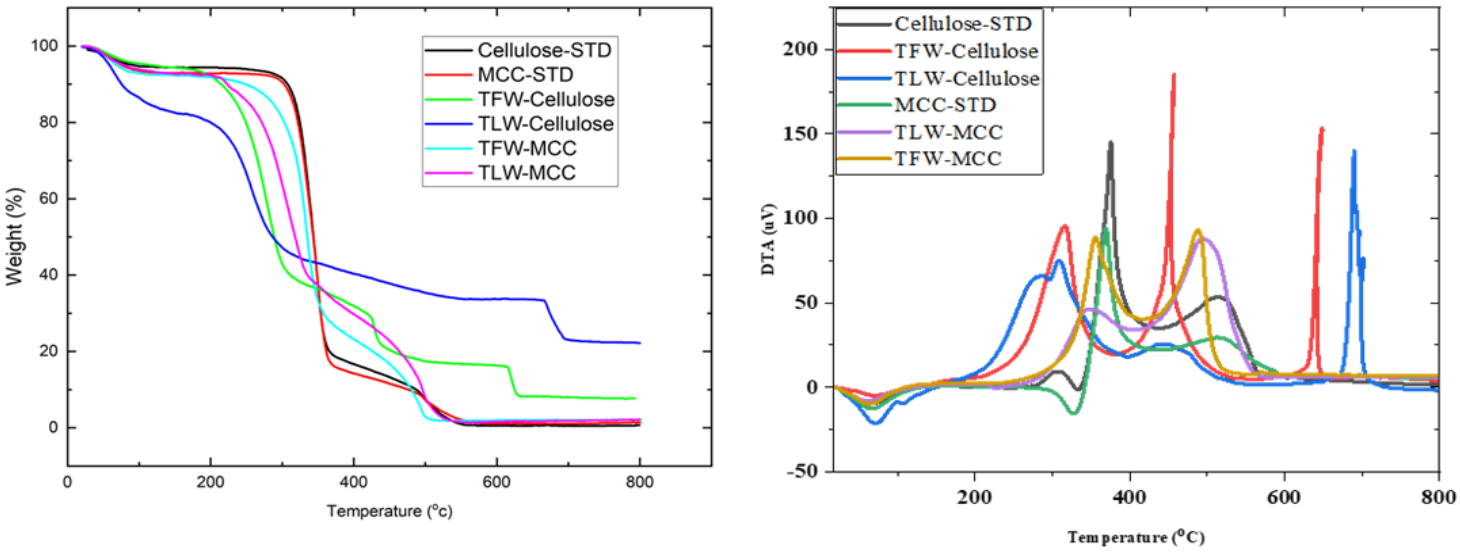

Figure 11. Thermogravimetric analysis (left) and differential thermal analysis (right) thermograms of Cellulose and MCC samples.

3.3.3. X-ray Diffraction Pattern Analysis

Based on the general analysis of XRD data, here are the observations to interpret the cellulose. The crystallinity of the peaks indicates crystallinity in the materials. The standard (STD-C) has sharper and more intense peaks, especially at 2θ values of around 22.5°, which is typical for cellulose I crystalline structure. Both TFW-C and TLW-C exhibit similar peak positions but have lower intensities, indicating reduced crystallinity compared to the standard. Peak Shifts and Patterns indicate that the major peak around 22.5° 2θ is present in all three samples, signifying a similar cellulose structure. However, its intensity is highest in STD-C, followed by TFW-C and TLW-C, indicating that the standard has a higher crystalline cellulose content. There are minor additional peaks at higher angles (in the range of 40–50° 2θ), which may correspond to other crystalline phases or impurities, although their intensity is minimal (Figure 12). This study is similar to a different literature result that was closely similar (Kane *et al*., 2016; Wathsala *et al*., 2021). Amorphous content observed at the lower intensities and broader peaks in TFW-C and TLW-C suggests a higher amorphous cellulose content in comparison to the STD-C. This may suggest that processing these samples lowered the degree of crystallinity.

XRD interpretation for MCC includes the following: crystallinity, peak analysis, and amorphous content. The standard sample (STD-MCC) shows the most prominent and sharpest peaks in crystallinity,

particularly around the 2θ value of 22.5°, which is characteristic of crystalline cellulose I. This indicates that STD-MCC has a high degree of crystallinity. Both TFW-MCC and TLW-MCC show similar peak positions but with lower intensities, implying that these samples have reduced crystallinity compared to the standard. Peak Analysis, as in the previous XRD pattern, the main peak around 22.5° corresponds to cellulose's crystalline structure; this peak is highest in STD-MCC. The secondary peak near 16° is also present in all three samples. Still, its intensity follows the same trend as the primary peak (STD-MCC > TFW-MCC > TLW-MCC), confirming the reduced crystallinity in TFW-MCC and TLW-MCC. There is a sharp peak in the red (TFW-MCC) curve at a higher angle, around 35-40°, which might indicate the presence of another phase or impurity. However, further investigation would be needed to identify it. Amorphous content, similar to the previous analysis, TFW-MCC, and TLW-MCC, shows broader peaks, suggesting that these samples have more amorphous cellulose (Tseng *et al*., 2022).

The broader and less intense peaks compared to the standard suggest a more disordered structure. This trend implies that the treatments applied to TFW-MCC and TLW-MCC might have broken down some of the crystalline structure, increasing the amorphous content. Tea leaf waste cellulose has the lowest crystallinity value, 60.95%, as determined by equation 1 (Table 7). Standard cellulose has the highest crystallinity Index value, 70.44 percent, which qualifies for the removal of the amorphous portion of cellulose by acid hydrolytic cleavage of 1,4-glycosidic bonds. The crystallinity index of cellulose and microcrystalline cellulose in this study ranged from 55% to 80%. The range of crystallinity in the sample and standards was comparable to that of a prior investigation (Nsor-Atindana *et al*., 2017). The crystal size increased from 2.21 nm to 9.53 nm, with standard cellulose having the smallest size and tea leaf waste cellulose having the largest. These values were also determined using Equation 3. Additionally, all the d-spacing values, calculated using Equation 3, are less than one. As a result, all parameters conducted on the cellulose and MCC crystallinity were comparable with a study reported by Getachew *et al*. (2023).

Table 7. Crystalline properties of cellulose and Microcrystalline cellulose powder.

Sample	Peak Positions	The area of the crystalline peaks	Total Area of the Crystalline Peaks	Total Area of the Crystalline & Amorphous Peaks	Crystallinity Index in percent CI%	Crystallite sizes L (nm)	d-spacing (d) value
STD-C	15.02	4946.84	16502.08	23426.14	70.44%	2.21	0.70
	22.46	9966.86					
	34.58	1254.88					
	43.94	333.5					
TFW-C	15.86	3260.88	10955.7	17023.11	64.36%	7.62	0.83
	22.4	6408.98					
	34.66	943.56					
	43.94	342.28					
TLW-C	16.56	750.64	8601.88	14112.18	60.95%	9.53	0.86
	21.64	4300.18					
	29.16	362.6					
	32.38	853.08					
	33.58	457.02					
	36.34	494.3					
	37.92	290.58					
	40.04	194.22					
	41.42	197.88					
	43.92	411.24					
	45.18	290.14					
STD-MCC	14.96	4201.2	13675.76	20959.92	65.25%	7.92	0.78
	22.58	8092.64					
	34.56	1103.6					
	43.94	278.32					
TFW-MCC	15.72	3361.98	11626.52	17613.39	66%	8.35	0.79
	22.22	6585.34					
	34.72	934.12					
	37.7	237.92					
TLW-MCC	15.96	3130.2	11127.6	17810.12	62.48%	8.64	0.78
	21.94	6893.92					
	34.9	870.18					
	43.98	233.3					

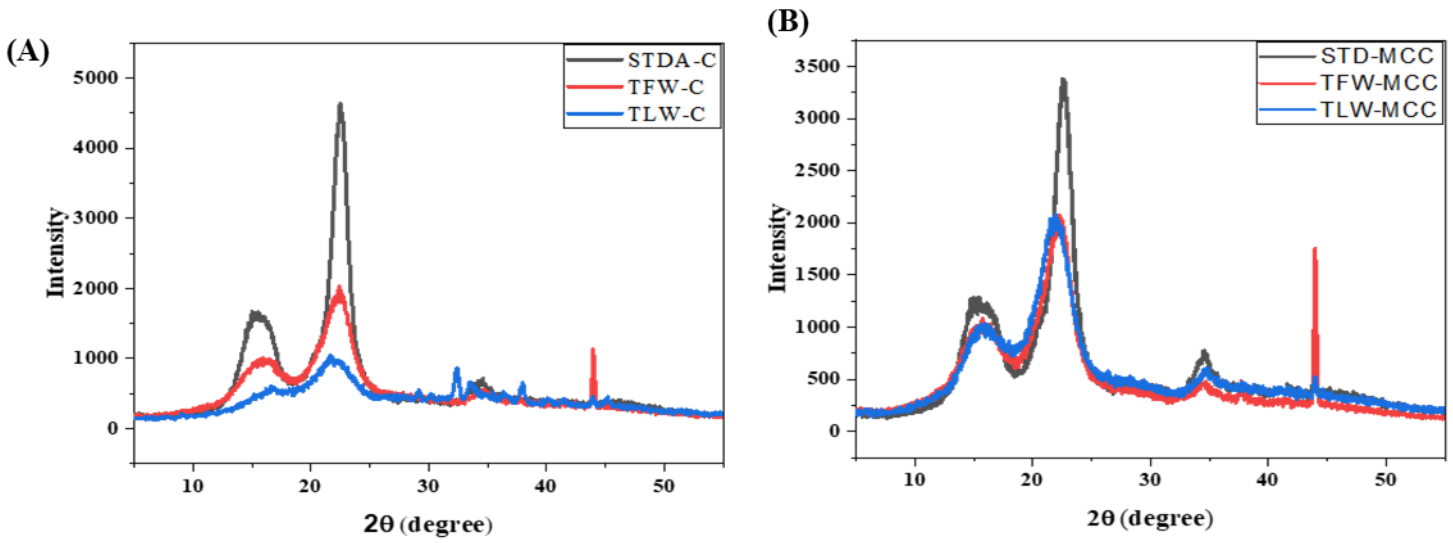

Figure 12. X-ray diffraction patterns of Cellulose (A) and Microcrystalline cellulose (B).

3.3.4. Morphology analysis of cellulose and MCC

Various scanning electron microscope images from tea waste extract samples, TFW, TLW, standard cellulose, and MCC are presented. Cellulose samples and standard cellulose exhibit a fibrous structure, typically characterized by long fibers and an interconnected network of fibrils. The surface of raw cellulose fibers may appear relatively smooth, with visible microfibrils running parallel to the fiber axis. Native cellulose fibers contain pores, grooves, or precipitates that are remnants of the plant cell wall structure. Generally, cellulose images reveal closely engaged microfibrils and ligaments. In contrast, SEM analysis displays a compact surface of the raw material, excluding natural complications, which leads to the formation of MCC (Figure 13) (Gabriel *et al*., 2020). The resulting MCC particles are irregularly shaped and compact, indicating a significant change in cellulose structure after hydrolysis. The alkali treatment and resulting structural changes have been shown in another study, where raw date fibers, initially in fine powder, transform into large spherical particles after alkaline treatment. This change indicates the self-organization behavior of the fibril structure. It suggests that the alkali treatment alters the fiber morphology. SEM observations of MCC indicate that the alkali treatment influences the fiber morphology. SEM observations from MCC, alongside standard MCC images of TFW and TLW samples, displayed a rough mine and softly wrapped morphology similar to standard MCC. These morphological features enhance the surface area of MCC and improve interfere interactions between hydroxyl groups (Tessema *et al*., 2023; Kunusa *et al*., 2018).

The increased surface area and interactions may contribute to the dry bond properties of MCCs. Morphological changes, such as enhanced surface area and rough texture, improve the functional properties of MCC, particularly binding capabilities. These results underscore the significance of chemical treatments in altering the structure and properties of cellulose, ultimately facilitating the production of MCCs with desirable characteristics for various applications (Figure 14). With its fragments and uneven surfaces, tea-waste cellulose resembles a complex, porous plant matrix. The fibrous and uneven appearance of cellulose powder preserves the shape of natural plant fibers. Higher purification and carefully regulated processing give MCC a uniform, crystalline, and granular appearance (Dignani *et al.*, 2020).

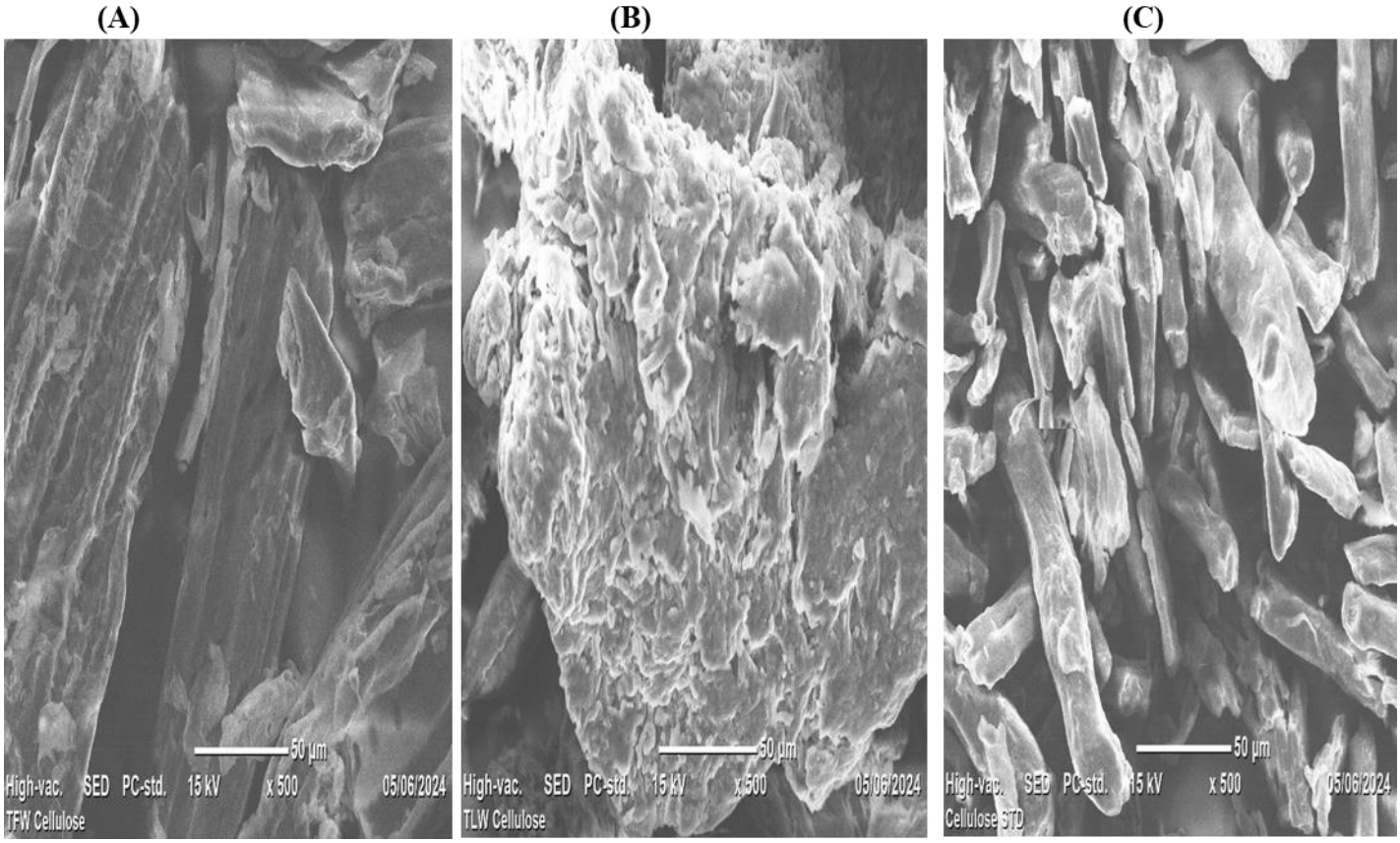

Figure 13. Scanning electron microscopy image of Cellulose Tea fiber waste (A), Tea Leaf Waste (B), and Standard cellulose (C).

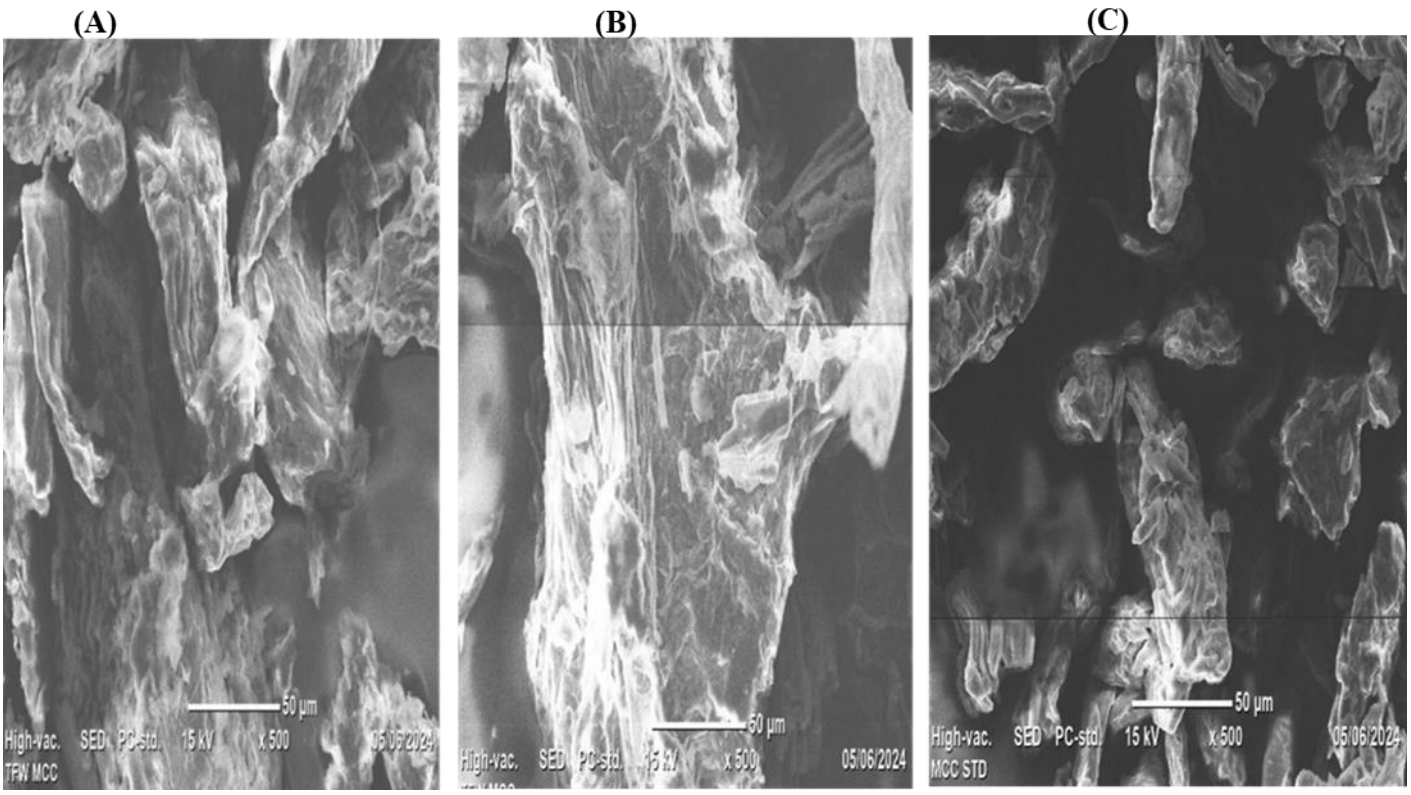

Figure 14. Scanning electron microscopy image of Microcrystalline cellulose, Tea fiber waste (A), Tea Leaf Waste (B), and Standard cellulose (C).

3.4. Physicochemical test and Powder property study

3.4.1. Physicochemical test of Microcrystalline cellulose powders

The physicochemical parameters, including identification and solubility, were compiled based on the pharmacopeia (Table 8). The pH value of TLW-MCC and TFW-MCC powder is slightly more acidic than Avicel PH-101. Ether-soluble substances of Avicel pH-101(3.3mg) powder are lower than TLW-MCC (4.5mg) and TFW-MCC (4.3mg), indicating an increase in carbon atoms in the molecule. Water-soluble substances of microcrystalline cellulose powder of the three samples were almost comparable; the result was less than 12.5 mg based on USP/BP. The total ash value of the TLW-MCC and TFW-MCC samples indicates a tiny amount, but in the case of Avicel PH-101 Nill, it is absent. Moisture content of the three samples of less than 3% indicates no moisture absorbed. Several studies have also reported that in the physicochemical analysis study of MCC, the results obtained from TLW and TFW did not vary from the

literature (Tessema *et al*., 2023; Nasution *et al*., 2017; Adeleye *et al*., 2022; Priyangga *et al*., 2021). The results of the physicochemical test were comparable to the literature and met the pharmacopeia limit.

Table 8. Some physicochemical parameters of Microcrystalline cellulose powders.

Parameter	Obtained Result			Limit based on the specification	Method used
	TLW-MCC	TFW-MCC	Avicel PH-101		
Identification	Complies	Complies	Complies	The substance takes on a violet-blue color.	USP/BP
Solubility	Complies	Complies	Complies	Practically insoluble in water, in acetone, in anhydrous ethanol, in toluene, in dilute acids, and solutions of sodium hydroxide	USP/BP
Organoleptic characteristics	Complies	Complies	Complies	Slightly white and odorless in physical appearance, MCC is a fine powder.	USP/BP
Degree of polymerization	208.15±2.17	236.75 ±4.88	238. 23 ±3.18	Acceptance criteria DP is NMT 350.	USP/BP
pH	5.5 ± 0.3	5.7 ± 0.2	6.0 ± 0.2	5.0–7.5	USP/BP
Ether-soluble substances	4.5 ± 0.1mg	4.3 ± 0.2mg	3.3 ± 0.2mg	Not more than 5.0 mg (0.05%)	USP/BP
Water-soluble substances	10 ±0.5mg	10.5 ±0.4 mg	8 ±0.5mg	Not more than 12.5 mg (0.25%)	USP/BP
Total ash (%)	0.05%	0.08%	Nill	Total ash (%) ≤0.1%	USP/BP
Moisture content	2 ± 0.25%	2.8 ± 0.5%	2.1 ± 0.25%	Not more than 7.0%	USP/BP

3.4.2. Comparative powder characteristics of isolated Microcrystalline cellulose Powder

In the comparison between the powder flow properties of the three samples, the angle of repose of TLW-MCC is lower than that of TFW-MCC and Avicel PH-101, which indicates that a lower angle of repose has better flowability (Table 9). The three MCC powders have similar bulk density but different tapped densities. TFW-MCC was lower, and Avicel PH-101 is higher. A lower tapped density for microcrystalline cellulose shows that the powder is less compactly packed. This can imply that the powder has good

flowability (Table 8). The Carr's Indices of the three MCC samples (TLW-MCC, TFW-MCC, and Avicel PH-101) were equivalent to 32.65 %, 31%, and 32.98%, respectively. TLW-MCC and TFW-MCC have lower Hausner's ratio values than Avicel PH-101, indicating packing properties and better flowability, which is important for direct compression tableting processes (Yohana Chaerunisaa *et al*., 2019). The true density of TLW-MCC, TFW-MCC, and Avicel PH-101 was comparable, with no exaggerated differences. The porosity of the powder depends on both bulk density and true density; however, the three MCC powders have similar bulk densities. In addition, TLW-MCC and TFW-MCC have a highly porous powder, but Avicel PH-101 has a lower porosity.

The swelling capacity of microcrystalline cellulose powder is an important property, particularly in the pharmaceutical industry (Rana *et al*., 2022). A high swelling capacity in MCC typically indicates its ability to absorb water and expand, and some key indications for high swelling capacity in MCC powder were binders in Tablet formulations, as a result, TLW-MCC (37.5%) and TFW-MCC (39.39%) powder had comparable swelling capacity, but Avicel PH-101 had a lower swelling capacity (Achor *et al*., 2014). Therefore, the high swelling property (TFW-MCC) helps to ensure that tablets remain intact during storage but disintegrate appropriately upon ingestion, aiding in the controlled release of the active ingredient (tablet). Almost similar densities and related powder properties were reported for MCC powders isolated from Teff Straw and *Cordia africana Lam.* Seeds by Getachew *et al*.2023 and Tessema *et al*.2023, respectively.

Table 9. Powder properties of microcrystalline cellulose.

Parameters	TLW-MCC (Mean ± SD)	TFW-MCC (Mean ± SD)	Avicel (Mean ± SD)
Angle of repose (°)	17.31±0.09	18.21±0.05	19. 37 ±0.11
Bulk density (g/mL)	0.16±0.1	0.16±0.1	0.16±0.1
Tapped density (g/mL)	0.24±0.2	0.23±0.2	0.44±0.3
Carr's index (%)	32.65±0.3	31±0.3	32.98 ± 0.2
Hausner's ratio	1.48±0.41	1.45±0.32	1.76±0.40
True density (g/mL)	1.357±0.10	1.372±0.111	1.523±0.145
Porosity (%)	88±0.5	88±0.6	81±0.5
Swelling capacity (%)	37.5±0.25	39.39±0.45	31.42±0.37

3.5. Moisture sorption capacity

The moisture sorption capacity indicates how sensitive a powder material is to moisture. Different cellulose sources and forms exhibit varying sorption capacities due to differences in their structure and surface properties. Moisture sorption in cellulosic materials mostly takes place in the bulk of disordered areas (Mihranyan *et al*., 2004). According to Ohwoavworhua and Adelakun (2010), the amount of amorphous cellulose present determines how much water cellulose can adsorb because the crystalline portion of cellulose cannot. Because it shows the physical stability of tablets under humid storage conditions, the moisture sorption capacity of MCC is essential (Pandey *et al.*, 2015). The moisture absorption capacities of TLW-MCC, TFW-MCC, and Avicel PH-101 are displayed in Figure 15 for 30 days at varying relative humidity (RH) levels (20, 30, 75, 85, and 100%). At 100% relative humidity, all three samples TLW-MCC, TFW-MCC, and Avicel PH-101, showed significant weight gain (24.1%, 23.2%, and 25.6%, respectively).

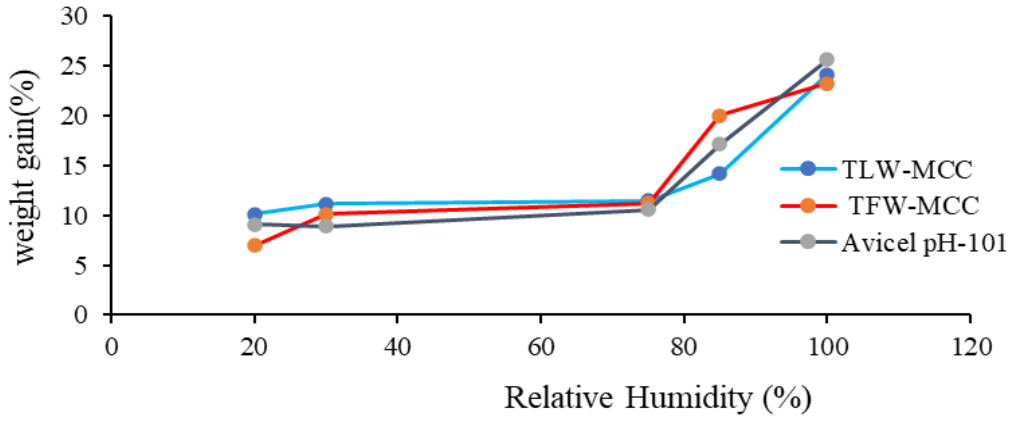

Figure 15. Moisture sorption pattern of Tea leaf waste -waste-Microcrystalline cellulose, Tea fiber waste-Microcrystalline cellulose, and Avicel PH-101 at room Temperature.

3.6. Particle size and Size distribution

Particle size and size distributions of MCC powders are presented in Table 10. It is common practice to include the following details when reporting the particle size and distribution of TLW, TFW, and Avicel-PH-101 powders: a summary of the average particle size (often provided as the median particle size, or D50) and the particle size distribution curve (often displayed as a percentage of particles across various size ranges) (Figure 16) (Fraser, 2013). The mean particle sizes for each sample were TLW at 143.3 µm, TFW at 139.59 µm, and Avicel-PH-101 at 78.26 µm. From these values, Avicel-PH-101 has the smallest

mean particle size, resulting in a larger surface area per unit mass, which can influence properties like reactivity and solubility. The size distribution percentiles D (v, 0.1), D (v, 0.5), and D (v, 0.9) indicated lower values for Avicel-PH-101, while TLW and TFW MCC powders showed comparable particle size distributions. TLW powder exhibited a meaningfully narrower particle size distribution (lower span value) compared to Avicel-PH-101 and TFW MCC powders. Both TLW and TFW MCC powders consisted of larger particles, typically with lower specific surface areas because they exposed less surface area per unit mass and contained more fragmented particles compared to Avicel-PH-101 (Annina Lähdeniemi *et al.,* 2024). A parallel study on the particle size distribution of MCC powder derived from wheat straw intended D (v, 0.1), D (v, 0.5), and D (v, 0.9), with slight variations in the values (Krivokapić *et al*., 2020).

Table 10. Volumetric mean particle size and size distribution of Microcrystalline cellulose powders.

Parameters	MCC powder		
	TLW	TFW	Avicel PH-101
Mean particle size (µm)	143.33±4.79	139.59±2.67	78.26±2.51
Size distribution percentile (µm)			
D (v, 0.1)	26.67±1.12	28.27±0.49	7.57±0.16
D (v, 0.5)	101.36±4.95	108.75±3.74	32..22±0.22
D (v, 0.9)	225.50±6.12	214.94±7.08	81.87±2.20
Span = [(D (0.9) -(0.1)/D (0.5]	2.48±4.06	2.16±3.71	2.306±0.86
Specific surface area (m^2/g)	0.245±0.04	0.260±0.03	0.30±0.03

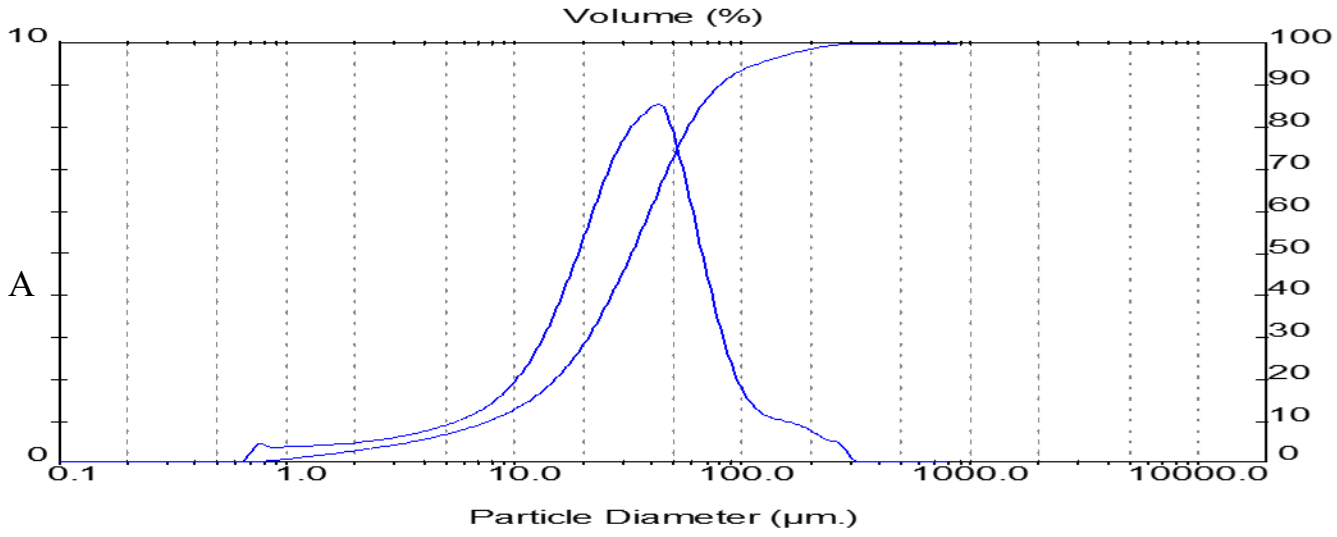

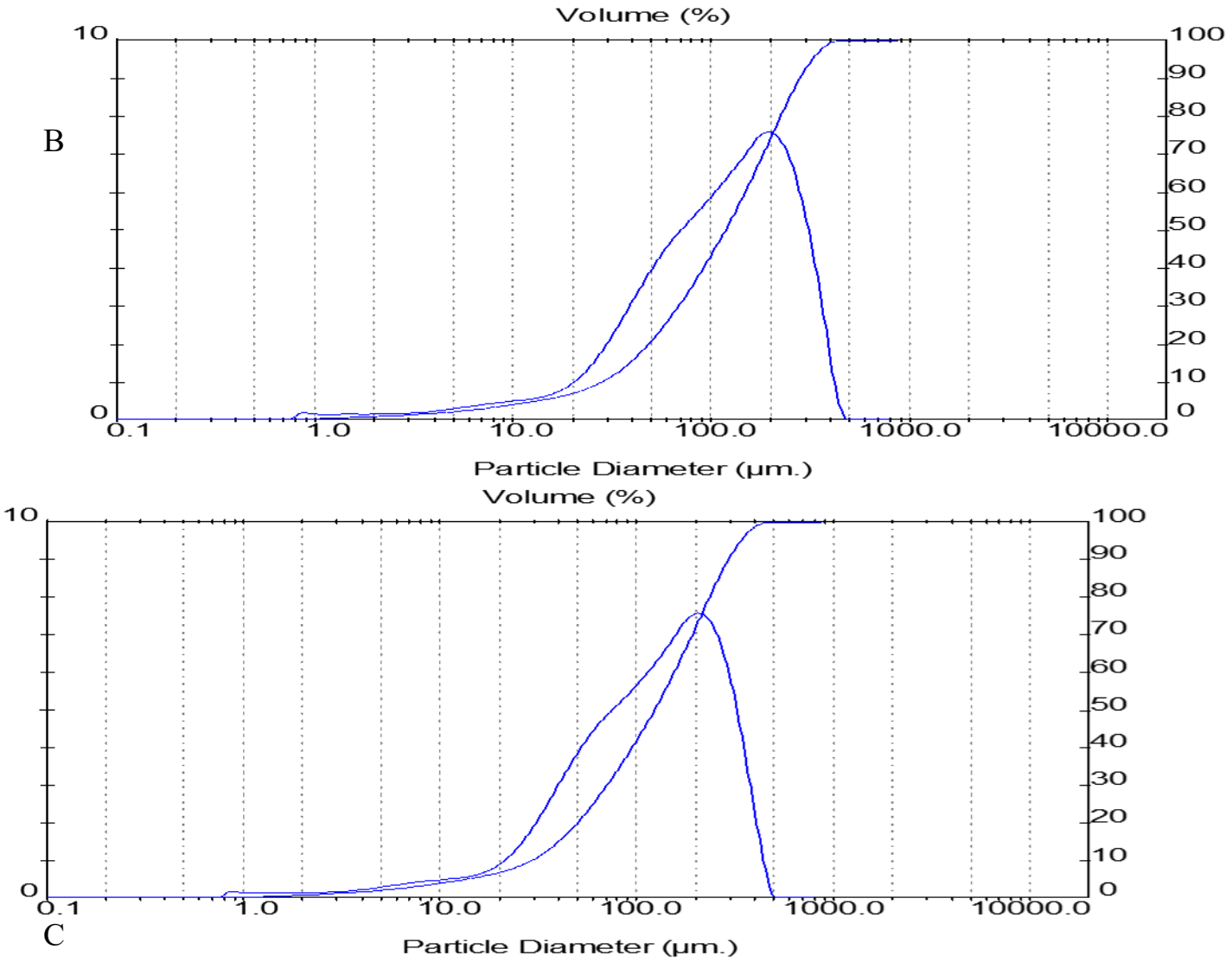

Figure 16. Particle size distribution of (A) Avicel PH-101, (B)Tea leaf waste, and (C)Tea fiber waste of Microcrystalline cellulose powders.

3.7. Compatibility study of a PCM drug with Microcrystalline cellulose excipient using FTIR

Compatibility studies of paracetamol and MCC often involve FTIR and measure the possible chemical or physical alterations in the drug and excipient at the molecular level. Incompatibilities, if any, are identified through the functional group of the compound and can alter the drug's molecular structure with an excipient (Diño *et al*., 2023). Paracetamol with MCC exhibits a distinct spectral form of hydroxyl O-H stretching at 3319 cm^{-1} broad peak, N-H stretching at 3100 cm^{-1}, carbonyl C=O stretching at 1650 cm^{-1}, C-H stretching at 2916cm^{-1}, and aromatic C=C benzene stretching near 1600 cm^{-1}. These spectra of paracetamol are of

MCC powder mixed with paracetamol and pure paracetamol. Paracetamol peaks are recognized for their distinct qualities from those of MCC, which also has paracetamol and exhibits a broad 3319 cm^{-1} peak assigned to hydroxyl groups O-H and C-C stretching around 2916 cm^{-1} due to aliphatic groups and C-O-C couple C-H-H ion 1050-1150 glycoside linkage, which are observed in all MCC spectra (Figure 17). The compatibility assessment enables the comparison of the spectra of physical mixtures and the components of various blends. The spectral patterns of the physical mixtures differ from those of the individual components in the blends. Changes in the stoichiometry and the identity of the components suggest the masking of functional groups or the formation of hydrogen bonds. Unwanted peaks during peak allude or disappearance peaks suggest possible reaction or degradation, but not unwanted peaks. In general, a compatible system did not meaningfully change the position or intensity of the characteristic peaks. The overlaid spectra of the mixtures should look something like a superposition of the individual spectra. FTIR spectra of physical mixtures compared to the individual spectra of their components, paracetamol and MCC, show no significant change, and these studies were comparable with recent literature (Dave *et al*., 2015; Shah, 2017).

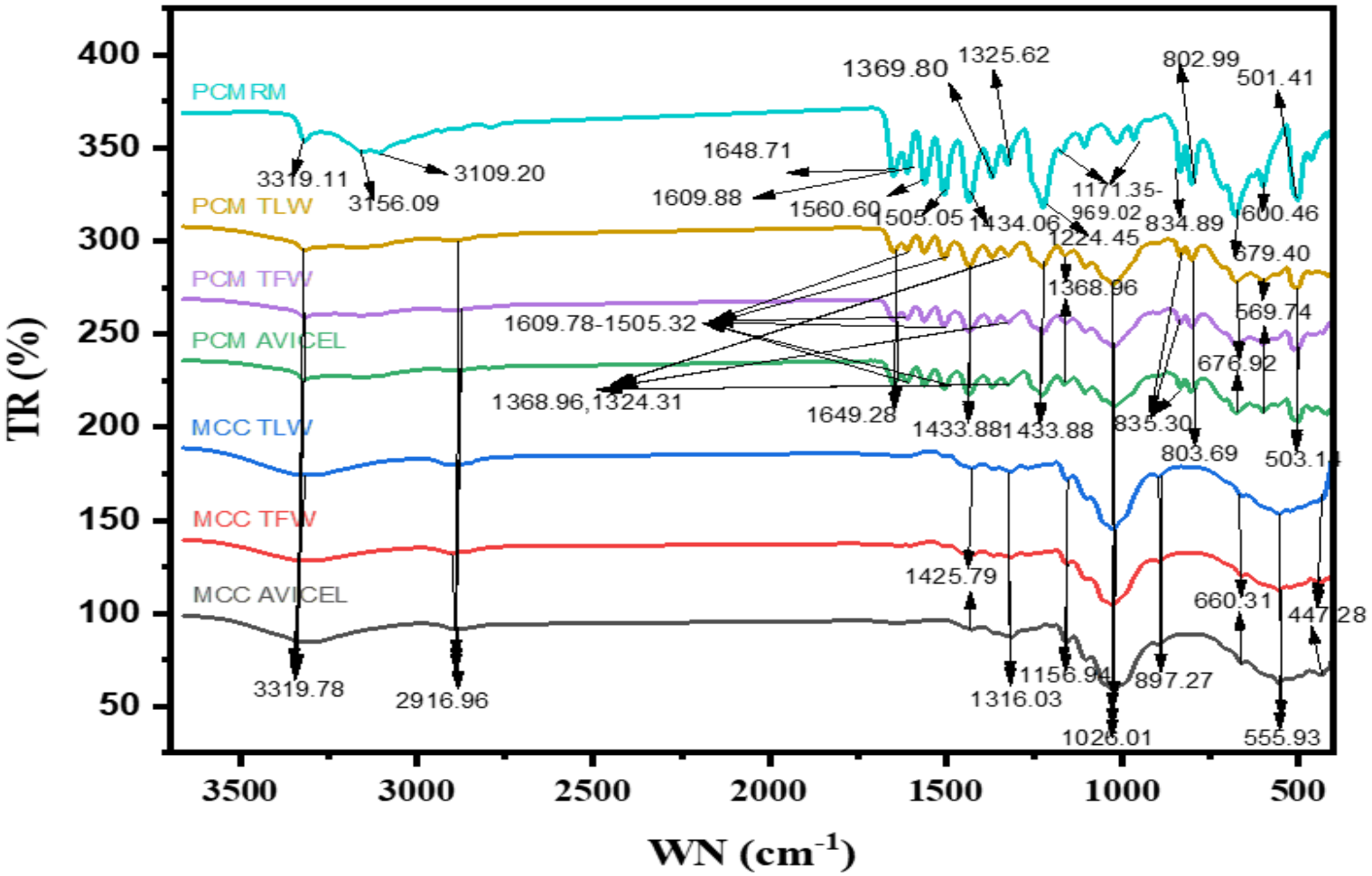

Figure 17. FTIR spectrum of Paracetamol DC Raw material, and Microcrystalline cellulose powder.

3.8. Result of Microbial Limits Testing of Microcrystalline cellulose

In the Total Aerobic Bacterial Count test, all samples of MCC (TLW, TFW, STD) showed negative results, indicating no bacterial colonies were present. In addition, a test of the total fungal count of all the samples of MCC (TLW, TFW, STD) is negative, and the result doesn't show any fungal colonies. All the samples of MCC (TLW, TFW, STD) have negative results in the *Escherichia coli* test. Moreover, it doesn't show the character of E. coli colonies, which are non-mucoid, brick-red colonies of Gram-negative rods. All the samples of MCC (TLW, TFW, STD) have negative results in *Salmonella* testing, and they didn't show the characteristics of Salmonella colonies, which are red colonies with or without a black center. All the samples of MCC (TLW, TFW, STD) are tested for *Staphylococcus aureus* result is negative. Moreover, it doesn't show the character of *Staphylococcus aureus*, which are yellow colonies with yellow zones. Finally, the specific microorganism tested showed negative results in all samples of MCC (TLW, TFW, STD), and

no colonies of *Pseudomonas aeruginosa* were observed, which are generally gray. The negative control of all tests remains negative throughout the incubation period, indicating that the test was valid (Figure 18). All the microbial tests and specific microorganism tests met the pharmacopeia requirements (USP, 2019, BP, 2009).

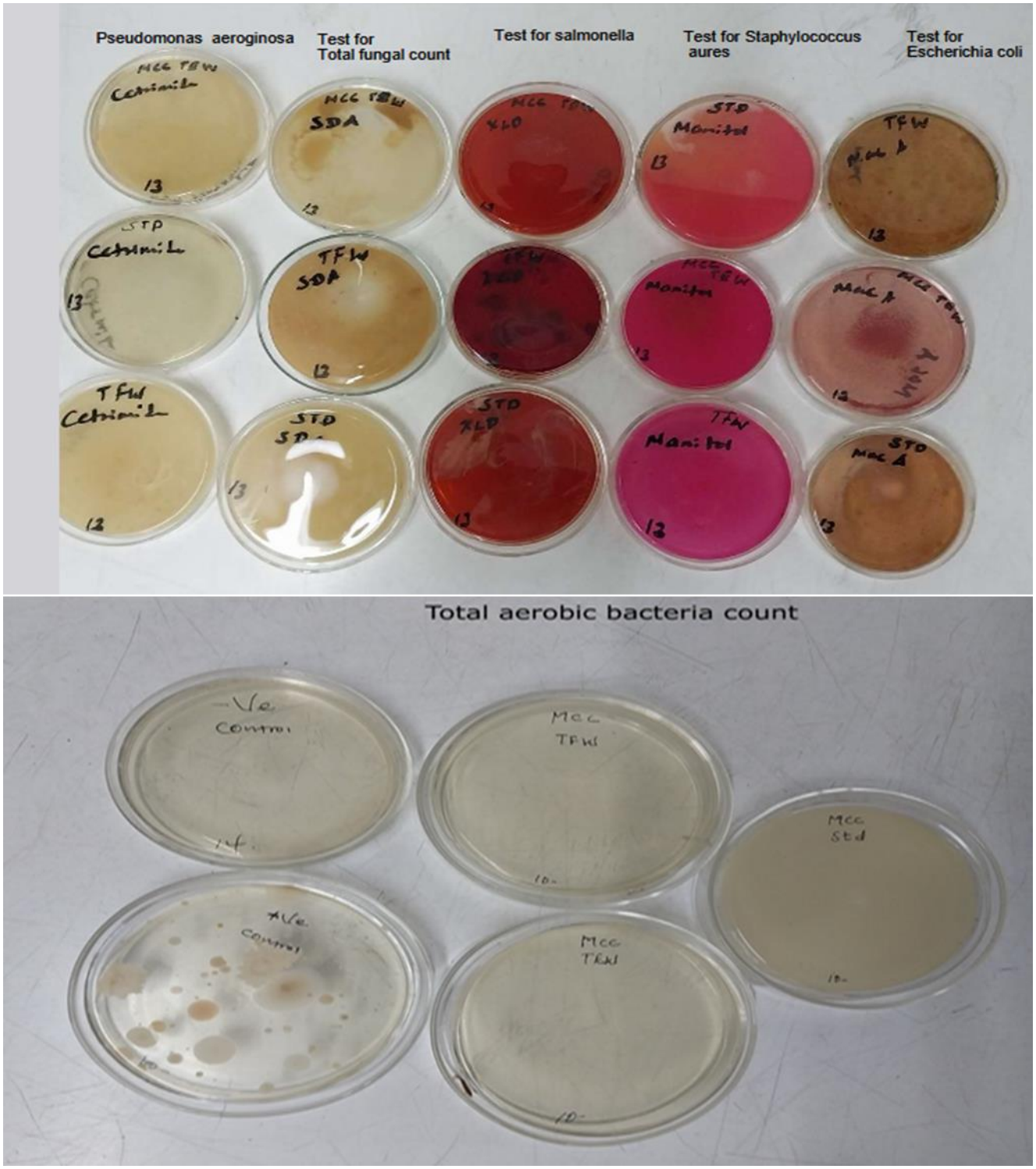

Figure 18. Image of Microbial Limits Testing of microcrystalline cellulose powder.

3.9. Evaluation of Formulated Tablet

3.9.1. Physical quality evaluation of Formulated tablet

The various physical properties include weight variation, friability, hardness, thickness, and diameter. The weight variation of the three formulations of paracetamol 250 mg, with an average weight of 355 mg, is within the pharmacopeia limit of ±5% (337.25-372.75 mg) (USP, 2012). Although it depends on the size of the blistering machine, paracetamol pills are normally about 4.10 mm thick, with a tolerance of ± 0.2 mm. The designed paracetamol pills exhibit low hardness when the compression force is low, and high hardness (7.3–9.8 kPa) when the compression force is high. Unfortunately, the compression force could not be adjusted manually (minimum, middle, and high) because the compression machine did not display the applied force. Generally, the size of the blended powder and the pressure used can affect how hard a tablet. The standard diameter is approximately 9.5 mm, with a tolerance of ± 0.2 mm. All designed paracetamol tablets normally have a friability of less than 1%. Regarding additional physical characteristics of paracetamol tablets, the uncoated tablets had a disintegration limit of less than 15 minutes, while the formulated tablets typically disintegrated in under a minute (Table 11). These results were consistent with pharmacopeial standards and previous literature.

Table 11. Common physical quality control parameters.

Quality parameters	F_1			F_2			F_3			RD
Compression force	Min	Mid	High	Min	Mid	High	Min	Mid	High	-
Weight variation*	354 ±7.4	356 ±8.5	357 ±7.5	358 ±8.14	353 ±6.7	356 ±6.81	353 ±5.5	356 ±8.5	350.5 ±6.35	5709± 3.1
% Friability*	0.82 ± 0.5	0.75 ±0.4	0.66 ±0.41	0.84 ±0.45	0.74 ±0.46	0.67 ±0.56	0.85 ±0.42	0.78 ±0.42	0.70 ±0.41	0.68± 23
Hardness (k. Pas) *	7.4±0. 4	8.5± 0.5	9.7±0. 6	7.3±0. 3	8.7±0. 2	9.8±0. 6	7.3± 0.6	8.7±0. 2	9.8± 0.4	9.8±1. 4
Thickness*	4.2±0. 12	4.2± 0.2	4.1±0. 2	4.12± 0.1	4.1±0. 12	4.2 ±0.15	4.12 ±0.2	4.11± 0.1	4.12 ±0.2	4.12 ±2
Diameter*	9.51±0 .12	9.53 ±0.1 5	9.51± 0.13	9.50± 0.16	9.47± 0.14	9.51± 0.16	9.51 ±0.1 2	9.49± 0.13	9.51 ±0.1 6	12.12 ±0.16
Disintegration time*(sec.)	30±5	40±6	50±7	31±4	42±5	45±5	30±5	34±4	48±6	55±3

* Mean ± SD; F1- Paracetamol tablet formulated using TLW-MCC; F2 -Paracetamol tablet formulated using TFW-MCC; F3- Paracetamol tablet formulated using Avicel PH-101.

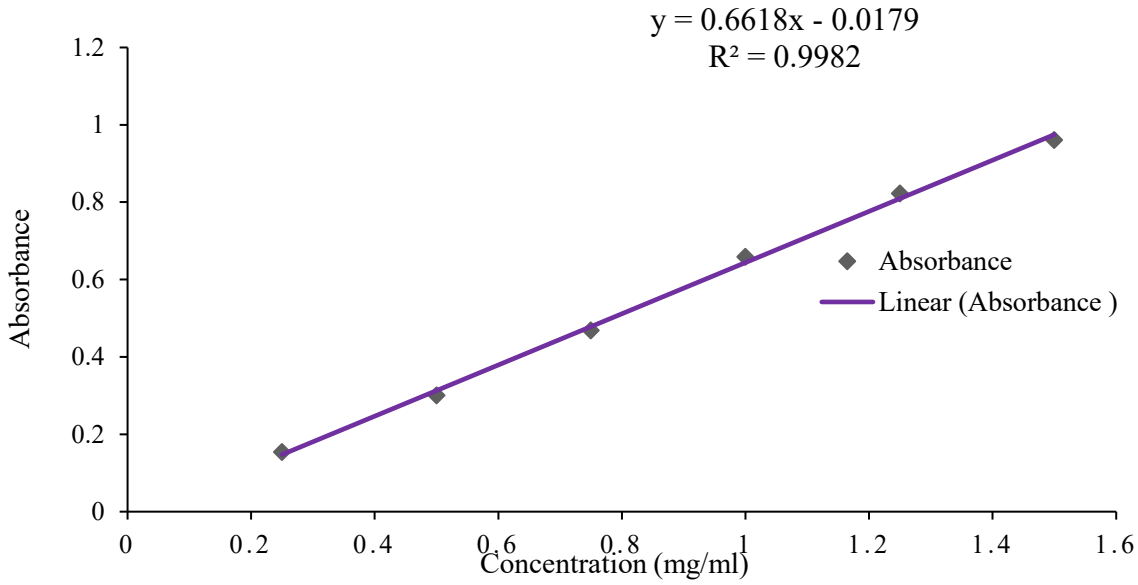

Figure 19. Calibration curve of Paracetamol Working reference standard.

3.9.2. Dissolution profile of paracetamol tablets

Dissolution profiles, shown in Figures 20A, B, and C, depict the dissolution behavior of the F_1, F_2, F_3, and reference drugs of paracetamol tablets. The results indicate that all formulations meet the British Pharmacopoeia requirements, which state that not less than 80% of the drug should dissolve within 60 minutes for conventional solid dosage forms. This requirement was satisfied by all tested formulations. As detailed in Table 12A and Table 12B, the highest percentage release was observed in F_1 at the middle compression force after 60 minutes, reaching 104.17%. The lowest percentage release was seen in the F_3 (High CF) sample at 10 minutes, with 86.23%. Generally, all *in vitro* releases of the formulations (F_1, F_2, and F_3) of paracetamol tablets exceeded 90% of the active pharmaceutical ingredient (API) within 10 minutes, indicating complete release. In F_1, drug release at 10 minutes was 89.24% at both high and middle compression forces, with a peak release of 104.17% (Figure 20). For F_2, the PCM also showed rapid release, with a minimum of 89.13% and a maximum of 103.62% at the lowest compression force. F_3 demonstrated a minimum dissolution rate of 86.23% at 10 minutes at high compression force and 99.40% at 20 minutes

at middle compression force. Lastly, the reference drug exhibited dissolution rates ranging from 88.91% to 94.53%, with the lower concentration recorded in the initially released (Tables 12A and 12B). This result contradicts the findings of studies conducted by Abdulmajed and Abdullah (2018, 2024), where all evaluated formulations passed the dissolution test. Similarly, in a study conducted in Bangladesh in 2020 by Vandy *et al.* (2024), all assessed samples also passed their dissolution tests

Table 12A. Drug release profile of the formulated paracetamol tablet of F_1 and F_2.

Time	F_1						F_2					
	Minimum CF		Middle CF		High CF		Minimum CF		Middle CF		High CF	
	Abs	%DR	Abs	%DR	Abs	%DR	Abs	%DR	Abs	%DR	Abs	%DR
10min	0.615	93.16	0.623	94.44	0.589	89.24	0.592	89.13	0.614	92.47	0.620	93.37
	±0.01	±1.04	±0.01	±1.55	±0.01	±1.55	±0.01	±1.24	±0.01	±0.73	±0.00	±0.42
20min	0.641	97.15	0.640	96.94	0.650	98.54	0.647	97.36	0.625	94.18	0.616	92.72
	±0.01	±0.93	±0.01	±1.61	±0.01	±1.38	±0.01	±2.07	±0.01	±1.04	±0.01	±1.41
30min	0.667	101.11	0.662	100.33	0.687	104.12	0.688	103.62	0.627	94.38	0.612	92.14
	±0.01	±1.59	±0.01	±1.82	±0.01	±0.96	±0.01	±1.19	±0.01	±1.72	±0.01	±1.29
40min	0.676	102.37	0.666	100.86	0.665	100.71	0.665	100.10	0.621	93.47	0.611	91.94
	±0.02	±2.28	±0.01	±1.63	±0.01	±1.10	±0.01	±1.48	±0.01	±1.11	±0.01	±1.31
50min	0.674	102.1	0.674	102.17	0.664	100.63	0.666	100.23	0.624	93.93	0.609	91.74
	±0.02	±2.45	±0.01	±0.88	±0.01	±1.27	±0.01	±1.99	±0.01	±2.22	±0.00	±0.38
60min	0.674	102.1	0.688	104.17	0.663	100.53	0.662	99.70	0.615	92.55	0.600	90.36
	±0.02	±2.45	±0.01	±1.07	±0.01	±1.13	±0.01	±0.961	±0.01	±2.01	±0.01	±1.41

F_1 was formulated by using TLW-MCC, F_2 was formulated by using TFW-MCC, CF- compression force, Abs- Absorbances, %DR- percent of drug released.

Table 12 B. Drug release profile of the formulated paracetamol tablet of F_3 and the reference drug.

Time	F_3						Reference drug (Commercial drug)	
	Minimum CF		Middle CF		High CF			
	Abs	%DR	Abs	%DR	Abs	%DR	Abs	%DR
10min	0.629	94.33	0.663	99.40	0.575	86.23	0.593	88.91
	±0.01	±1.56	±0.01	±1.96	±0.01	±1.36	±0.01	±1.44
20min	0.636	95.08	0.663	99.40	0.582	87.18	0.627	94.06
	±0.02	±2.33	±0.01	±1.96	±0.01	±1.73	±0.01	±0.84
30min	0.634	95.08	0.650	97.53	0.580	86.88	0.649	97.36
	±0.02	±2.67	±0.02	±2.79	±0.01	±2.99	±0.01	±1.83
40min	0.641	96.03	0.647	96.95	0.600	89.91	0.658	98.7
	±0.02	±2.85	±0.01	±1.68	±0.01	±1.22	±0.02	±3.46
50min	0.648	97.10	0.624	93.55	0.621	93.10	0.662	99.38
	±0.04	±5.94	±0.04	±5.44	±0.01	±1.64	±0.01	±1.05
60min	0.595	89.18	0.619	92.85	0.616	92.30	0.670	100.53
	±0.01	±1.24	±0.02	±0.97	±0.01	±1.30	±0.01	±1.62

F_3 was formulated by using Avicel PH 101-MCC, CF- Compression force, Abs- Absorbances, %DR- percent of drug released.

One important criterion for managing and evaluating drug quality is the similarity of the dissolution profiles, which is assessed using the f2 factor determined by Equation (18). For two curves to be statistically similar, the dissolution values of the reference batch and the test batch must be between $50 < f2 < 100$. High f2 values indicate small average differences (Shah *et al*., 1999). Scatter diagrams of the f2 values were generated using the proposed method for each formulation. The f2 values for formulation F1 at minimum CF, middle CF, and high CF were 55.28, 54.28, and 60.61, respectively, all above 50, indicating good similarity with the reference batch. For formulation F2, the f2 values at minimum CF, middle CF, and high CF were 63.60, 61. 34, and 56. 98, respectively. These values, closer to 100, suggest a strong similarity between the reference and test batches. In contrast, the f2 values for formulation F3 at minimum CF, middle CF, and high CF were 55.49, 49. 22, and 50. 02, respectively. Notably, the middle CF value for F3 fell below 50, indicating reduced similarity with the reference batch; however, the minimum CF and high CF

values were above 50, suggesting greater similarity to the reference batch (refer to Tables 13A, 13B, and 13C). Additionally, the f1 factor measures the percentage difference between the dissolution profiles of the reference and test products at each time point (Equation (17)). The f 1 values for all batches were below 15: for F_1 (minimum CF, middle CF, and high CF), they were 3.29, 3. 45, and 2.56, respectively, with higher values closer to zero indicating greater similarity. In formulation F_2, the f_1 values were 2.22, 2.47, and 3.03 at minimum CF, middle CF, and high CF, respectively, all near zero, which implies strong similarity and minimal dissimilarity with RD. For formulation F_3, the f1 values at minimum CF, middle CF, and high CF were 3. 29, 4. 36, and 4. 20, respectively, with all values close to zero, indicating they are more similar to F_1 relative to the reference batch, thus showing less dissimilarity (refer to Tables 13 A, 13 B, and 13 C). These findings also suggest that the suggested approach is dependable for carrying out precise and consistent drug dissolution testing (Hassouna *et al*., 2012).

Table 13 A. Comparison of the Similarity of the dissolution profiles of F_1 Paracetamol tablet.

Time interval in minute	Minimum CF		Middle CF		High CF	
	Rt	Tt	Rt	Tt	Rt	Tt
10	88.91	93.16	88.91	94.44	88.91	89.24
20	94.06	97.15	94.06	96.94	94.06	98.54
30	97.36	101.11	97.36	100.33	97.36	104.12
40	98.7	102.37	98.7	100.86	98.7	100.71
50	99.38	102.1	99.38	102.17	99.38	100.63
60	100.53	102.1	100.53	104.17	100.53	100.53
	Sum Rt=578.94		Sum Rt=578.94		Sum Rt=578.94	
	Sum (Rt-Tt) =19.02		Sum (Rt-Tt) =19.97		Sum (Rt-Tt) =14.83	
	Sum (Rt-Tt) ^{2}=362.90		Sum $(Rt-Tt)^2$ =398.80		Sum $(Rt-Tt)^2$ =219.93	
	Similarity factor f_2 =55.28		Similarity factor f_2 =54.28		Similarity factor f_2 =60.61	
	Difference factor f_1 = 3.29		Difference factor f_1 = 3.45		Difference factor f_1 =2.56	

F_1 was formulated by using TLW-MCC, CF- compression force, Abs- Absorbances, %DR- percent of drug released.

Table 13 B. Comparison of the Similarity of the dissolution profiles of F_2 Paracetamol tablet.

Time interval In minute	Minimum CF		Middle CF		High CF	
	Rt	Tt	Rt	Tt	Rt	Tt
10	88.91	89.13	88.91	92.47	88.91	93.37
20	94.06	97.36	94.06	94.18	94.06	92.72
30	97.36	103.62	97.36	94.38	97.36	92.14
40	98.7	100.10	98.7	93.47	98.7	91.94
50	99.38	100.23	99.38	93.93	99.38	91.74
60	100.53	99.70	100.53	92.55	100.53	90.36
	Sum Rt=578.94		Sum Rt=578.94		Sum Rt=578.94	
	Sum (Rt-Tt) =12.86		Sum (Rt-Tt) =14.32		Sum (Rt-Tt) =17.59	
	Sum $(Rt-Tt)^2$ =165.38		Sum $(Rt-Tt)^2$ =205.06		Sum $(Rt-Tt)^2$ =309.41	
	Similarity factor f_2 =63.60		Similarity factor f_2 =61.34		Similarity factor f_2 =56.98	
	Difference factor f_1 = 2.22		Difference factor f_1 =2.47		Difference factor f_1 =3.03	

F_2 was formulated by using TFW-MCC, CF- compression force, Abs- Absorbances, %DR- percent of drug released.

Table 13C. Comparison of the Similarity of the dissolution profiles of F_3 Paracetamol tablet.

Time interval in minute	Minimum CF		Middle CF		High CF	
	Rt	Tt	Rt	Tt	Rt	Tt
10	88.91	94.33	88.91	99.40	88.91	86.23
20	94.06	95.08	94.06	99.40	94.06	87.18
30	97.36	95.08	97.36	97.53	97.36	86.88
40	98.7	96.03	98.7	96.95	98.7	89.91
50	99.38	97.10	99.38	93.55	99.38	93.10
60	100.53	89.18	100.53	92.85	100.53	92.30
	Sum Rt=578.94		Sum Rt=578.94		Sum Rt=578.94	
	Sum (Rt-Tt) =19.02		Sum (Rt-Tt) =25.25		Sum (Rt-Tt) =24.34	
	Sum $(Rt-Tt)^2$ =361.76		Sum $(Rt-Tt)^2$ =638.07		Sum $(Rt-Tt)^2$ =592.44	
	Similarity factor f_2 =55.49		Similarity factor f_2		Similarity factor f_2	
	Difference factor f_1 = 3.29		=49.22		=50.02	
			Difference factor		Difference factor f_1= 4.20	
			f_1=4.36			

F_3 was formulated by using Avicel PH101-MCC, and formulated by using TLW-MCC, CF- compression force, Abs- Absorbances, %DR- percent of drug released.

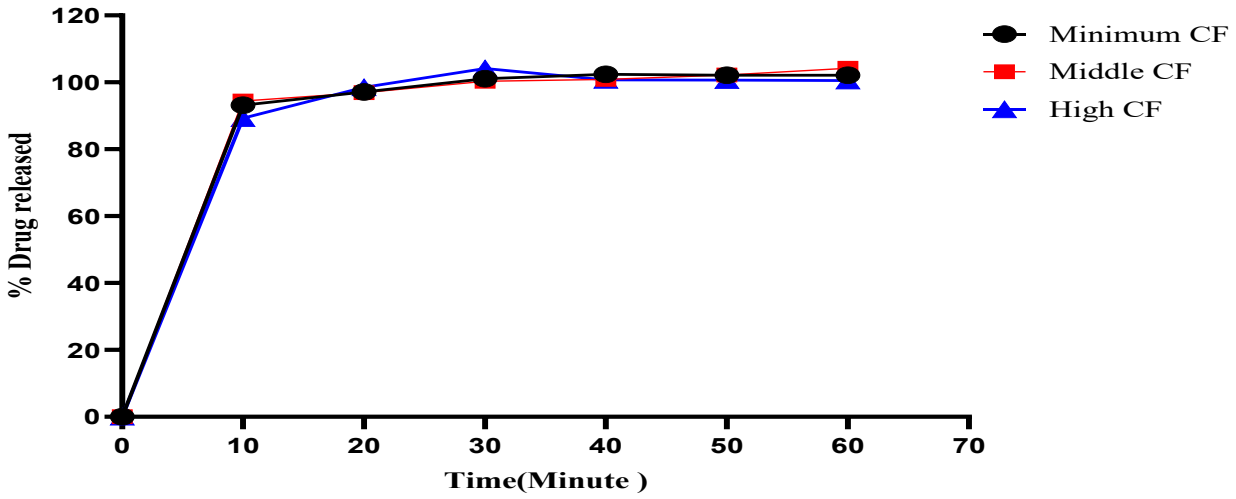

Figure 20A. Dissolution profiles of F_1 paracetamol tablets.

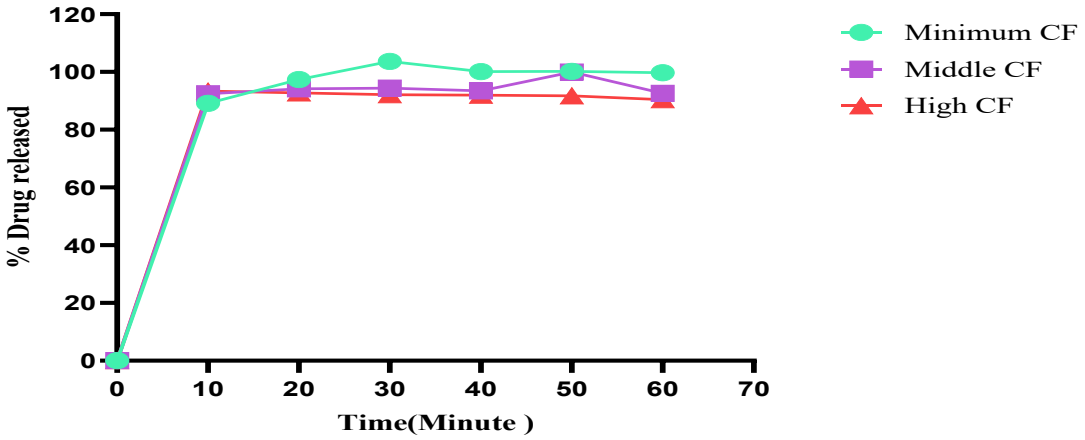

Figure 20B. Dissolution profiles of F_2 paracetamol tablets.

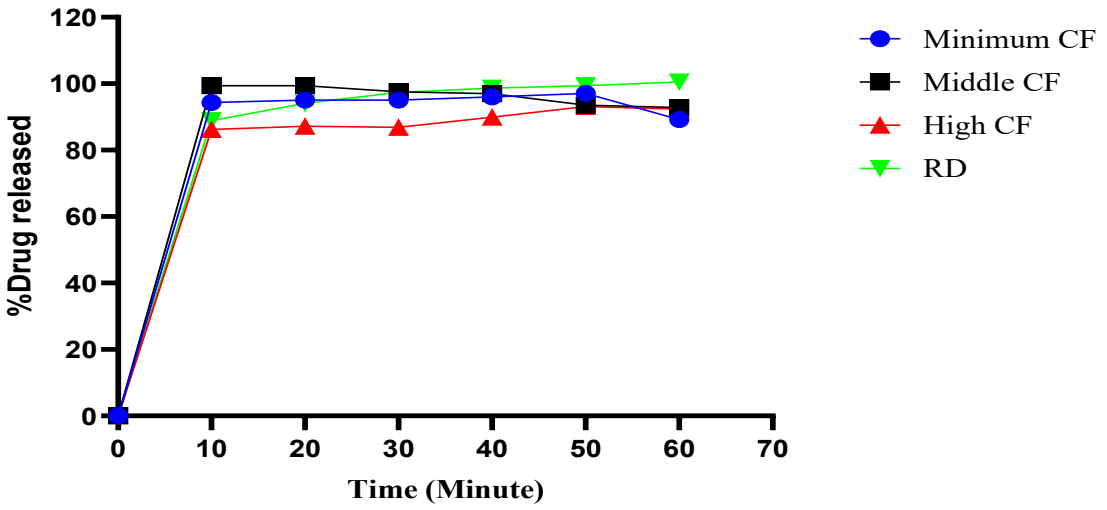

Figure 20C. Dissolution profiles of F_3 and Reference drug paracetamol tablets.

3.9.3. Assay of paracetamol tablets and identification test

The percentage of the active ingredient in each sample was ascertained by performing a drug content analysis on paracetamol tablets. Table 14 summarizes the assay test results, including peak area, height, retention time, tailing factor, theoretical plates, and concentration. The retention time of drug concentration is crucial for identifying samples, and it aligns with the reference samples within a similar range of 4.96 to 5.03. The tailing factor assesses column quality, with a maximum acceptable limit of two; all tested samples yielded results below this limit, ranging from 1.410 to 1.265. Both height and theoretical plates are important parameters for evaluating the system suitability of the column and mobile phase during HPLC analysis (Figures 22, 23, 24). The results of all sample analyses met the required standards and complied with the BP or USP pharmacopeia.

Peak area is a key parameter for determining the active pharmaceutical ingredient (API) concentration. A high peak area indicates a high concentration, while a low peak area suggests a low concentration. In these sample analyses, RD verified a high peak area (424807), F_2 at middle compression force showed a low peak area (372205), and the working reference standard exhibited an average peak area (398067).

The test percentages or concentrations for the various samples (F_1, F_2, F_3, and the reference drug) ranged from 93.62±1.162% (F_2 at the middle compression force) to 106.85±0.242% (the reference drug). According to the British Pharmacopoeia (BP), paracetamol concentration in the formulation is acceptable,

within the 90-110% range (Ramzi Abdulhameed *et al*., 2016). As demonstrated by the collective evidence, all the formulations assessed in this study had the required amount of paracetamol as their active ingredient. This study is comparable to others, and one sample was run in triplicate to minimize the error and calculate the relative standard deviation (RSD). The concertation of paracetamol at each formulation F1at minimum compression force 96.72%, F1at middle compression force 94.98% F1at high compression force 99.69%, F_2 at minimum compression force 94.78%, F_2 at middle compression force 93.62% F2 at high compression force 93.66%, F_3 at minimum compression force 94.60%, F_3 at middle compression force 95.24% F_3 at high compression force 100.79%, References drug106.85% and concentration of Working references standard 100.0% (Figure 21). All samples and RD contained paracetamol as the active ingredient, which complied with BP or USP these results are comparable to those reported (Achille *et al*., 2022, Marisa *et al*., 2024). However, statistical analysis exposed a statistically significant change between the paracetamol F_1, F_2, and F_3 formulations and the reference drug ($P \leq 0.05$ and $P \geq 0.05$), as shown in Table 13.

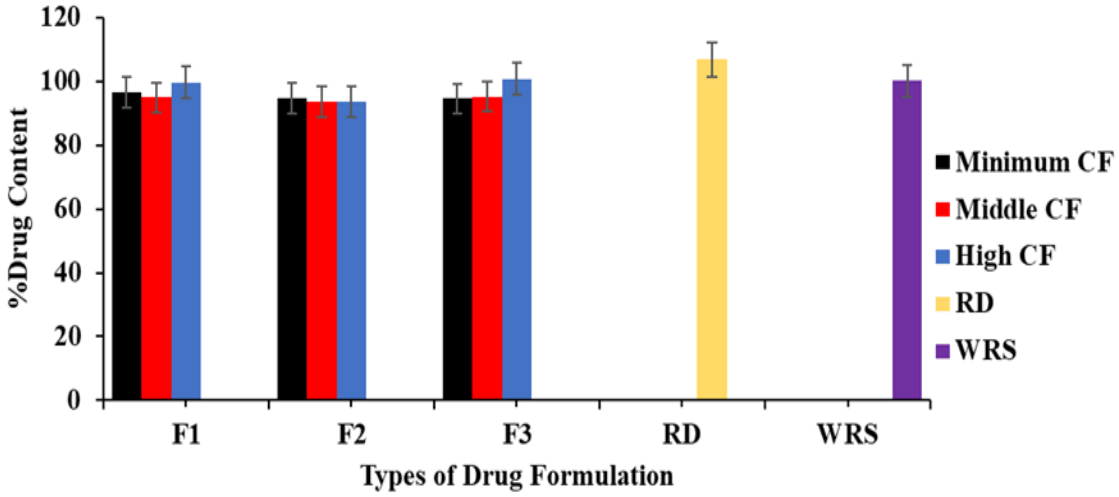

Figure 21. Paracetamol drug content concerning compression force strength.

Table 14. High-performance liquid chromatography, Chromatograms data for the drug content of the formulated Paracetamol tablet.

CF point	Peak Area	Height	Ret. time	Tailing factor	Theoretical plate	Con.
F_1Min CF	384995±0.46	41934±0.412	4.96±0.23	1.293±1.65	6773±1.63	96.72±0.47
F_1Mid CF	377594±0.14	41091±0.114	4.98±0.06	1.330±0.72	6590±0.02	94.98±0.14
F_1High CF	396334±0.07	43244±0.110	4.99±0.03	1.337±0.24	6558±0.07	99.69±0.07
P-value	Min CF, no association exists between the middle CF and high CF, but the middle CF and high CF are more associated (p-value < 0.05).					
F_2Min CF	376820±0.20	40635±0.14	4.99±0.04	1.362±0.40	6531±0.22	94.78±0.21
F_2Mid CF	372205±1.16	40120±1.35	5.00±0.02	1.374±0.19	6549±0.18	93.62±1.16
F_2High CF	372376±0.72	40009±0.33	5.00±0.42	1.383±0.36	6487±0.51	93.66±0.72
P-value	Min CF, Mid CF, and high CF have no significant association (P-value> 0.05).					
F_3Min CF	376563±0.09	40770±0.35	5.01±0.03	1.400±0.30	6480±0.60	94.60±0.09
F_3Mid CF	379125±0.21	40873±0.14	5.00±0.13	1.410±0.20	6482±0.66	95.24±0.21
F_3High CF	429078±0.49	47865±0.13	5.02±0.46	1.382±0.81	6463±0.29	100.79±0.49
P-value	The association exists between Min CF and high CF (p-value < 0.05), but the middle CF is not associated with either of them.					
RD	424807±0.24	45315±0.20	5.03±0.20	1.397±0.410	6328±0.04	106.85±0.24
P-value	Reference drug suggesting an association exists in F_1, F_2, F_3, and WRS, no statistically significant difference between the formulations (p-value < 0.05).					
WRS	398067±0.29	43495±0.66	4.95±0.43	1.265±1.947	6455±2.15	100.16±0.29
P-value	WRS suggests an association observed in F_1, F_2, F_3, and RD, with no statistically significant difference between the formulations (p-value < 0.05).					

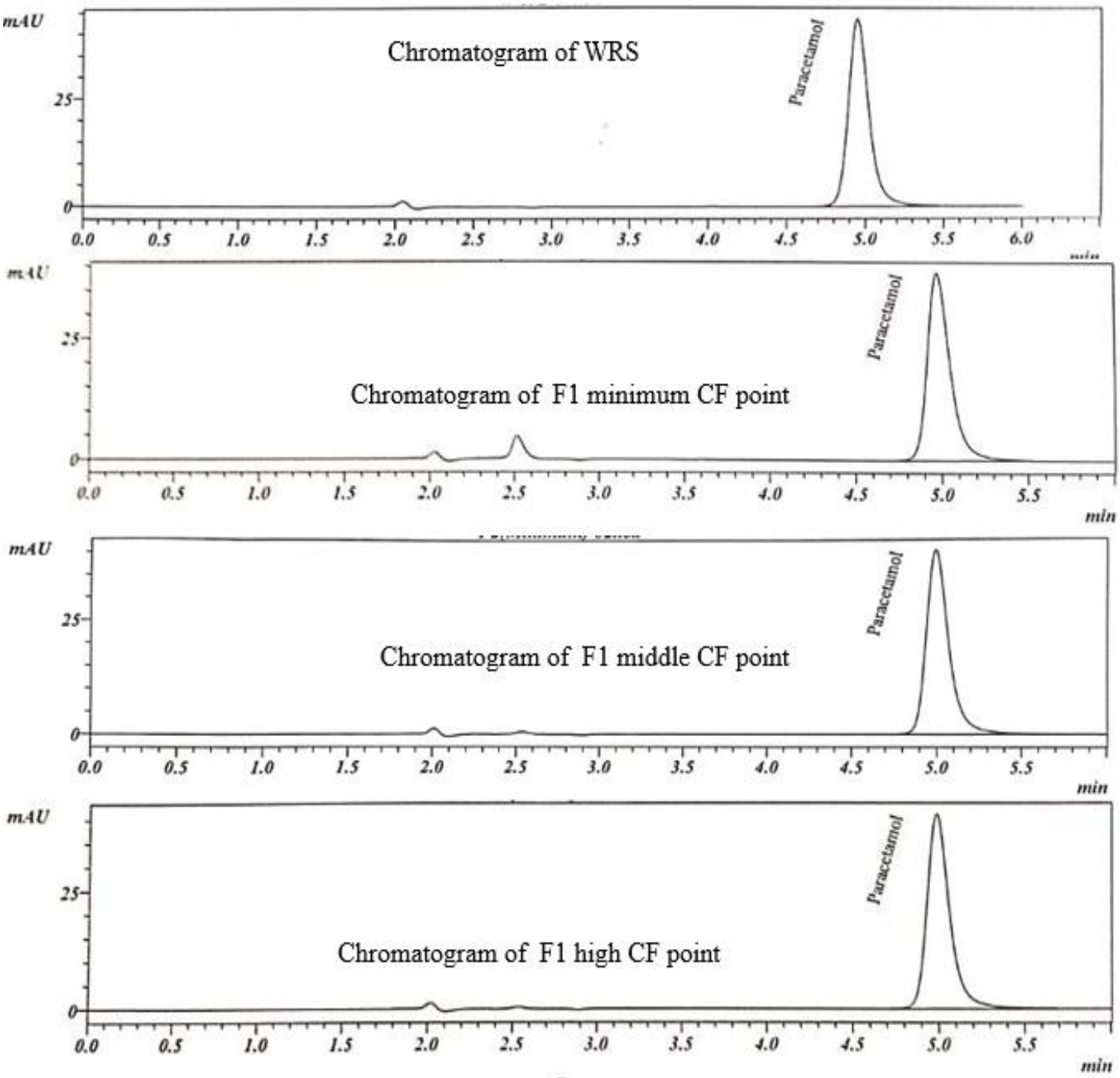

Figure 22. Assay results from High-performance liquid chromatography, Chromatograms of Working Reference standard and F_1, respectively.

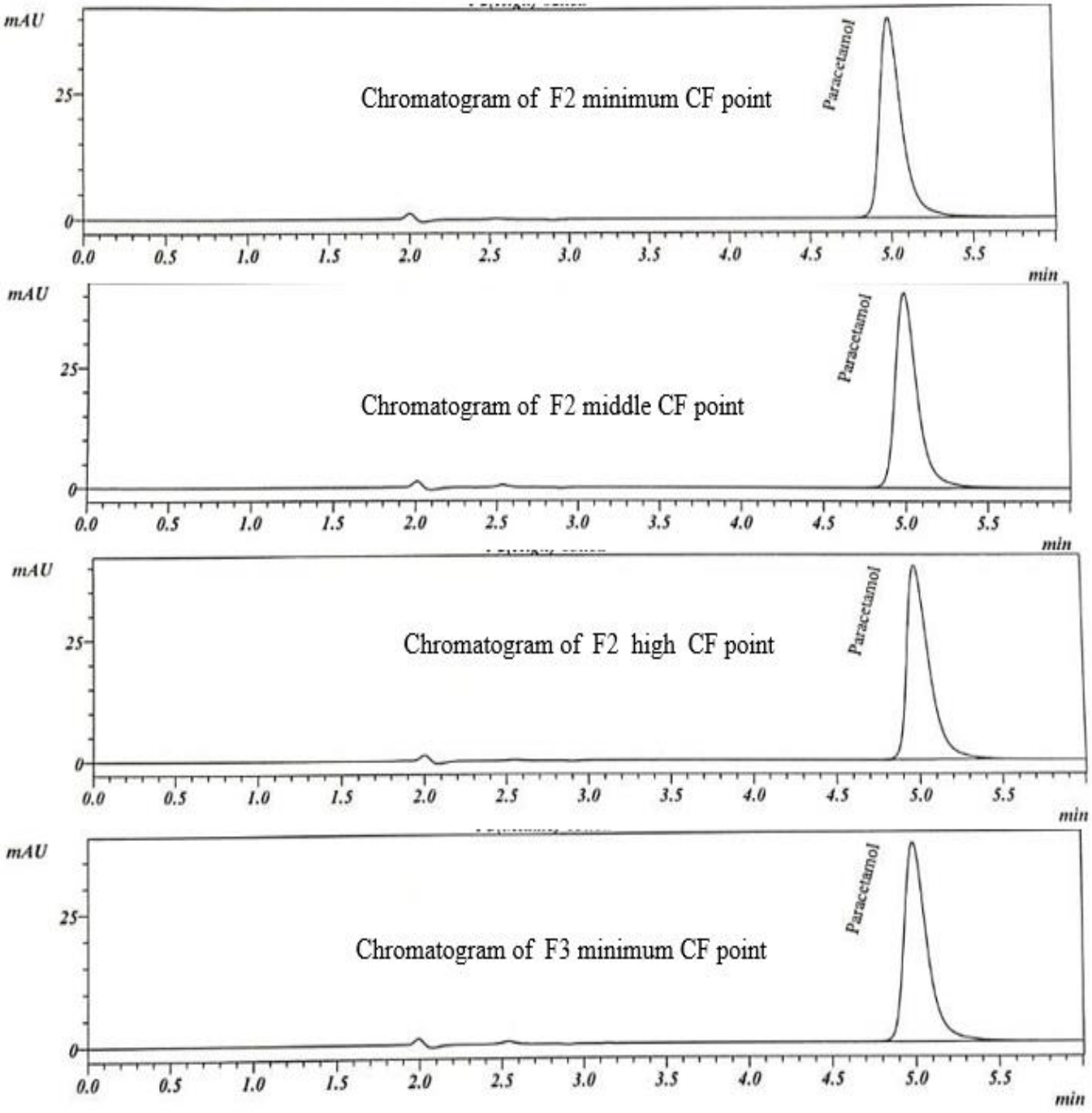

Figure 23. Assay results from High-performance liquid chromatography, Chromatograms of F_2 and F_3 (minimum CF), respectively.

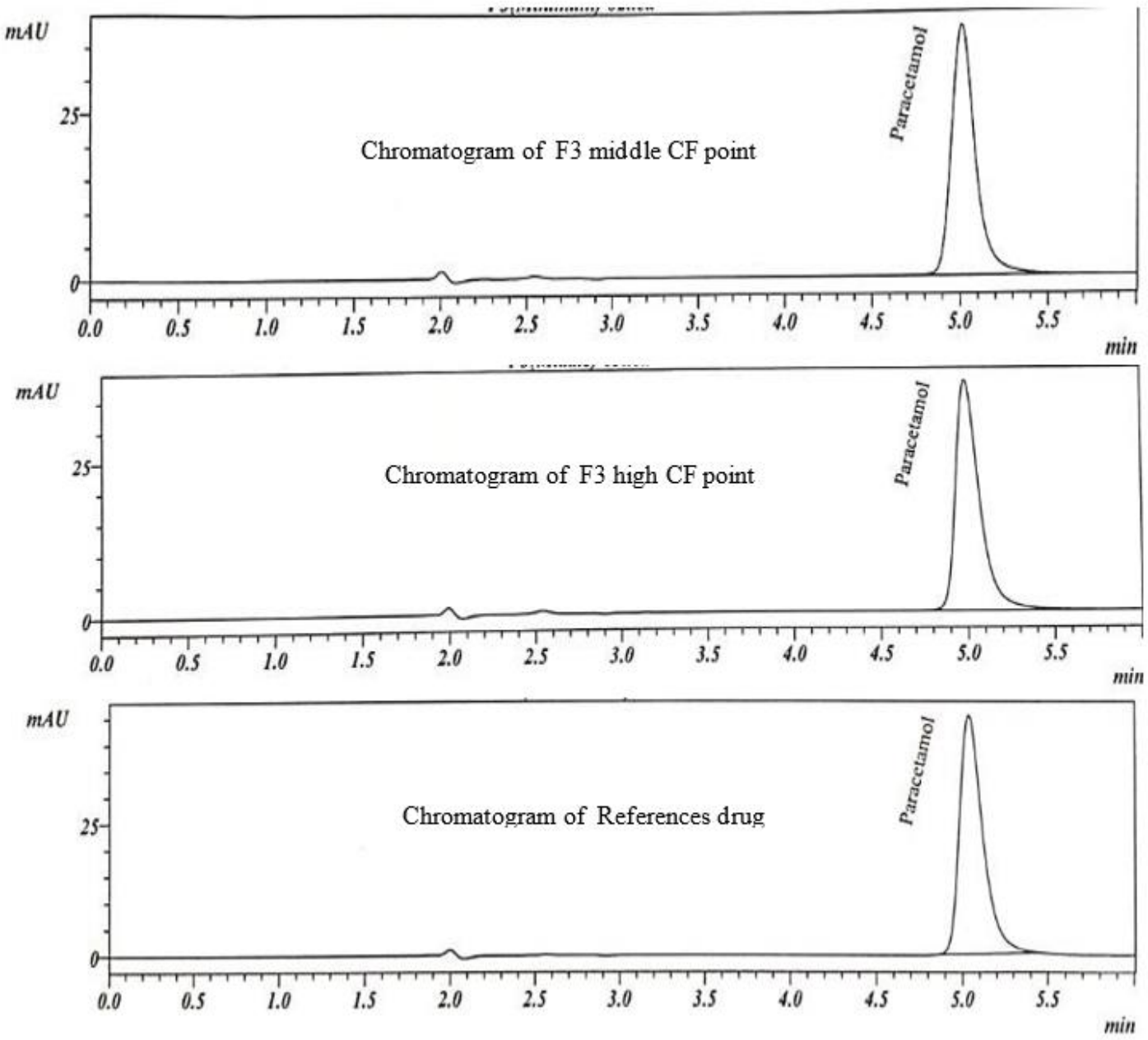

Figure 24. Assay results from High-performance liquid chromatography, Chromatograms of F_3 (Middle and High) and RD, respectively.

4. CONCLUSION

This study successfully demonstrated the isolation, characterization, and application of microcrystalline cellulose (MCC) derived from tea leaf waste (TLW) and tea fiber waste (TFW) as a sustainable alternative to conventional excipients. Optimization of the extraction process yielded up to 86.52% MCC under controlled hydrolysis conditions, highlighting the efficiency of tea waste valorization. Comprehensive characterization using FTIR, XRD, SEM, and thermal analyses confirmed that the structural, morphological, and thermal properties of TLW- and TFW-derived MCC were equivalent to the commercial standard, Avicel PH-101. Crystallinity indices ranging between 60.95% and 70.44% fell within literature-reported values, while SEM imaging revealed distinct morphological features distinguishing native cellulose from MCC.

Physicochemical evaluations, including polymerization degree, pH, solubility, moisture content, flow properties, and microbial quality, aligned with pharmacopeial specifications. Importantly, MCC from tea waste exhibited satisfactory compressibility and flowability, making it suitable for direct compression. The practical application was validated through the successful formulation of paracetamol tablets, which met BP standards for physical quality, dissolution profile, and assay, demonstrating equivalent performance to tablets prepared with Avicel PH-101.

Overall, these findings establish tea waste as a cost-effective, cellulose-rich, and abundantly available raw material that can be transformed into high-quality MCC. This strategy encourages waste valorization, environmental sustainability, and local capacity building in addition to addressing the shortage of pharmaceutical excipients. Hence, tea leaf and fiber waste represent a promising substitute source for MCC in pharmaceutical industries, offering both industrial and ecological benefits.

5. SUGGESTIONS FOR FURTHER WORK

Further studies on microcrystalline cellulose as a direct compressible excipient can also explore its potential applications in various formulations within drug delivery systems, such as controlled-release, delayed-release, or extended-release formulations. The study should be made on the inherent properties of MCC. Additionally, mixing MCC with other excipients, such as polymers or starches, may develop new functionalities and ensure optimized release profiles for various therapeutic applications.

It is recommended to develop a comprehensive method for evaluating the performance of isolated TLW MCC and TFW MCC in compatibility with various active pharmaceutical ingredients and as directly compressible excipients. This method would not only assess the suitability of these MCC variants for paracetamol formulations but also extend the evaluation to other commonly used drugs, such as ibuprofen, metformin chloride, aspirin, and others.

Also, detailed stability check-ups on mixes using MCC as a main ingredient are very important. Both accelerated and long-term stability check-ups should be conducted to see how things like temperature, humidity, and light affect the formulation's stability and drug quality. Regular check-ups would assist in confirming that the assistant maintains its intended characteristics over time and that its latest responses are up to the standards of quality, safety, and effectiveness.

6. REFERENCES

Abu-Thabit, N. Y., Judeh, A. A., Hakeem, A. S., Ul-Hamid, A., Umar, Y., & Ahmad, A. (2020). Isolation and characterization of microcrystalline cellulose from date seeds (Phoenix dactylifera L.). International Journal of Biological Macromolecules, 155, 730–739. https://doi.org/10.1016/j.ijbiomac.2020.03.255

Achille, Y. L., Engelbert, A. J., Gabin, A. A., Pauline, A., Parfait, D., Habib, G., & Djang'eing'a, R. M. (2022). Quality Control of Paracetamol Generic Tablets Marketed in Benin and Search of Its Two Impurities, P-Aminophenol and P-Nitrophenol by HPLC-UV/Visible. American Journal of Analytical Chemistry, 13(11), 449–460. https://doi.org/10.4236/ajac.2022.1311030

Achor, M., Oyeniyi, Y. J., & Yahaya, A. (2014). Extraction and characterization of microcrystalline cellulose obtained from the back of the fruit of Lageriana siceraria (water gourd). Journal of Applied Pharmaceutical Science, 4(1), 57–60. https://doi.org/10.7324/JAPS.2014.40109

Adel, A. M., El-Wahab, Z. H. A., Ibrahim, A. A., & Al-Shemy, M. T. (2010). Characterization of microcrystalline cellulose prepared from lignocellulosic materials. Part I. Acid-catalyzed hydrolysis. Bioresource Technology, 101(12), 4446–4455. https://doi.org/10.1016/j.biortech.2010.01.047

Adeleye, O. A., Bamiro, O. A., Albalawi, D. A., Alotaibi, A. S., & Iqbal, H. (2022). Cellulose Isolated from Cocoa Pod Husk as a Potential. Materials, 1–17. https://doi.org/doi.org/10.3390/ma15175992.

Akhabue. (2017). Optimization of extraction of microcrystalline cellulose from orange peel waste using response surface methodology, Akhabue C. E, and Osubor N. T. 19(2), 227–235.

Alemdar, A., & Sain, M. (2008). Isolation and characterization of nanofibers from agricultural residues - Wheat straw and soy hulls. Bioresource Technology, 99(6), 1664–1671. https://doi.org/10.1016/j.biortech.2007.04.029

An, N. N. (2023). Extraction of microcrystalline cellulose from cotton fiber, and application to block natural rubber as reinforcing agent. Vietnam Journal of Chemistry, 61, 73–80. https://doi.org/10.1002/vjch.202300070

Andersson, S. (2006). A Study of the Nanostructure of the Cell Wall of the Tracheids of Conifer Xylem by X-Ray Scattering. In Report Series in Physics (Issue January).

Angupale, J. R., Okello, A., Ashante, C., Ainembabazi, S., Nalubega, L., Job, I., Nalimu, F., Anyase, R. A., Oloro, J., & Casim, U. T. (2023). Comparison of Physicochemical and Binding Properties of Novicel ™ Microcrystalline Cellulose and Avicel ® PH 101 in Direct Compression of Ascorbic Acid

Tablets. Journal of Pharmaceutics & Drug Development, 10(3), 1–15.

Aridi et al. (2010). Structural FTIR analysis of cellulose functional groups isolated from Leucaena leucocephala pods using different bleaching agents. Cmc.

Azubuike, C. P., & Okhamafe, A. O. (2012). 10.1186%2F2251-7715-1-9.pdf. Journal of Recycling of Organic Waste in Agriculture, 1(9), 1–7.

Azum, N., Jawaid, M., Kian, L. K., Khan, A., & Alotaibi, M. M. (2021). Extraction of microcrystalline cellulose from washingtonia fibre and its characterization. Polymers, 13(18), 1–11. https://doi.org/10.3390/polym13183030

Bacakova, L., Pajorova, J., Bacakova, M., Skogberg, A., Kallio, P., Kolarova, K., & Svorcik, V. (2019). Versatile application of nanocellulose: From industry to skin tissue engineering and wound healing. Nanomaterials, 9(2). https://doi.org/10.3390/nano9020164

Bahreini, Z. (2022). A Study on Preparation and Characterization of Microcrystalline Cellulose from Lucerne (alfalfa) Waste Fibers. 1–16.

Bandelin, F. J. (1999). Compressed Tablets by Wet Granulation. In Pharmaceutical Dosage Forms : Tablets Volume 1.

Borhana, A., Mohammed, A. A. B. A., Sapuan, S. M., Ilyas, R. A., Asyraf, M. R. M., Koloor, S. S. R., & Petrů, M. (2021). Micro-and nanocellulose in polymer composite materials: A review. Polymers, 13(2), 1–30. https://doi.org/10.3390/polym13020231

BP. (2009). British Pharmacopeia (BP) (2009). Version 11, Published on the Recommendation of the Medicines Commission Pursuant to the Medicine Act 1968. Her Majesty's Stationery Office, London. BioMed Research International. https://doi.org/10.1155/2024/9437835

Chen, W. S., Yu, H. P., Chen, P., Jiang, N. X., Shen, J. H., Liu, Y. X., & Li, Q. (2011). Preparation and morphological characteristics of cellulose micro/nano fibrils. Materials Science Forum, 675 677(c), 255–258. https://doi.org/10.4028/www.scientific.net/MSF.675-677.255

Chijioke, O., Philomena, K. I., Joseph, T. N., Charles, O. N., & Paschal, E. O. (2020). Artificial Intelligence in Agriculture: Evaluation of optimization techniques in predicting optimum moisture content reduction in drying potato slices. Artificial Intelligence in Agriculture, 4, 39–47. https://doi.org/10.1016/j.aiia.2020.04.001

Chowdhury, A., Sarkar, S., Chowdhury, A., Bardhan, S., Mandal, P., & Chowdhury, M. (2016). Tea waste management: A case study from West Bengal, India. Indian Journal of Science and Technology, 9(42). https://doi.org/10.17485/ijst/2016/v9i42/89790

Dave, V. S., Sayles, M., & Popielarczyk, M. (2015). Fisher Digital Publications Drug-Excipient Compatibility Studies in Formulation Development : Current Trends and Techniques 9–15. https://doi.org/https://fisherpub.sjf.edu/pharmacy_facpub/212 and

Debnath, B., Duarah, P., & Purkait, M. K. (2023). Microwave-assisted quick synthesis of microcrystalline cellulose from black tea waste (Camellia sinensis) and characterization. International Journal of Biological Macromolecules, 244, 1–5. https://doi.org/10.1016/j.ijbiomac.2023.125354

Dechassa, N., & Merga, M. (2022). Tea (Camellia sinensis) Production, Opportunities, Challenges, and Future Prospects in Ethiopia. Advances in Agriculture, 2022. https://doi.org/10.1155/2022/1942666

Demirayak, Ş. (2016). Development of Directly Compressible Excipients from Phoenix dactylifera Mucilage and Microcrystalline Cellulose using Co-Processing Techniques. International Journal in Pharmaceutical Sciences.

Diño, S. F., Edu, A. D., Francisco, R. G., Gutierrez, E., Crucis, P., Lapuz, A. M., Carandang, R. R., & Miranda, K. J. (2023). Drug-Excipient Compatibility Testing of Cilostazol Using FTIR and DSC Analysis. 152(May), 2129–2137.

Dinte, E., Bodoki, E., Leucuta, S., & Adela Iuga, C. (2013). Compatibility studies between drugs and excipients in the preformulation phase of buccal mucoadhesive systems. Farmacia, 61(4), 703–712.

Edrees1*, W. H. A., Abdullah1, Q. Y. M., AL-Kaf2, A. G., & Naji, K. M. (2017). Review article- A review on comparative study between the physicochemical and biological processes for paracetamol degradation. Article Info : 2(2), 32–41.

Foroughi, F., Ghomi, E. R., Dehaghi, F. M., Borayek, R., & Ramakrishna, S. (2021). A review on the life cycle assessment of cellulose: From properties to the potential of making it a low carbon material. Materials, 14(4), 1–23. https://doi.org/10.3390/ma14040714

Fortunati, E., Puglia, D., Monti, M., Peponi, L., Santulli, C., Kenny, J. M. and Torre, L. (2013). Extraction of Cellulose Nanocrystals from Phormium tenax Fibres. Journal of Polymers and the Environment. (pp. 319-328.).

Gabriel, T., Belete, A., Syrowatka, F., Neubert, R. H. H., & Gebre-Mariam, T. (2020). Extraction and characterization of celluloses from various plant byproducts. International Journal of Biological Macromolecules, 158, 1248–1258. https://doi.org/10.1016/j.ijbiomac.2020.04.264

Gangolu, J., Balaiah, S., Nandi, S., & Roy, H. (2019). Optimization and Quest of HPMC-loaded Stavudine Controlled Release Dosage Development by Central Composite Design utilizing Reduced Factorial Screening Technique. 1–21.

Gawshinde, A., Solanki, D., Tikariya, K., Atneriya, U., & Chaurasia, P. (2024). Formulation, Development, and Evaluation of Paracetamol Tablet by Moisture-Activated Dry Granulation (MADG) Process. 07. https://doi.org/10.37421/2952-8100.2024.07.467

Getachew, M., Gabriel, T., Belete, A., & Gebre-Mariam, T. (2023). Extraction and Characterization of Cellulose and Microcrystalline Cellulose from Teff Straw and Evaluation of the Microcrystalline Cellulose as Tablet Excipient. Journal of Natural Fibers, 20(2). https://doi.org/10.1080/15440478.2023.2245565

Gholizadeh-Hashjin, A., lotfipour, farzaneh, & Hallaj-Nezhadi, S. (2019). Quality Control of Non-Sterile Drug Product According to United States' Pharmacopeia Instruction. Iranian Journal of Medical Microbiology, 13(5), 321–345. https://doi.org/10.30699/ijmm.13.5.321

Haafiz, M. K. M., Hassan, A., Zakaria, Z., & Inuwa, I. M. (2014). Isolation and characterization of cellulose nanowhiskers from oil palm biomass microcrystalline cellulose. Carbohydrate Polymers, 103(1), 119–125. https://doi.org/10.1016/j.carbpol.2013.11.055

Haji Badri, K. (2016). Thermal Characteristics of Microcrystalline Cellulose From Oil Palm Biomass. Malaysian Journal of Analytical Science, 20(5), 1112–1122. https://doi.org/10.17576/mjas-2016-2005-17

Hitesh Chaturvedi1*, A. G., and U. S. R. (2022). Post-Compression Evaluation Parameters for Tablets. European journal of pharmaceutical and Medical Research, 4(March), 526–530.

Hospodarova, V., Singovszka, E., & Stevulova, N. (2018). Characterization of Cellulosic Fibers by FTIR Spectroscopy for Their Further Implementation to Building Materials. American Journal of Analytical Chemistry, 09(06), 303–310. https://doi.org/10.4236/ajac.2018.96023

Jamshaid, A., Hamid, A., Muhammad, N., Naseer, A., Ghauri, M., Iqbal, J., Rafiq, S., & Shah, N. S. (2017). Cellulose-based Materials for the Removal of Heavy Metals from Wastewater – An Overview. ChemBioEng Reviews, 4(4), 240–256. https://doi.org/10.1002/cben.201700002

Kačuráková, M., & Wilson, R. H. (2001). Developments in mid-infrared FT-IR spectroscopy of selected carbohydrates. Carbohydrate Polymers, 44(4), 291–303. https://doi.org/10.1016/S0144-8617(00)00245-9

Kale, R. D., Bansal, P. S., & Gorade, V. G. (2018). Extraction of Microcrystalline Cellulose from Cotton Sliver and Its Comparison with Commercial Microcrystalline Cellulose. Journal of Polymers and the Environment, 26(1), 355–364. https://doi.org/10.1007/s10924-017-0936-2

Kamlesh B. Shah, Dayton, N. J. (2012). Method for preparing a direct compression granulated

acetaminophen composition. United States Patent, 19, 1–12.

Kane, S. N., Mishra, A., & Dutta, A. K. (2016). Preface: International Conference on Recent Trends in Physics (ICRTP 2016). Journal of Physics: Conference Series, 755(1). https://doi.org/10.1088/1742-6596/755/1/011001

Kharismi, R. R. A. Y., Sutriyo, & Suryadi, H. (2018). Preparation and characterization of microcrystalline cellulose produced from betung bamboo (dendrocalamus asper) through acid hydrolysis. Journal of Young Pharmacists, 10(2), s79–s83. https://doi.org/10.5530/jyp.2018.2s.15

Khili, F., Borges, J., Almeida, P. L., Boukherroub, R., & Omrani, A. D. (2019). Extraction of Cellulose Nanocrystals with Structure I and II and Their Applications for Reduction of Graphene Oxide and Nanocomposite Elaboration. Waste and Biomass Valorization, 10(7), 1913–1927. https://doi.org/10.1007/s12649-018-0202-4

Kian, L. K., Jawaid, M., Ariffin, H., & Alothman, O. Y. (2017). Isolation and characterization of microcrystalline cellulose from roselle fibers. International Journal of Biological Macromolecules, 103, 931–940. https://doi.org/10.1016/j.ijbiomac.2017.05.135

Kokott, M., Lura, A., Breitkreutz, J., & Wiedey, R. (2021). Evaluation of two novel co-processed excipients for direct compression of orodispersible tablets and mini-tablets. European Journal of Pharmaceutics and Biopharmaceutics, 168(May), 122–130. https://doi.org/10.1016/j.ejpb.2021.08.016

Krivokapić, J., Ivanović, J., Djuriš, J., Medarević, D., Potpara, Z., Maksimović, Z., & Ibrić, S. (2020). Tableting properties of microcrystalline cellulose obtained from wheat straw measured with a single-punch bench-top tablet press. Saudi Pharmaceutical Journal, 28(6), 710–718. https://doi.org/10.1016/j.jsps.2020.04.013

Kumar, V., & Sartaj Ahmad BhatC, Sunil KumarA, Pradeep VermaD, Irfan Anjum BadruddinF, Juliana Heloisa Pinê Américo-Pinheiro eH, Ravishankar Sathyamurthy g, J, A. E. A. i. (2006). Tea byproducts biorefinery for bioenergy recovery and value-added products development: A step towards environmental sustainability. January 2006.

Kunusa, W. R., Isa, I., Laliyo, L. A. R., & Iyabu, H. (2018). FTIR, XRD and SEM Analysis of Microcrystalline Cellulose (MCC) Fibers from Corncorbs in Alkaline Treatment. Journal of Physics: Conference Series, 1028(1). https://doi.org/10.1088/1742-6596/1028/1/012199

Landín, M., González, M. P., Souto, C., Concheiro, A., Gómez-Amoza, J. L., & Martínez-Pacheco, R. (1993). Comparison of Two Varieties of Microcrystalline. 19(10).

Liang, Z., Li, X., Li, M., & Hong, Y. (2023). Study on the Preparation and Properties of Jute

Microcrystalline Cellulose Membrane. Molecules, 28(4). https://doi.org/10.3390/molecules28041783

Liya Teklu, E. A. and A. A., & Department. August (2014). Quality Evaluation of Paracetamol Tablets obtained from the Common Shops (Kiosks) in Addis Ababa, Ethiopia, International Journal of Pharmaceutical Sciences and Research https://doi.org/10.13040/IJPSR.0975-8232.5(9).3502-10

Mansor, A. M., Lim, J. S., Ani, F. N., Hashim, H., & Ho, W. S. (2019). Characteristics of cellulose, hemicellulose and lignin of MD2 pineapple biomass. Chemical Engineering Transactions, 72(March 2018), 79–84. https://doi.org/10.3303/CET1972014

Marisa, G., Kapala, J., Mafuru, T., Matinde, R., Kimaro, E., & Kaale, E. (2024). Quality Evaluation of Locally Manufactured Paracetamol Tablets in East Africa. BioMed Research International, 2024, 9437835. https://doi.org/10.1155/2024/9437835

Mihranyan, A., Llagostera, A. P., Karmhag, R., Strømme, M., & Ek, R. (2004). Moisture sorption by cellulose powders of varying crystallinity. International Journal of Pharmaceutics, 269(2), 433–442. https://doi.org/10.1016/j.ijpharm.2003.09.030

Nasution, H., Yurnaliza, Veronicha, Irmadani, & Sitompul, S. (2017). Physicochemical properties and characteristics of microcrystalline cellulose derived from the cellulose of oil palm empty fruit bunch. IOP Conference Series: Materials Science and Engineering, 223(1), 1–8. https://doi.org/10.1088/1757-899X/223/1/012056

Newman, R. H., Davies, L. M., & Harris, P. J. (1996). Solid-state 13C nuclear magnetic resonance characterization of cellulose in the cell walls of Arabidopsis thaliana leaves. Plant Physiology, 111(2), 475–485. https://doi.org/10.1104/pp.111.2.475

Nsor-Atindana, J., Chen, M., Goff, H. D., Zhong, F., Sharif, H. R., & Li, Y. (2017). Functionality and nutritional aspects of microcrystalline cellulose in food. Carbohydrate Polymers, 172, 159–174. https://doi.org/10.1016/j.carbpol.2017.04.021

Ogemdi, I. K. (2019). A Review on the Properties and Uses of Paracetamol. 5(3), 31–35. https://doi.org/10.11648/j.ijpc.20190503.12

Osubor, A. and E. (2017). Optimization of extraction of microcrystalline cellulose from orange peel waste using response surface methodology. Ife Journal of Science Vol., 19(2), 227–235.

Ouwmeester, H. A. N. S. B. (2015). REVIEW A Review of Analytical Methods for the Identification and Characterization of Nano Delivery Systems in Food. 8231–8247.

Owolabi, A. F., Ghazali, A., Khalil, H. P. S. A., Hassan, A., Arjmandi, R., Fazita, M. R. N., & Haafiz, M. K. M. (2016). Isolation and Characterization of Microcrystalline Cellulose from Oil Palm Fronds

Using Chemomechanical Process. Wood and Fiber Science, 48(4), 260–270.

Pachuau, L., Vanlalfakawma, D. C., Tripathi, S. K., & Lalhlenmawia, H. (2014). Muli bamboo (Melocanna baccifera) as a new source of microcrystalline cellulose. Journal of Applied Pharmaceutical Science, 4(11), 87–94. https://doi.org/10.7324/JAPS.2014.41115

Panaitescu, D. M., Vizireanu, S., Stoian, S. A., Nicolae, C. A., Gabor, A. R., Damian, C. M., Trusca, R., Carpen, L. G., & Dinescu, G. (2020). Poly(3-hydroxybutyrate) modified by plasma and TEMPO-oxidized celluloses. Polymers, 12(7), 1–16. https://doi.org/10.3390/polym12071510

Picker, K. M., & Hoag, S. W. (2002). Characterization of the thermal properties of microcrystalline cellulose by modulated temperature differential scanning calorimetry. Journal of Pharmaceutical Sciences, 91(2), 342–349. https://doi.org/10.1002/jps.10018

Priyangga, A., Pambudi, A. B., Atmaja, L., & Jaafar, J. (2021). Physicochemical properties of microcrystalline cellulose doped imidazole membrane for direct methanol fuel cell. AIP Conference Proceedings, 2349(8), 1–8. https://doi.org/10.1063/5.0051533

Rahman, N. H. A., Chieng, B. W., Ibrahim, N. A., & Rahman, N. A. (2017). Extraction and characterization of cellulose nanocrystals from tea leaf waste fibers. Polymers, 9(11), 1–11. https://doi.org/10.3390/polym9110588

RAJ.R, A. (2013). Disintegrating Agents in Aceclofenac Tablet Formulation. International Journal of Pharmacy and Pharmaceutical Sciences, 5(2), 30–33.

Ramzi Abdulhameed, B., Salih Mohamed, S., Ramzi Abdulhameed, S., & Fatah Aziz, D. (2016). Assay of paracetamol tablets from different manufacturing sources Assay of paracetamol tablets from different manufacturing sources in Sulaimani market in Iraq. In Sulaimani Market in Iraq Diyala Journal of Medicine, 15(1).

Rana, R. H., Rana, M. S., Tasnim, S., Haque, M. R., Kabir, S., Amran, M. S., & Chowdhury, A. A. (2022). Characterization and tableting properties of microcrystalline cellulose derived from waste paper via hydrothermal method. Journal of Applied Pharmaceutical Science, 12(6), 140–147. https://doi.org/10.7324/JAPS.2022.120613

Santos Júnior, A. de F., Barbosa, I. S., dos Santos, V. L., Silva, R. L., & Caetite Junior, E. (2014). Test of dissolution and comparison of in vitro dissolution profiles of coated ranitidine tablets marketed in Bahia, Brazil. Brazilian Journal of Pharmaceutical Sciences, 50(1), 83–89. https://doi.org/10.1590/S1984-82502011000100008

Sayed, H. M. (2025). Optimization of microcrystalline cellulose-based pharmaceutical formulations using

design of experiments (DoE) and Process Analytical Technology. 14(1), 87–93.

Sergejs Trusovs, Northridge. (2002). Cellulose and Cellulose Derivatives: United States Patent, 1(12), 1–4.

Shah, Y. (2017). And in vitro evaluation of the sublingual film of isosorbide World Journal of Pharmaceutical Research formulation development and in vitro evaluation of. World Journal of Pharmaceutical Research, August. https://doi.org/10.20959/wjpr201711-9426

Sharma, A., Thakur, M., Bhattacharya, M., Mandal, T., & Goswami, S. (2019). Commercial application of cellulose nano-composites – A review. Biotechnology Reports, 21(2018), e00316. https://doi.org/10.1016/j.btre.2019.e00316

Shlieout, G., Arnold, K., & Müller, G. (2002). Powder and mechanical properties of microcrystalline cellulose with different degrees of polymerization. AAPS PharmSciTech, 3(2), 1–10. https://doi.org/10.1208/pt030211

Shwetha Margaret JL, & Madhavi BLR. (2019). Study of Direct Compression Method for the Preparation of Quinapril Hydrochloride Tablets. Asian Journal of Pharmaceutical and Clinical Research, 13(1), 202–211. https://doi.org/10.22159/ajpcr.2020.v13i1.34005

Sikdar, D., Goswami, S., & Das, P. (2020). Activated carbonaceous materials from tea waste and its removal capacity of indigo carmine present in solution: synthesis, batch and optimization study. Sustainable Environment Research, 30(1). https://doi.org/10.1186/s42834-020-00070-8

Tarchoun, A. F., Trache, D., & Klapötke, T. M. (2019). Microcrystalline cellulose from Posidonia oceanica brown algae: Extraction and characterization. International Journal of Biological Macromolecules, 138, 837–845. https://doi.org/10.1016/j.ijbiomac.2019.07.176

Tessema, T. A., Feroche, A. T., Workneh, G. A., & Gabriel, T. (2023). Physicochemical Characterization of Cellulose and Microcrystalline Cellulose from Cordia africana Lam. Seeds. Journal of Natural Fibers, 20(2). https://doi.org/10.1080/15440478.2023.2198278

Tiwari, R., Agarwal, S. K., & Tiwari, S. (2013). International Journal of Drug Delivery 5 (2013) 206-213 Formulation and multivariate optimization of microcrystalline cellulose pellets of highly water soluble drug. 5, 206–213.

Tomar, M., Sinha, A. R., & Singh, A. K. (2017). Process And Development Of Co-Processed Excipient Silicified Microcrystalline Cellulose And Manufacture Paracetamol Tablet By Direct Compression. International Journal of Pharmaceutical Sciences Review and Research, 42(1), 191–196.

Trache, D., Donnot, A., Khimeche, K., Benelmir, R., & Brosse, N. (2014). Physico-chemical properties

and thermal stability of microcrystalline cellulose isolated from Alfa fibres. Carbohydrate Polymers, 104(1), 223–230. https://doi.org/10.1016/j.carbpol.2014.01.058

Trache, D., Hussin, M. H., Hui Chuin, C. T., Sabar, S., Fazita, M. R. N., Taiwo, O. F. A., Hassan, T. M., & Haafiz, M. K. M. (2016). Microcrystalline cellulose: Isolation, characterization and bio-composites application—A review. International Journal of Biological Macromolecules, 93, 789–804. https://doi.org/10.1016/j.ijbiomac.2016.09.056

Tseng, A., Lau, W. J., Tung, K.-L., Setnickova, K., Asif, M., Ahmed, D., Ahmad, N., Tariq Qamar, M., Alruwaili, N. K., Nasir, S., & Bukhari, A. (2022). Extraction and Characterization of Microcrystalline Cellulose from Lagenaria siceraria Fruit Pedicles. Polymers , 14(1867), 1–11. https://doi.org/10.3390/polym14091867

USP. (2012). Microcrystalline Cellulose Microcrystalline Cellulose and Carboxymethylcellulose Sodium (Issue c).

USP. (2019). Excipient Monographs 2: Microcrystalline Cellulose. United States Pharmacopeia, Stage 4 Harmonization, 31(5), 3306.

USP. (2022). United State Pharmacopoia 41the ed.National formulary 36 ed. The United 100 States Pharmacopeial Convention - U.S. Pharmacopeia National Formulary., 30(6), 1–7.

Victoria, A., John, P., Keeran, H., & Ries, M. E. (2023). Design of experiments in the optimization of all - cellulose composites. Cellulose, 30(17), 11013–11039. https://doi.org/10.1007/s10570-023-05535-8

Wathsala, K. P. T., Weerakkody, K. M., & Weragoda, V. S. C. (2021). Isolation and characterization of microcrystalline cellulose from rice straw. MERCon 2021 - 7th International Multidisciplinary Moratuwa Engineering Research Conference, Proceedings, 13(Mcc), 670–675. https://doi.org/10.1109/MERCon52712.2021.9525752

Widodo, R. T., Hassan, A., Liew, K. Bin, & Ming, L. C. (2022). A Directly Compressible Pregelatinised Sago Starch: A New Excipient in the Pharmaceutical Tablet Formulations. Polymers, 14(15). https://doi.org/10.3390/polym14153050

Yildirim, M., & Candan, Z. (2020). Usage Potential of Lignocellulosic Nanomaterials in Eco-Friendly Applications. 10th International Ecology Symposium, March. https://www.researchgate.net/profile/Nazli-Ersoez-

Yohana Chaerunisaa, A., Sriwidodo, S., & Abdassah, M. (2019). Microcrystalline Cellulose as Pharmaceutical Excipient. Pharmaceutical Formulation Design - Recent Practices. https://doi.org/10.5772/intechopen.88092

Zeleke, N. M., Sinha, D. K., & Kumar, S. (2024). Multi-objective optimization of micro crystalline cellulose and montmorillonite-filled poly lactic acid bio–composite and its characterizations. Journal of Engineering and Applied Science, 1–20. https://doi.org/10.1186/s44147-024-00525-4

Zeleke, N. M., Sinha, D. K., & Mengesha, G. A. (2022). Chemical Composition and Extraction of Microcrystalline Cellulose from Outer Skin Isolated Coffee Husk. Advances in Materials Science and Engineering, 2022. https://doi.org/10.1155/2022/7163359

Zhao, T., Chen, Z., Lin, X., Ren, Z., Li, B., & Zhang, Y. (2018). Preparation and characterization of microcrystalline cellulose (MCC) from tea waste. Carbohydrate Polymers, 184(December 2017), 164–170. https://doi.org/10.1016/j.carbpol.2017.12.024